Ultrasonic-time-domain-reflectometry as a real time non-destructive visualisation technique of concentration polarisation and fouling on reverse osmosis membranes

by

Louis Johannes Koen

Thesis submitted in partial fulfilment of the requirements for the degree of

Master of Science in Engineering

at the

University of Stellenbosch.

Supervisors:

Prof R.D.Sanderson

Prof. L.Lorenzen

Stellenbosch 2000

Declaration

I, the undersigned, hereby declare that the work contained in this thesis is my own original work and has not previously in its entirety or in part been submitted at any university for a degree.

16-11-2000

Date

ABSTRACT

Fouling is readily acknowledged as one of the most critical problems limiting the wider application of membranes in liquid separation processes. A better understanding of fouling layer formation and its monitoring is needed in order to improve on existing cleaning techniques. Plant operation can be optimised if fouling can be monitored by noninvasion means either on the plant itself or on an attached monitoring device.

The overall scope of this research was to develop a non-destructive, real-time, in situ visualisation technique or device for concentration polarisation and fouling layer monitoring. Ultrasonic-time-domain-reflectometry (UTDR) was employed as a visualisation technique to provide real-time characterisation of the fouling layer.

A 24 cm-long rectangular flat sheet aluminium cell was designed and used as separation device for a desalination system. The experimental results obtained using this module confirmed that there are an excellent correspondence between the flux decline behaviour and the UTDR response from the membrane. The ultrasonic technique could effectively detect fouling layer initiation and growth on the membrane in real-time. In addition to the measurement of fouling, the ultrasonic technique was also successfully employed for monitoring membrane cleaning. Since no real-time permeation data is available during cleaning operations in industrial applications, a UTDR monitoring device may prove to be a very valuable technique in optimising cleaning strategies.

The technique was further tested on an 8-inch diameter spiral wrap industrial module and good results were obtained. Stagnant zones, as well as flux flow behaviour inside the module could be determined. However, more research is needed to fully understand the complex phenomena inside a spiral wrap module.

Overall, the UTDR technique and its use in monitoring devices have a major impact in the membrane industry due to its extremely powerful capabilities.

Opsomming:

Membraan-bevuiling of -verstopping is die grootste struikelblok wat die algemene aanwending van membrane vir verskillende watersuiweringsprosesse negatief beinvloed. 'n Beter begrip van membraan-bevuiling, asook beter metingsmetodes daarvan is nodig om op bestaande skoonmaaktegnieke te verbeter.

Die hoofdoel van hierdie studie was die ontwikkeling van 'n nie-destruktiewe-in-lyn visuele tegniek vir die meting van konsentrasie polarisasie en membraan-bevuiling. Deur gebruik te maak van ultrasoniese klank golwe, is 'n tegniek ontwikkel wat 'n direkte visuele aanduiding kon gee van die toestand van membraan-bevuiling binne-in die module.

'n Reghoekige aluminium-module, 24 cm lank, is ontwerp en gebou waarbinne die membraan geplaas is vir die skeidingsproses. Resultate dui daarop dat daar 'n uitstekende verband bestaan tussen die afname in permeaatvloei en die ultrasoniese eggo vanaf die membraan. Die ultrasoniese tegniek kon die vorming van en toename in membraan-bevuiling doeltreffend karakteriseer. In teenstelling hiermee, is die tegniek ook suksesvol aangewend om die skoonmaak-proses van membrane te ondersoek. Met min of geen data beskikbaar vir die skoonmaak-proses van membrane in die industriële sektor, het die tegniek enorme potensiaal in die optimisering van bestaande skoonmaak-tegnieke.

Die tegniek is verder aangewend op 'n industriële 8-duim deursnee spiraal-module en goeie resultate is verkry. Stagnante sones asook vloed-vloei-patrone binne-in die module kon suksesvol bepaal word. Baie navorsing is egter nog nodig om die ingewikkelde data wat gegenereer word tydens die ondersoek van 'n spiraal-module ten volle te verstaan.

Die enorme potensiaal en moontlikhede van die ultrasoniese tegniek kan die begin wees van 'n revolusie in die membraan-industrie.

INDEX

List of Figures

Acknowledgements

I would like to thank the following people without whom this study would have been impossible:

Prof. R.D. Sanderson and **Prof. L. Lorenzen**, my promoters, for their help and support.

The **Water Research Commission** of South Africa for funding this project.

All the staff at the Institute for Polymer Science for their assistance.

My parents for their love and support throughout this study.

Mineral Water Development for supplying RO equipment, as well as their technical staff for their help.

All my friends, but especially Ria Strydom, for making the time at Stellenbosch "the best years of my life."

Our heavenly Farther for His guidance and for giving me the opportunity to undertake such a study.

1 Introduction

Although the phenomenon of osmosis has been observed and studied for over 200 years, its application to the desalination of water has only been intensively studied for the last 40-50 years. Historically, the first recorded study of membrane phenomena was conducted by Abbe' Jean Antoine Nollet in 1748 (Lonsdale, 1982). He immersed wine contained in an animal bladder in pure water and observed that water permeated through the bladder into the wine.

However, it was not until the early twentieth century that the first commercial membranes for practical applications were developed by Zsigmondy (Lonsdale, 1982) and manufactured by Sartorius in Germany. In the years since formulation of the first practical, synthetic asymmetric semi-permeable membrane, reverse osmosis (RO) technology has evolved as a highly competitive process involving multi-million dollar installations around the world. Whereas RO was originally regarded as a method of producing potable water from the sea or from brackish sources, the technology is now being applied on large scale in municipal and industrial wastewater treatment, and has found additional applications on a smaller scale, in a wide variety of industrial processes.

Distillation technology dominated the desalination scene until about 1970. Since then, improvements in reverse osmosis (RO) and electrodialysis (ED) technologies have resulted in substantial increases in their application. Today there are approximately 8900 desalting units comprising over 15.6 million m^3/day of installed capacity (Mallevialle et al., 1996). Distillation technologies account for approximately 60 percent of the worlds desalting capacity, whereas RO and ED account for 35 and 6 percent, respectively. However, over the past years, the percentage of worldwide desalting capacity by membrane processes has increased, while the reverse has been observed for distillation. RO treatment capacity has increased from 20 to more than 30 percent, while distillation has decreased from 68 to 56 percent (Mallevialle et al., 1996). Although there is greater desalting capacity by distillation, there is a greater number of treatment plants employing membrane

processes. Today, membrane plants account for almost 70 percent of the total number of desalination plants constructed.

Low energy costs have been the prime motivation for the surge in RO desalting activity. In the late 70's, RO desalination of seawater, the least efficient application because of high osmotic pressures, required only one third the energy of thermal desalting processes (Kremen, 1979). Over the last few years there have been a lot of improvement in membrane technologies and this figure is even better.

Probably the most promising application of RO is in the field of affordable seawater desalting and water recycling. Limited availability of traditional surface and groundwater supplies, combined with increasingly stringent industrial and municipal discharge standards, have frequently made recycling the most economically attractive solution to a water supply problem. In the new millennium, the lack of sufficient water supplies to fulfil everyone's needs might soon become a problem, which will further strengthen the importance of recycling.

However, fouling is still a major problem that limits the wider application of membrane processes for desalination purposes. A more effective method of monitoring fouling initiation, as well as a means of measuring fouling layer growth, is necessary for a better understanding of this complex problem. Differences in flux flow as well as pressure induced changes are presently the only two indicators of fouling, and are often not enough to monitor fouling.

The development of a non-invasive technique to monitor the presence and growth of a fouling layer under realistic operating conditions in real time is thus of great importance.

1.1 Focus of this research

The objective of this study is to describe the development of ultrasonic-time-domain-reflectometry and its use as a real-time visualisation technique for concentration polarisation and fouling layer monitoring on RO membranes, and to compare these results with traditional methods of fouling indicators such as

permeate flux changes, as well as visual samples of the membrane surface covered by the fouling layer.

In order to achieve these objectives, the following goals were set:

- Develop a firm knowledge in ultrasonics and various ultrasonic equipment available on the market.
- Find all the necessary hardware i.e. pulsar-receiver, oscilloscope, probes etc. for usage in the study.
- Design a suitable desalination cell and system for salt separation.
- Define the operating conditions, fouling agents and membranes that will be used. As calcium carbonate and calcium sulphate are the two most dominant fouling species in RO processes, it was decided to use them for fouling the membranes. The fact that both species have well defined chemical characteristics also makes them very suitable.
- Implement the ultrasonic equipment on the desalination system to visually monitor membrane fouling.
- Correlate the UTDR response with membrane performance and corroborate the results *via* morphological characterisation of the fouling layer.
- Model the ultrasonic reflections inside the cell.
- Investigate the possibility of using the technique on an industrial spiral-wound module.

1.2 Thesis structure

As a result of above mentioned features, this thesis is organised into ten chapters. Chapter 2 presents an overview of prior research in the field of membrane fouling, as well as all relevant background information on membrane desalination processes. It also provides a thorough overview on the ultrasonic technique. Chapter 3 explains the overall experimental approach for this research, as well as the experimental strategy that evolved for the development of UTDR in monitoring membrane fouling. In Chapter 4 a model of the reflections inside the flat sheet cell and its correlation with the actual cell dimensions is given, while Chapter 5 presents the

results as well as the interpretation of the results for the experimental studies undertaken with the flat sheet and spiral wrap module. Major conclusions are summarised in Chapter 6. Areas where more research is needed is discussed in Chapter 7, while Chapters 8 and 9 present the References and Appendix respectively. Chapter 10 is a glossary.

2 Historical and technical background

2.1 Visualisation techniques

Over the last ten years a number of non-invasive techniques have been used to study concentration polarisation and particle polarisation at the membrane surface. McDonogh et al. (1995) reported two non-invasive techniques for the study of concentration polarisation during filtration of bovine serum albumen (BSA) and dextran blue. A radio isotope technique was used to measure the adsorption of species in the polarised layer. Mackley and Sherman (1992) conducted an in-situ direct observation of particle deposition during filtration of sub-millimetre particles. Using a 15 x magnification video camera they were able to record the growth of cake and particle motions on the cake surface. Wakeman (1994) used a high-speed camera and a high magnification zoom lens to record the development of the cake layer at the centre axis of the membrane. Altman and Ripperger (1997) used a laser triangulometer in situ to measure the cake layer height under various filtration conditions.

These studies provided valuable information on polarisation profiles and cake thickness, but little information on the phenomenon occurring at the membrane-solution interface as particle deposit. Li et al. (1998) reported observations of particle deposition on membrane surfaces using in-situ, non-invasive continuous direct observation through a membrane (DOTM). The image observed by the microscope was recorded and viewed via a video camera attached to a super-VHS video recorder and monitor. The filtration tests were conducted in the imposed flux mode, so that the flux could be controlled at below, or above, the "critical flux." The "critical flux" is the flux rate (dependant on the crossflow velocity) which controls particle deposition on the membrane surface. Below the critical flux, particle deposition is negligible and above the critical flux, particle layers forms rather quickly on the membrane surface. The results demonstrated that DOTM is a powerful technique with which the fundamentals of particle deposition and the interaction between particles and the membrane can be studied.

Kools et al. (1998) had some success in employing ultrasound for real-time visualisation of thickness changes during the evaporative casting of polymeric films, while Peterson et al. (1998) employed ultrasound for real-time measurement of compressive strain during membrane compaction.

Mairal et al. (1999) described the first, and so far the only systematic attempt to adapt and employ ultrasonic-time-domain-reflectometry (UTDR) for the non-invasive measurement of membrane fouling in real-time. UTDR is a versatile measurement technique that is used in a wide variety of industrial, medical and military applications. The technique uses ultra sound waves to measure the location of a moving or stationary interface and can provide information on the physical characteristics of the media through which the waves travel. UTDR thus appears to be ideally suited for the real-time monitoring of membrane fouling, as well as other phenomena of interest such as membrane compaction. Although Mairal was not able to see or measure a fouling layer, his results showed a decline in the membrane signal amplitude (Figure 2-1), as a fouling layer started to develop and grow on the membrane.

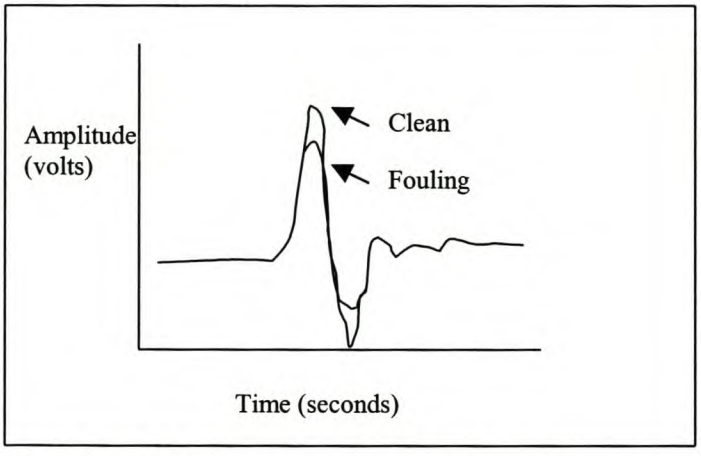

Figure 2-1 – Mairal's ultrasonic amplitude decline

Further research in this area was deemed most necessary. The present study was conducted in an effort to use UTDR for the improved visualisation of membrane fouling.

2.2 Cleaning ability of ultrasound

Although the scope of this research did not include the cleaning ability of ultrasound, (but the visualisation potential of ultrasound), the use of ultrasound cleaning was investigated. This was considered necessary in order to ensure that the visualisation technique was not responsible for cleaning.

Several patents deal with the application of ultrasound in water treatment. Hurvey (1965) used an acoustic liquid whistle or transducer to produce cavitation on the membranes. It is believed that the formation of air bubbles during cavitation suppresses fouling. When a cavitating air bubble is oscillating near a solid surface, it generates microjets of very high velocities that can effectively decrease the boundary layer thickness. In effect, mass transfer is enhanced.

Schimichi (1995) proposed the application of ultrasound in a purification process where water was passed through an ion-exchange resin bed. Li et al (1995) investigated the effect of ultrasound on the diffusion of electrolytes through a cellophane membrane. He found that the diffusion velocity of electrolyte through the membrane was faster when ultrasound was applied.

Band (1997) studied the influence of specially mounted ultrasound signals on water desalination through special polymeric ion-exchange hollow fibres. Both Na^+ and H^+ ion exchange were enhanced under ultrasound.

Chai et al (1999) used ultrasound to clean polymeric UF and MF membranes that were fouled with peptone. Ultrasound with a frequency of 45 kHz and an output power of 27.3 kW/m^2 was used.

In all these studies, ultrasound with low frequencies (kHz) and high power outputs were used. Frequencies in the order of 40 – 50 kHz showed the best cleaning abilities. In contrast with this, the visualisation technique needs good spatial resolution, and thus a shorter wavelength is required. Ultrasound with higher frequencies (more than 1 MHz) is therefore needed. At this high frequency it has no cleaning ability (ultrasound of frequency 5 – 7.5 MHz is used for visualisation in the

human body) and is therefore suitable to study concentration polarisation and fouling.

2.3 Osmosis

The term "osmosis" is generally used to describe the spontaneous flow of pure water into an aqueous solution, or from a less to a more concentrated aqueous solution, when separated by a semi-permeable membrane. The reason for this behaviour is that a concentration gradient exists between the two solutions, and the flow is in the direction of lower chemical potential in order to establish equilibrium. Under isothermal conditions, in both 'osmosis' and 'reverse osmosis', the preferential transport of material through the membrane is always in the direction of lower chemical potential.

In order to obtain potable water from saline or brackish water in a similar process, the direction of flow of the pure water must be reversed; i.e. pure water must flow from a more to a less concentrated solution. This is done by applying pressure on the concentrated solution, by which pure water is forced through the membrane to the less concentrated solution, i.e. reverse osmosis.

2.4 Membrane processes

The different types of membrane processes are:

2.4.1 Microfiltration (MF)

Microfiltration is a pressure-driven process that dynamically separates micron-size or sub-micron particles from a liquid or gaseous feed stream by a membrane. Thus, MF typically operates at low transmembrane pressures to minimise build-up of the suspended solids at the membrane surface. Pressures of 0.3-3.3 bar (5-50 psi) and cross-flow velocities of up to 3-6 m/s in tubular modules are common. On an industrial scale, MF is usually implemented as a multistage (stages-in-series) operation in a feed-and-bleed mode of operation. MF is the "loosest" of the membrane processes with a pore size ranging from 0.05 to 5 μm and can be operated under ultra-low-pressure conditions. As a consequence of its large pore size, it is

used primarily for particle and microbial removal. It separates macro-materials and suspended solids like starch, bacteria, moulds, yeast and emulsified oils.

2.4.2 Ultrafiltration (UF)

UF is a low-pressure fractionation of selected components by size. Ultrafiltration separates dissolved solutes of 0.005 to 0.1 microns. This corresponds to a molecular weight cut-off of about 1,000 to 500,000. Depending on the molecular weight cut-off selected, the membrane will concentrate high molecular weight species while allowing dissolved salts and lower molecular weight materials to pass through the membrane. UF membranes are used in numerous industries for concentration and clarification of large process streams.

2.4.3 Nanofiltration (NF)

The NF membrane displays excellent rejection of divalent ions while allowing a majority of monovalent ions to pass. Organic molecules in the 200-300 molecular weight range are also highly rejected. The unique separation capability of NF provides the opportunity to selectively concentrate either valuable or undesirable substance from a process stream with greater effectiveness, consistency, reliability and economy.

Nanofiltration (NF) is a membrane technology on the rise because it is more cost effective than reverse osmosis (RO) membranes in certain applications. In most water sources, there will be single-charged ions such as sodium ions (Na^{+}) and chloride ions (Cl^{-}) and double charged ions such as calcium ions (Ca^{+2}) and sulphate ions (SO_4^{-2}). The single-charged, positive ions do not generally participate in scale formation, so they may be considered soft ions. The double-charged positive ions such as calcium and magnesium, in conjunction with certain negatively charged ions can form hard scales within water treatment equipment and piping and are called hardness ions. Depending upon the membrane, water chemistry, and operating conditions, NF membranes can remove more than 90% of feed water's hardness ions. NF membranes also remove large colour molecules and many of the trihalomethane (THM) precursors. Nanofiltration can treat the same amount of water, or more, at half the pressure. Since NF membranes can remove the double-charged scaling ions like calcium and magnesium ions, another term for NF is

membrane softening. The largest users of the NF technology are municipal drinking water plants. A future trend is for NF to replace lime softening to achieve an industry standard of 50 parts per million (ppm) of alkalinity plus meet the federal THM limits. NF is well established in the dairy industry for cheese-whey desalting. Other growing markets are in RO pre-treatment; pharmaceutical concentration; kidney dialysis units; and maple sugar concentration.

2.4.4 Reverse Osmosis (RO)

RO is the most complex technique in membrane separation. RO membranes concentrate low molecular weight organic materials and salts while allowing water and solvents to pass. High pressures of about 35-100 atmospheres are required in order to overcome the high osmotic pressures across the membrane. This permits water to flow from the concentrated feed stream to the dilute permeate - a direction that is just the reverse of what would occur naturally during osmosis. RO has been the most widely used technology for desalinating seawater and reclaiming brackish well water. The reverse osmosis membranes rejects organic molecules such as sugar related entirely to the size and shape of the organic molecules. An RO membrane typically will reject all of the organic molecules over 150 molecular weight and a percentage of those between 25 and 150 MW. It is generally used for the production of very high purity water used in boilers, microelectronics processing and pharmaceutical formulation.

2.4.5 Electrodialysis

Electrical energy supplies the driving force in eletrodialysis (ED) for ion-migration through the membranes. Electrolytes are usually transferred from a less concentrated solution through the ion-exchange membranes to a more concentrated solution with the aid of electrical current. If membranes are more permeable to cations than to anions or vice versa, the concentration of ionic solutions increases or decreases, so that concentration or depletion of electrolyte solutions is possible. Since in electrodialysis only ionic species are transferred directly, removal of ionic species from non-ionic products can be accomplished, so that purification is possible. Electrodialysis reversal (EDR) is an electrodialysis process in which the polarity of the electrodes is reversed on a prescribed time cycle, thus reversing the direction of ion movement in a membrane stack.

2.4.6 Pervaporation

Pervaporation (PV) is the separation of liquid mixtures by partial vaporisation through a permselective membrane. Unlike the other membrane processes, a phase change occurs when the permeate changes from liquid to vapour during its transport through the membrane. PV in fact is an enrichment technique similar to distillation. The heart of the PV is a non-porous membrane, which either exhibits a high permeation rate for water but does not permeate organics, or vice versa, permeates organics but does not permeate water. A gradient in the chemical potential of the substances on the feed side and the permeate side is the driving force for the process. The driving force is kept at a maximum by applying low pressure to the permeate side of the membrane, combined with immediate condensation of permeated vapours.

The following table summarises the various membrane treatment processes, their application(s), as well as comparable traditional treatment methods:

Membrane separation technology	Substances removed	Comparable traditional water treatment methods
Microfiltration	Bacteria and larger colloids; separation of precipitates and coagulates	Ozonation-ultraviolet radiation, chlorination, sand filters, bioreactors and coagulation-settling tanks
Ultrafiltration	All of the above, plus viruses, high-molecular weight proteins, organics and pyrogen	Sand filters, bioreactors and activated carbon
Nanofiltration	All of the above, plus divalent ions, larger monovalent ions, colour and odour	Lime-soda softening and ion exchange
Reverse osmosis	All of the above, plus monovalent ions	Distillation, evaporation, ion exchange, ED, EDR
Electrodialyses (ED) and Electrodialyses reversal (EDR)	Dissolved ionic salts	Ion exchange, Reverse osmosis

2.5 Scaling and/or fouling

2.5.1 Scaling of boilers

The formation of hard lime scale on the container walls of boiler and pipe systems is a consequence of the scarcity of nucleation centres in ordinary water. When the concentration of $CaCO_3$ exceeds solubility, solidification can begin only at appropriate starting points, mostly at foreign matter. If no foreign matter is present in the form of particles in the liquid, solidification can start only at the walls of the container. Ordinary water tends to surround any foreign particulate with complexes of 100-200 water molecules each. The water molecules agglomerate around every foreign particle in ordinary water. They form cages around them, which makes them ineffective as nuclei. The container walls are then the only non-water substances available where crystal growth can start. The crystals form a few starting points attached firmly to the wall and extended systems of crystals cling to one another and to the wall around the starting point. The dendritic crystallisation mode is the initiation of the formation of hard lime scale, which, if further solidification of the mineral occurs, grows layer-over-layer on the first set of dendrites.

2.5.2 Reverse Osmosis fouling

Membrane fouling is a major problem in brackish and seawater desalination and in wastewater reclamation by the process of reverse osmosis. The most common Reverse Osmosis foulants encountered are the following (Faller, 1999):

1. suspended solids
2. colloids
3. metal oxides
4. scales (i.e. $CaCO_3$, $CaSO_4$, $Mg(OH)_2$, $BaSO_4$, $SrSO_4$, CaF_2 , SiO_2)
5. biological slime
6. organics
7. oil and grease

The formation of one or more of these types of foulants on the surface of a membrane is inherently a function of the nature of the feedwater to the membrane and the nature and degree of pre-treatment applied to the RO system. Other factors include membrane material, permeator configuration, and the efficiency of operation as well as quality control. In seawater desalination by RO, the first five types of foulants are most likely to occur, with calcium carbonate as the most dominant scalant. In brackish water desalination, calcium sulphate scaling is widely encountered due to the high content of sulphate ions in well waters. Biological fouling (micro-organisms) and organic fouling are the most dominant types of fouling in industrial and wastewater reclamation by RO.

The scaling behaviour exhibited by $CaCO_3$ is further complicated by pressure induced changes in crystal habit. Research has shown (Kronenberg, 1998) that $CaCO_3$ deposits in RO modules as aragonite and vaterite, which are unstable at ambient temperatures and pressure. Aragonite is a meta-stable crystalline form of $CaCO_3$. It transforms into the more stable calcite, with a half-life of about 24 hours. When the pH exceeds 9, the crystalline transformation occurs more rapidly and may be completed within one hour.

Supersaturation is the main driving force for scale formation and this can be considerably augmented by the superimposed effect of concentration polarisation. Other factors, such as temperature, pH, or feedwater composition deviations, can also induce precipitation at the membrane surface. Under these fluctuating conditions, the efficiency of the pre-treatment system can often be undermined, and ineffective performance or operation shutdowns can often induce scaling in a relatively short time-span.

2.5.3 Concentration polarisation and fouling

Concentration polarisation may be defined as the presence of a higher concentration of a rejected species (e.g. NaCl) at the surface of a membrane than in the bulk solution, due to convective transport of both solute and solvent. RO membranes achieve a net rejection of solute because the flux of solvent (e.g. water) through the membrane is much higher than the flux of rejected solute. At steady state, it is assumed that solute does not accumulate on the membrane, so that solute transport by diffusion away from the membrane surface must occur simultaneously, with convective diffusion towards the membrane. For this reverse diffusion to occur, a negative concentration gradient must exist, with a higher solute concentration at the surface than in the bulk.

Negative aspects associated with concentration polarisation are:

1. An increase in chemical potential at the surface reduces the driving force for the separation.
2. If the wall concentration of solute reaches the saturation concentration, precipitation of a gel on the membrane surface increases the hydrostatic resistance.
3. High concentration of solute at the membrane interface increases the risks for changes in composition of the membrane material due to chemical attack.
4. The deposition of solute on the surface can change the separation characteristics of the membrane.

As a consequence of all these negative factors, the transmembrane fluxes in commercial desalination plants are only 2-10% of the transmembrane fluxes for pure water. Therefore it is of the utmost importance to reduce concentration polarisation. However, it is not always possible to explain the flux behaviour as a consequence of concentration polarisation only. Fouling also occurs.

Fouling is an accumulation of material on the surface of the membrane and in the membrane pores that decreases the permeate flux. In some cases fouling is an irreversible adsorption of macromolecules while gel formation caused by concentration polarisation in its true sense is reversible lacking forces between the macromolecules in the gel. If the gel is strongly attached to the membrane surface, the membranes become very hard to alter even by washing procedures.

According to DuPont (1982), cleaning of RO membranes is recommended in any of the following cases:

- When there is a significant increase of permeate conductivity under constant feed water parameters.
- When, at a constant feed water temperature, the delivery pressure of the high-pressure pumps must be increased by more than 8-10% to retain the rated permeate flow rate.
- When, at a constant flow volume and temperature, the differential pressure between inlet and outlet of the RO system rises between 25 and 50%.

However, flux decline as well as pressure increases are not necessarily sensitive to fouling initiation. Any way of tracking or monitoring fouling at an early stage of development would be of valuable interest. This is where the information using UTDR could be helpful.

2.6 Prediction of fouling

For the design of RO facilities, it would be desirable to have an analytical procedure available to predict quantitatively how rapidly or severely a given feed will foul a membrane. The Silt Density Index, (Potts et al., 1980) is the only widely accepted test for fouling prediction in the RO industry, although two other models are also available i.e. the Modified fouling Index (Schippers et al., 1980) and the Langelier Saturation Index. (Du Pont, 1977)

The Silt Density Index test is performed in the following manner:

RO feed is pumped through a 0.45μm cellulose acetate Millipore filter at a constant pressure. The time required to collect the first 500-ml of filtrate is noted and recorded as t_i. Fifteen minutes after the start of the test, another 500 ml is collected and the time is recorded as t_f. The plugging factor (%P) is computed as follows:

Eq. 1.....$\%P = 100(1- t_i / t_f)$

The silt density index is computed by dividing %P by the time of the test, i.e., 15-min in this case. Shippers applied a filtration theory to the SDI test and derived a formula for a modified fouling index (MFI). With the SDI no linear relationship exists between the index and the colloid or suspended matter concentration, while the MFI is directly proportional to colloidal concentration. The relation has the form:

Eq. 2.....$MFI = (\eta 20/ \eta)(\Delta P/210)\tan\alpha$

where $\eta 20$ = viscosity at 20 °C

η = viscosity at water temperature

ΔP = applied pressure in kPa

$\tan\alpha$ = slope of the straight line portion of a plot of reciprocal volumetric flowrate (t/V_{tot}) vs. accumulated volume of filtrate

Mathematical models of fouling are found in the literature, but are very complex and tedious. The following models are available:

1. Model by Kimura and Nakao (1975)
2. Model by Carter and Hoyland (1976)
3. Model by Gutman (1977)
4. Model by Belfort and Marx (1979)
5. Model by Hiddink et al (1980)

2.7 Technology dealing with fouling

Techniques used to reduce fouling include turbulence promotion, periodic depressurisation of membrane tubes, flow reversal, pre-coating of membrane surfaces, enzyme immobilisation, flushing and modification of membrane polymeric structure. Mechanical and ultrasonic vibration of membranes has been tried, but with little success. (Belfort, 1977)

Due to the increasing pumping costs at high flowrates, current research (Baker et al., 1997) is directed towards turbulence promotion at lower flowrates. These methods (Jagannadh, 1996) often involve the use of secondary flow or vortices produced by placing inserts in the flow channel. These inserts may be shaped, have a rough surface and/or rotate in order to promote cyclic flow. Although these methods seem promising, they can only be applied to flat or tubular membranes and with high costs. Some technology has proven commercially feasible and highly successful with tubular membranes. It uses sponge balls to scrape away the fouling layer on the membrane.

2.7.1 Interaction of dispersed phase

The presence of a dispersed phase seems to have an effect in controlling the size of eddy formation and the rate of energy dissipation in the fluid medium. The dispersed phase acts simply as a turbulence promoter. Studies by Parvatiyar (1996) showed that the mass transfer coefficient decreases with an increase in eddy size at a given void fraction. Furthermore, smaller eddies seem to be the most effective in enhancing the mass transfer coefficient. It was also observed that eddy size decreases with an increase in the Reynolds number.

Conclusions drawn from these studies are the following:

1. Smaller eddies and high-energy dissipation rates per unit mass of the fluid are favourable conditions for the increase of the mass transfer coefficient.
2. High void fraction and large particle diameter induce the growth of large eddies.

3. The ratio of the membrane tube diameter to the particle diameter is the most significant parameter in affecting the mass transfer coefficients and the concentration polarisation.
4. Concentration polarisation in a membrane tube can be controlled by placing inert solid particles as a suspension or dispersed phase in a module.

2.7.2 Application of external fields (electric, magnetic, ultrasonic)

The first known patent on this subject was issued to France and Cabell in 1890 (France, 1890). Although the method has been used worldwide since the pioneering work of Vermeiren, a Belgian engineer who founded the EURO company in the early 1940's (Vermeiren, 1953), commercial units using magnets to treat water were only introduced in the early 1950's. A South African company (Cooray, 1998), applied magnetic fields to membrane processes and they seem to be very successful. They have recently patented their technique.

Subsequent studies (mostly conducted for prevention of protein fouling of microfilters) have suggested the rate of fouling is dependent upon electric field strength and frequency, colloidal concentration, particle size and shape, and its surface properties. For maximum effect the electrodes need to be as close as possible to the membrane, but not so as to impede the flow. A recent review of the use of DC electric fields (Jagannadh, 1996) suggests the most probable antifouling mechanisms as electrophoresis (i.e. the particles are driven away from the membrane) and electroosmosis (i.e. effects occurring on interstitial water at the membrane/water interface.) Current research in this area is directed towards development of corrosion resistant anodes and to their optimum placement in commercial modules. The ultimate development would be a membrane material that could also act as an electrode. This has been researched by Tony Fane et al. (Fane, 2000)

Membrane permeability to both charged and uncharged solutes have also been changed under the influence of an applied electric field. This behaviour, exhibited for 'deformable' membranes has been attributed to electric field control of membrane pore size. Grodzinsky and Weiss (1985) favour the mechanism of

'electrodiffusion' in which the intramembrane pH or ionic strength is modified. The result is an increase in repulsive forces between structural elements of the membrane, which are balanced by their mechanical strength. These effects, which have been found to be fully reversible, have implications for use in controlled delivery systems. Blokhra (1994) have found similar results when a strong magnetic field is applied perpendicular to the direction of flow across a cellulose acetate membrane. One could argue for a similar mechanism since an electric field will also be generated in this case.

The use of magnetic pre-treatment to prevent crystalline scale formation has only been done by Lin and Nadiv (1988). In this case a commercially available magnetic treatment device was used on the high pressure feed line to the reverse osmosis cell in a fully recycled system using hard tap water at a pH of 10.5.

Chai et al (1999) had some success in removing peptone fouling from ultrafiltration and microfiltration membranes by using ultrasound. The ultrasound used had a frequency of 45 kHz and an output power of 27.3 kW/m^2.

2.8 The working of ultrasonics

Vibrational waves of a frequency above the hearing range of the normal human ear are referred to as ultrasonic, and the term therefore includes all those waves of a frequency of more than about 20 000 cycles. Frequencies of 20 000 to 100 000 cycles are used for sound ranging, submarine signalling and communication. Those of 100 000 to 10 000 000 cycles are used in testing materials for flaws etc.

The quartz crystal has the property of expanding and sending out an ultrasonic wave when a voltage, generated by a pulsar-receiver, is applied to it. It can also produce an electrical signal when it is mechanically vibrated. The transducer sends out this high frequency signal into the medium which needs to be investigated.

Any material that has elasticity can propagate ultrasonic waves. The propagation takes the form of a displacement of successive elements of the medium. If the substance is elastic, there is a restoring force that tends to bring each element of material back to its original position. Since all such media also posses inertia, the particle continues to move after it returns to the position from which it started and finally reaches another different position, past the original one. From this second point it returns to its starting position, about which it continues to oscillate with constantly diminishing amplitude. The elements of material will therefore execute different movements or orbits as the waves pass through them. It is the differences in these movements that characterise basic types of ultrasonic waves; but no matter what the wave type, the general properties of ultrasonics remain.

As the wave travels through the material, successive elements in it experience these displacements, each such element in the wave path moving a little later than its neighbour. In other words, the phase of the wave or vibration changes along the path of wave transmission. This displacement can be plotted, and the graph is descriptive of the wave.

2.8.1 Types of waves

An ultrasonic wave being transmitted through a substance may be of several types. Each type causes a specific movement in the elements of the medium and the paths that these elements follow as they move in response to the wave are called their orbits. These orbits may be essentially parallel to the line of propagation, in which case the wave is *longitudinal.* On the other hand, they may be executed normal to the direction of propagation. Such waves are called *transverse* or *shear.*

2.8.1.1 Longitudinal waves

Longitudinal waves exist when the motion of particles in a medium is parallel to the direction of wave propagation. This kind of wave, also called the L wave, will travel in liquids, solids and some gases and is easily generated and detected. L waves have a high velocity of travel in most media, and the wavelengths in common materials are usually very short in comparison with the cross-sectional area of the transducer. This property allows the energy to be focused into a sharp beam from which it diverges only slightly. If the energy is to remain in a beam, the frequency (and therefore the wavelength) must be the proper ratio to the area of the surface that is being vibrated. In order to make use of these oscillations, since they travel with very great velocities, and since their frequencies are generally high; the systems that are used with them must be capable of responding to such frequencies and of resolving signals following each other closely in time.

2.8.1.2 Shear waves

When shear waves, also called an S wave, are used, the movement of the particles in the medium is at right angles to the direction of wave propagation. If the wave movement is in the x-direction, the particle displacement is in the y-direction. These waves may also exist in a limited area of, or entirely throughout a body. Usually, however, they are in the form of a beam of small cross section in comparison with the cross-sectional area of the piece in which they travel. The beam does not ordinarily extend to a surface parallel to the direction of travel. Shear waves have a velocity that is approximately one-half of that of L waves. Due to this lower velocity, the wavelength of shear waves is much shorter that that of L waves.

Shear waves have certain advantages, because their lower velocity makes the electronic timing circuits with which they are used less critical. However, the shorter wavelength makes them more sensitive to small inclusions, and they are therefore more easily scattered within a material. Moreover, since the vibration is in a specific direction, rotation of the transmitting element changes this direction, and therefore polarisation effects may be noticed. In other words, the results in a material that is not absolutely uniform may differ with rotation of the transducer. Shear waves will not travel in liquids and gases, since there is no elasticity to shear in such materials

2.8.1.3 Surface or Rayleigh Waves

These waves can be propagated over the surface of a part without penetrating below that surface to any extent. These waves are roughly analogous to water waves which travel over a body of water. Their velocity depends upon the material itself and is about nine-tenths of S-wave velocity. The wavelength of a surface wave is always extremely short, and the plate on which it travels is at least several wavelengths thick. Under such conditions the displacement of particles a few wavelengths below the surface is negligible. Surface waves consist of both L and S types of particle motion. These types of waves can be used for exploration of materials for defects, for measuring thickness by resonance, or for measuring other characteristics of the material on which the wave travels.

2.8.2 Reflection of waves

The ultrasonic signal is reflected by a change in acoustic impedance, which happens when it reaches a layer with different acoustic impedance than the medium it is travelling through. When this happens, part of the energy travels forward as one wave through the second medium, while the rest of the signal is reflected back into the first medium, usually with a phase change. These reflections can be seen on an oscilloscope for interpretation. Consider such an example where a plane acoustic wave is transmitted from one medium to another as in Figure 2-2. (Ford, 1970)

Figure 2-2 – Reflection and transmission of plane waves at a boundary.

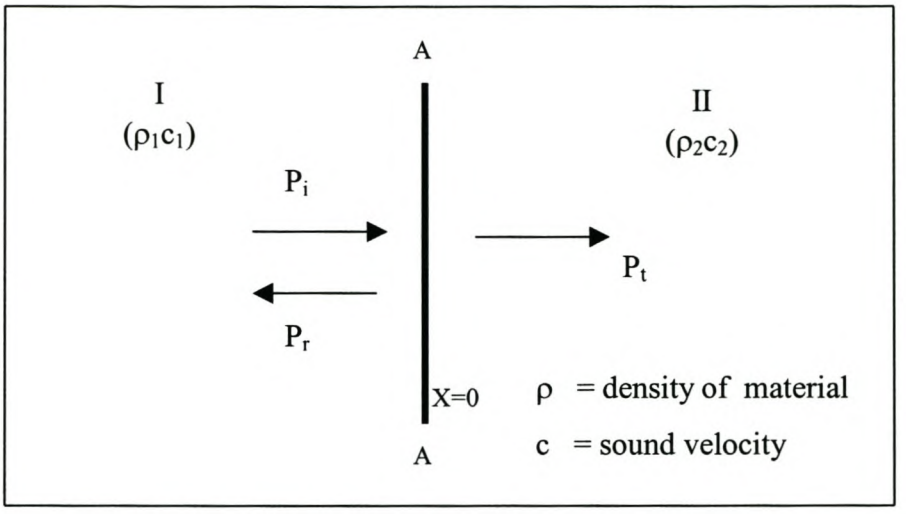

Let AA denote the plane of the boundary between medium I, of characteristic impedance $\rho_1 c_1$, and medium II, of characteristic impedance $\rho_2 c_2$, and consider a plane wave in medium I travelling in the positive x direction at right angles to the plane of the boundary.

This incident wave can be represented by

Eq. 3..... $P_I = A_1 e^{j(wt-k1x)}$

where

w = $2\pi f$ with f in rad/s

t = time

k = wavelength constants

x = distance

A_1 is a complex constant representing the complex pressure amplitude P_+. Upon striking the plane of the boundary between the two media at x=0, a reflected wave

Eq. 4..... $P_r = B_1 e^{j(wt+k1x)}$

and a transmitted wave

Eq. 5..... $P_t = A_2 e^{j(wt+k2x)}$

are produced. The transmitted wave always has the same frequency as the incident wave, but as a result of the difference between the velocities c_1 and c_2 in the two media, the values of the wavelength constants, $k_1=w/c_1$ in medium I, and $k_2=w/c_2$ in medium II, are different.

There are two boundary conditions that must be satisfied at all times and at all points on the plane surface separating the two media:

1. The acoustic pressures on the two sides of the boundary are equal and
2. The particle velocities normal to the interface are equal.

The first condition of continuity of pressure results from the fundamental law that pressure in a fluid is a continuous, single-valued, scalar function, and the second condition is equivalent to the requirement that the two media remain in constant contact at the boundary. Since pressure is a scalar quantity, the pressure at a point in medium I is given by $P_i + P_r$. By setting this expression equal to P_t at the boundary, one obtains.

Eq. 6.....$A_1 e^{j(wt-k1x)} + B_1 e^{j(wt+k1x)} = A_2 e^{j(wt+k2x)}$

so that

Eq. 7.....$A_1 + B_1 = A_2$

The particle velocities u_i, u_r and u_t can be represented by

Eq. 8.....$u_I = P_i/\rho_1 c_1$

Eq. 9.....$u_r = P_r/-\rho_1 c_1$

Eq. 10.....$u_t = P_t/\rho_2 c_2$

The velocity of a particle in medium I is $u_i + u_r$, which makes the second boundary condition

Eq. 11..... $u_i + u_r = u_t$

Substituting Eq. 8, Eq. 9 and Eq. 10 into Eq. 11 gives

Eq. 12.....$P_i/\rho_1 c_1 - P_r/\rho_1 c_1 = P_t/\rho_2 c_2$

By introducing the respective expressions for the pressure at x=0, this equation can be reduced to

Eq. 13.....$\rho_2 c_2(A_1 - B_1) = \rho_1 c_1$

Further, Eq. 7 and Eq. 13 can be combined to eliminate A_2, which gives

Eq. 14.....$B_1 = A_1[(\rho_2 c_2-\rho_1 c_1)/(\rho_2 c_2+\rho_1 c_1)]$

The amplitude of the reflected wave is thus related to the incident one as

Eq. 15.....$B_1/A_1 = [(\rho_2 c_2-\rho_1 c_1)/(\rho_2 c_2+\rho_1 c_1)]$

In the case of an air-solid boundary practically 100 per cent of the energy is reflected. It should be remembered that in a reflection system, the energy passes through an interface twice, once going and once returning. All these calculations are entirely independent of attenuation and scattering. The amount of energy actually reflected may differ vastly from that calculated theoretically. Energy may be dissipated at a boundary or in a material in several ways. The formulas given refer only to an absolutely perfect boundary between two infinite media. If there is any discontinuity, no matter how minute, these relationships no longer apply. It is accordingly difficult to get actual values of reflected energy except by experiment.

2.8.3 Transformation of waves

When a wave of any kind strikes a boundary between two media of different acoustic impedances at an angle other than 90 deg, a transformation may take place and the wave may be changed into another type. An example would be an L wave passing from a liquid to a solid and hitting the solid at an angle. At the boundary

between the liquid and the solid, reflected L and S waves and transmitted L and S waves may form with different amplitudes and different angles of travel, depending on the angle at which the wave hits and also on the impedance's of the materials. Since S waves will not travel in liquid, only the reflected L wave and the transmitted L and S waves remain. Thus, under certain appropriate conditions the type of wave may be changed. Changes such as these can be very misleading to an investigator who does not take into account all the type of waves that may appear at such a boundary. It should also be noted that in the case of liquids incident on solids, the results would be misleading unless the liquid wets the solid. Wetting agents may be included to assist in obtaining intimate contact.

The case of liquids incident upon solids is of practical interest in studying earthquakes and in the design of transducers where a volume of liquid is imprisoned between the transducer and the medium. It is also of concern in testing objects that are inspected in a liquid bath.

Waves travelling in a metal or solid part supported in air exhibit the same tendency, and a number of misleading signals will be observed, which are caused by the originally generated wave hitting a boundary at an angle. This results in the generation of different types of waves, which, in turn, again hit a boundary and repeat the phenomena. In this a large number of extraneous signals may be generated, each travelling at its own velocity and in a different direction. When observed, the resulting signal is so confused that it is impossible to interpret.

2.8.4 Beams

A beam of ultrasonics is propagated through a material with very little divergence. Although such a beam can be considered to be confined to the projection of the face of the transducer, in reality there is always some spreading. This spread is a function of the ratio y/D where y is the wavelength of the ultrasonic wave and D is the distance across the transducer interface. In an ordinary quartz plate the energy is located in a cone whose angle of spread is given by:

Eq. 16……..……sin A = 1.2(y/D)

This formula will not give exact experimental results, because the way in which the crystal is mounted affects its beaming characteristics. For example, edge effects may produce secondary beams. These secondary rays are not determined by the relation above but have greater angles of spread. However, in practical work the basic beam is the only one of consequence.

When ultrasonic waves hit the face of a material in which they are to be propagated, only the main beam will be transmitted through the interface and actually enter the medium, since the transmitted energy depends on the angle at which the waves hit. There is such great refraction in the ordinary case of an oil-to-metal surface that any beam diverging at more than a comparative small angle is totally refracted. This angle is about 15 deg from the normal and is determined in the usual way by the ratio of the velocities of the ultrasonics in the two media, the one from which the waves are transmitted and the one that they enter. The beam may be scattered in other ways than by its normal divergence. For example, if the medium in which it travels is full of small dispersed discontinuities or is of very large grain size, the ultrasonic energy will be broken up and reflected and refracted in a haphazard manner. This may occur even between neighbouring crystals of different elastic properties. In this way the energy may be diffused by continuous reflection.

This difficulty can be minimised by lowering the frequency of transmission, thus initially widening the beam. However, because of the now longer wavelength, the energy will not be affected by the small discontinuities but will pass through them without reflection. In other words, with a given transducer size, the beam spread becomes greater as the frequency goes down but the internal scattering becomes less. Thus the higher frequency transducer you are using, the better resolution you will have, but your penetration depth decreases.

2.9 *Ultrasonic equipment*

2.9.1 Ultrasonic set-up

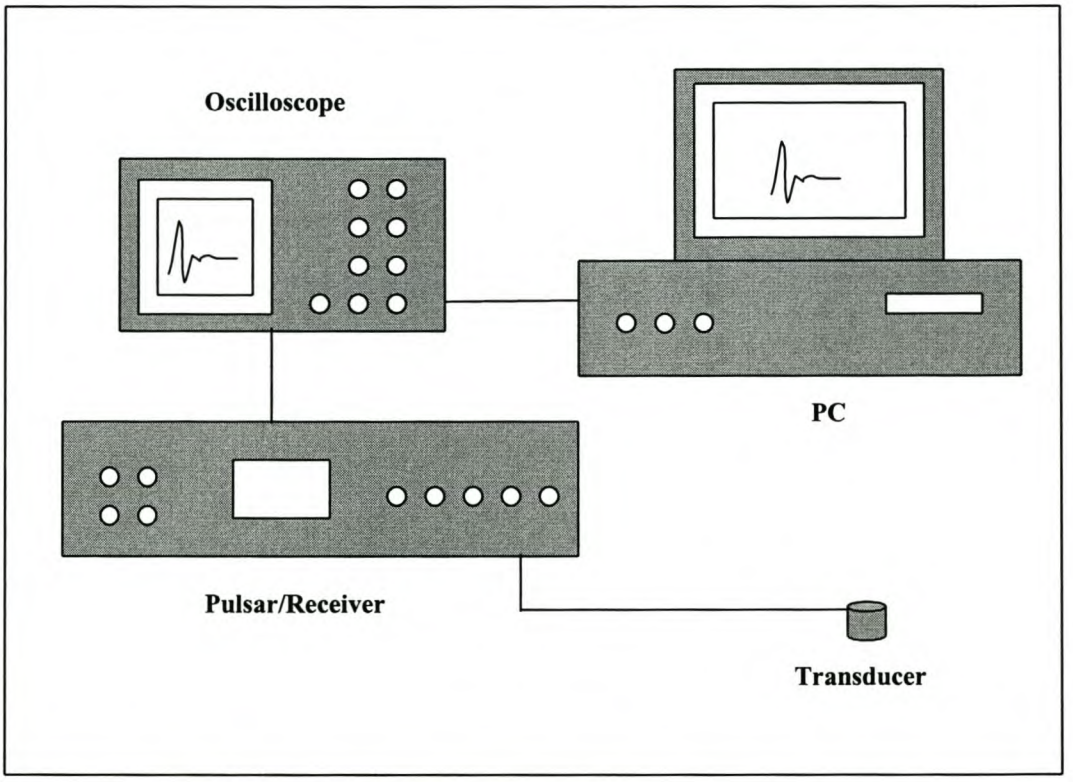

Figure 2-3 – Ultrasonic set-up for UTDR pulse-echo operation

Figure 2-3 is a simplified drawing of all the hardware in the ultrasonic set-up. A Pulsar/Receiver generates the Voltage signal that triggers the transducer to send out an ultrasonic wave. The oscilloscope that is connected to the Pulsar/Receiver captures and displays the data as amplitude changes on its front panel. These data can be stored on a computer's hard drive.

2.9.2 Pulsar/Receiver

A Panametrics Model 5058PR High Voltage Pulsar-Receiver was used. It is designed especially for ultrasonic test and measurement applications that require a high material penetration capability. The pulsar section of the Model 5058PR can

deliver up to 900 volts in an impulse-type excitation pulse to appropriate low frequency transducers. The receiver section provides 60dB RF gain, with an additional 30dB available from an integral auxiliary preamplifier. A full range of front panel controls permits either discrete, calibrated settings or continuous adjustments for all important instrument functions. Pulse voltage is continuously adjustable in four values from 100 to 900 volts with a front panel meter displaying the available voltage to the transducer. Receiver gain is selectable as 40 or 60 dB, while receiver attenuation is adjustable from 0 to 80dB in 1dB steps with a ±1dB vernier for precise setting. The Model 5058PR includes an internal preamplifier that can be used to create an additional 30dB gain. Echo pulses can be selected as either normal or inverted 180° for peak detection applications.

The 5058PR can be internally triggered at any of seven PRF rates from 20Hz to 2KHz, or externally triggered at any frequency up to 2KHz. Pulse damping is continuously adjustable over a range of 50 to 333 ohms, or in stepped values of 50, 100, 200, or 500 ohms. All transducer and RF output connectors are front panel mounted for easy access.

FEATURES

- High voltage pulsar, switched settings or continuously adjustable to 900 volts
- High gain, low noise broadband (10MHz) receiver
- Pulse-echo and through transmission modes
- High isolation (80dB) in through transmission mode
- 60dB RF Gain
- Additional 30dB gain available from integral auxiliary preamplifier
- Receiver attenuation range of 0 to 80dB in 1dB steps
- ±1dB vernier for fine adjustment
- Switchable high pass and low pass filters
- PRF rate switch selectable from 20Hz to 2KHz
- Controls permit either discrete, calibrated settings or continuous adjustment
- Compatible with Panametrics Stepless Gates, Gated Peak Detectors, and Gated Threshold Alarms

2.9.3 Oscilloscope

The choice of the correct oscilloscope is very important, as real-time signal changes are displayed on it. The oscilloscope should have a digitising capability for real-time processing and display of the ultrasonic signals as well as appropriate time-domain resolution and sensitivity for accurate measurement of fouling layer growth. A Hewlett Packard oscilloscope with the following characteristics was used.

Hewlett Packard Oscilloscope Model 54602B

- 150 MHz bandwidth
- 2+2 Input channels
- Sweep speeds from 5s/div to 2 ns/div
- Up to 1.5 million points per sec screen update rate
- I/O function
- 1 mV/div sensitivity

HP 54602B (2+2) Channel 150 MHz Oscilloscope

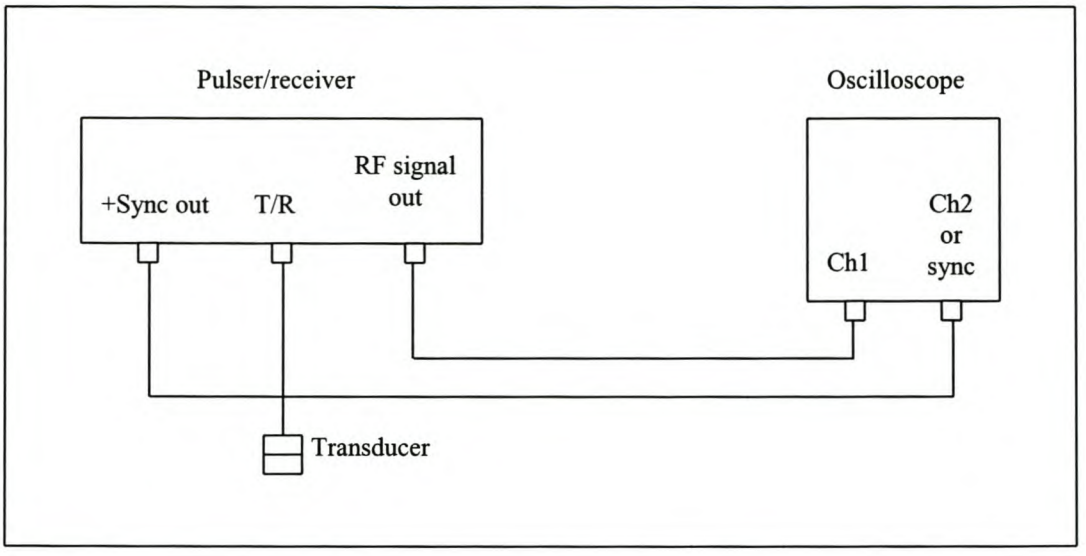

Figure 2-4 - Pulsar/receiver-oscilloscope set-up for pulse-echo operation

2.9.4 Transducers

The transducer is one of the most critical components of any ultrasonic test system. As a result a good deal of attention should be paid to selecting the proper transducer for the application. Of equal importance is the performance of the system as a whole. Variation in instrument characteristics and settings as well as material properties and coupling conditions play a major role in system performance.

Most often the transducer is chosen to enhance either the sensitivity or the resolution of the system. A system with good sensitivity has the ability to detect small variations at a given depth in the test material. A system with good resolution has the ability to produce simultaneous and distinct indications from reflectors lying at nearly the same depth and position with respect to the sound beam. In applications where good resolution is of primary importance it is common to select a highly dampened transducer. A high degree of damping will help to shorten interface ringdown or recovery time and allows the system to resolve closely positioned reflectors.

The specific transducer configuration also has an impact on system performance. Consideration should be given to the use of focused transducers, transducers with wear surfaces that are appropriate to the test material, and the choice of the appropriate frequency and element diameter.

In this study Panametrics Videoscan transducers were used. Videoscan transducers are untuned transducers, which provide heavily damped broadband performance. They are the best choice in many applications where good axial or distance resolution is necessary or in tests that require improved signal-to-noise in attenuating or scattering materials.

2.9.5 Theoretical resolution:

The theoretical resolution of a specific frequency transducer can be calculated if the speed of the sound wave in the media that is under investigation is known. The wavelength can be calculated with Eq. 17 where

Eq. 17.....$\psi = c/f$

with ψ = wavelength
c = speed of soundwave
f = frequency

The smallest detail that the transducer would pick up is that which is 0.25 of the soundwave's wavelength, (explained in Figure 2-5), The theoretical resolution can thus be calculated with Eq. 18 where

Eq. 18.....Resolution = 0.25ψ

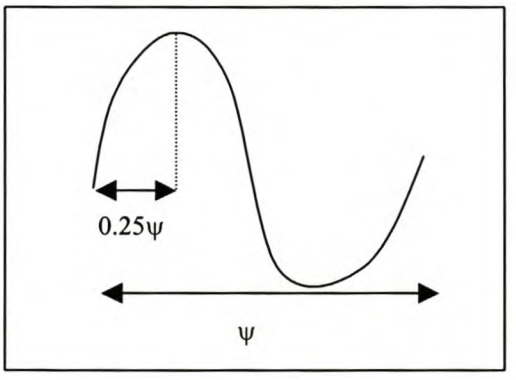

Figure 2-5 –Typical sound wave

The possible theoretical resolution (in water) of the range of transducers that were used during this study is:

Transducer type	Frequency MHz	Resolution µm
V106-RB	2.25	159
V182-RB	3.5	102
V109-RB	5	72
V120-RB	7.5	48
V111-RB	10	36

3 Experimental

3.1 Desalination system

The selection of an appropriate membrane separation system involves the choice of a separation process, a feed solution containing one or more potential foulants, a membrane, a separation module, and an associated flow system. The separation process should further be adaptable to laboratory scale, but still be industrially relevant while affected by fouling during operation. The feed solution chemistry is also predicated by the commercial importance; in particular, the potential foulant chosen must occur frequently in the industry. Additionally, the foulant should have a well-characterised and reproducible chemistry, be readily available in high purities, and produce environmental friendly disposable waste. The operating conditions should be relevant to real fouling conditions in practice and must provide stable and reproducible performance. The module should also allow safe and continuous operation under existing process conditions.

Figure 3-1 is a drawing of the experimental set-up of the system. The assembly consisted of a 40 litre feed tank for storage and supply of the fouling solution, a high pressure positive displacement pump for pressurisation of the feed solution, the rectangular test module, system cooling on the feed tank, analog pressure gages and valves, and a by-pass line parallel to the test module. The by-pass line is necessary in order to vary both the flowrate and the pressure inside the cell separately. Pressure was controlled with the back-pressure valve on the outlet line of the cell.

It must be understood that most membrane systems use a cross-flow filtration technique. In cross-flow, only a portion of the water fed to the membrane passes through the membrane. The remaining flow passes across the membrane and through the treatment system as waste (also called concentrate, reject or brine). This waste-or concentrate-flow is necessary to keep fouling materials from building up too rapidly on the surface of the membrane. Therefore the cross-flow membrane system has one feed stream entering the system, one concentrate stream (brine) and

one permeate stream (purified water) leaving the system. These 3 streams are circulated back to the feed tank in the experimental set-up.

System cooling was necessary as the circulating system experienced an increase in temperature resulting from line frictions as well as heat gained from the pump. A coil with running cooling water at 8 °C was used as heat exchanger in the feed tank. A thermocouple (accuracy ~ 0.5 °C) was used to measure the feed tank temperature and a solenoid valve was fitted in the cooling water line to vary the cooling water flowrate. The solenoid valve was controlled by the measured feed temperature. Feed flow to the cell was measured with a rotameter and manually controlled with a valve. Permeate was measured manually with a stopwatch.

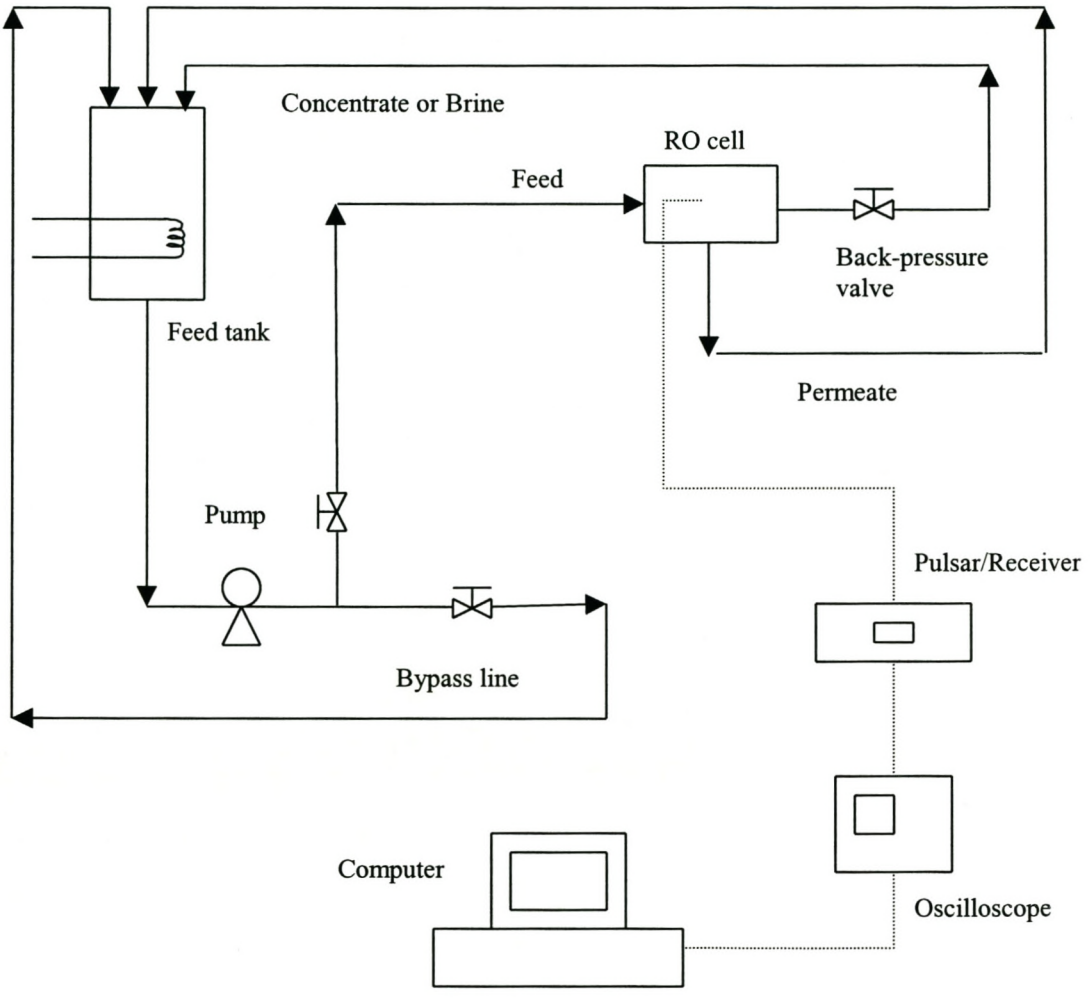

Figure 3-1 – Experimental set-up

3.2 Test cell

The characteristic properties of the material that is chosen for construction of the cell is very important, as the ultrasonic signal must be able to penetrate it. The acoustic impedance difference between the cell and the quartz crystal should be kept at a minimum, while the material's grain size should also be as small as possible. This would ensure better penetration with less attenuation and scattering. Aluminium, with specific acoustic impedance of 1.70 is very suitable (89 %) compared to that of quartz at 1.52.

Figure 3-2 shows a drawing of the test cell. It was designed for safe operation under high-pressure RO conditions while enabling the ultrasonic transducer to function with a sufficient signal-to-noise ratio and to provide representative sampling. The dimensions of the cell are 25mm x 100mm x 240mm with an effective membrane area of 85 cm^2. The thickness of the top part was 10 mm. A sintered copper plate (GKN Sinter metals, 100 µm pore size, 3 mm thick) was used as support for the membrane, while a spacer was also necessary due to the geometric dynamics of the cell.

The topside of the top part of the cell had a 4mm x 50mm x 160mm trench. It was filled with commercial grade honey, which was used as coupling agent between the transducer and the cell. A rectangular channel of 1mm x 50mm x 170mm was also cut at the bottom of the top part, to form the actual flow channel. The ultrasonic signals thus had to traverse through only half the thickness of the top plate, rather than through the whole 10 mm.

The membrane with a support-plate/spacer combination was seated into the bottom plate (see Figure 3-3) and the unit was sealed with a dual o-ring combination. The complete module assembly was clamped together with sixteen 6mm-diameter bolts.

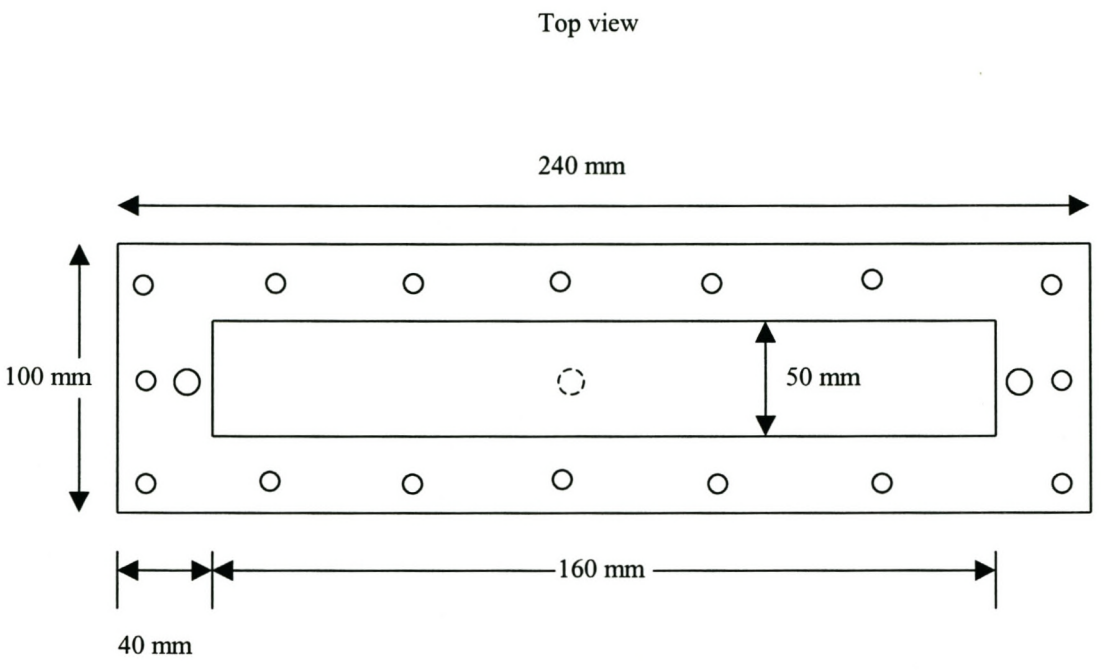

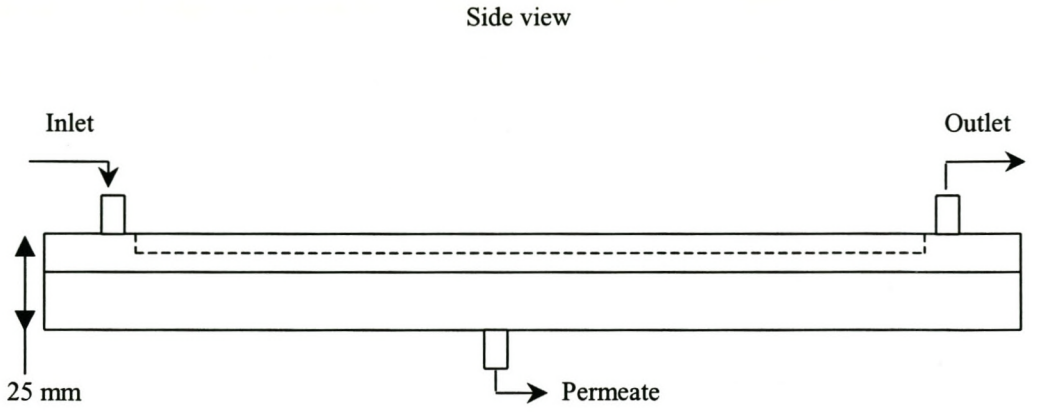

Figure 3-2 - Test cell

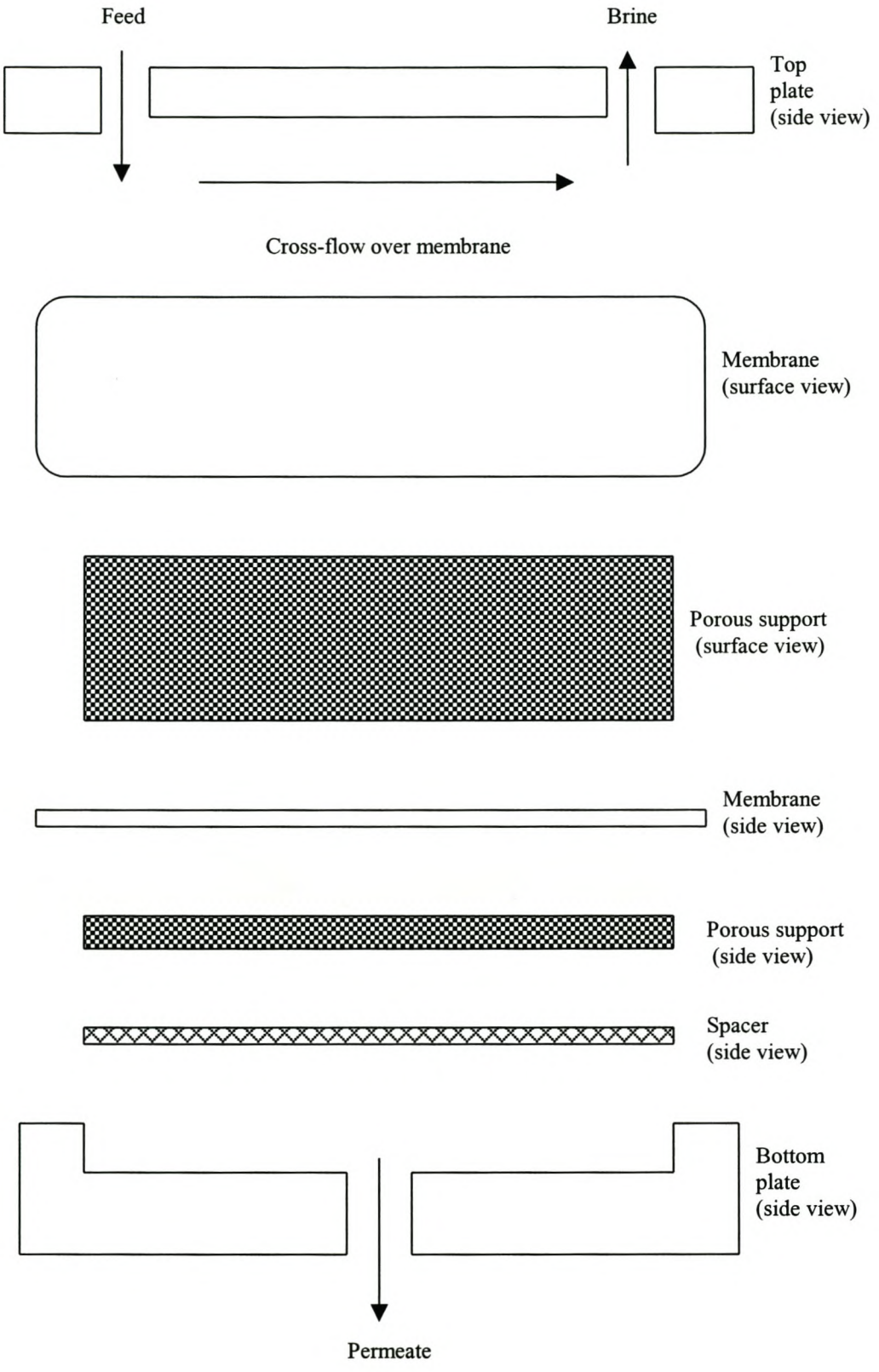

Figure 3-3 Placement of membrane in cell

3.2.1 Hydrodynamic entrance length of rectangular cell.

The hydrodynamic entrance length for the rectangular test module that was used in this study is given by Sakiadis (1984).

Eq. 19.....$L_{hy}/h = 0.625 + 0.022N_{Re}$

Where L_{hy} is the entrance length, h is the height of the channel, and N_{Re} is the Reynolds number based on the hydraulic diameter D_H. D_H is given by 2hw/(h+w) where w = the width of the channel.

The density and viscosity of the diluted feed solution (max of 2 g/l) can be assumed to be the same as that of pure water. Cross-flow velocities of no more than 5 cm/s were employed in this study. The Reynolds number at this velocity is 360, which is in the laminar region.

According to Eq. 19, the calculated entrance length under these circumstances is 13 mm. Since the length of the channel is 170 mm, the flow can be assumed to be fully developed before salt separation is initiated.

3.3 Experimental cell reflections

Figure 3-4 is a cross-sectional view of a typical flat-sheet cell with a membrane placed between two aluminium plates and an externally mounted transducer in contact with the top plate (Mairal, 1999). The high-pressure feed solution flows on top of the membrane and the permeate is withdrawn from the bottom side. Suppose a fouling layer with thickness dS is present on the surface of the membrane, and the reflected echoes A, B and C are generated from the various interfaces within the cell.

In Figure 3-5 the corresponding time-domain response is shown. The top plate/feed solution interface is represented by echo A, and the initial feed solution/membrane interface by B.

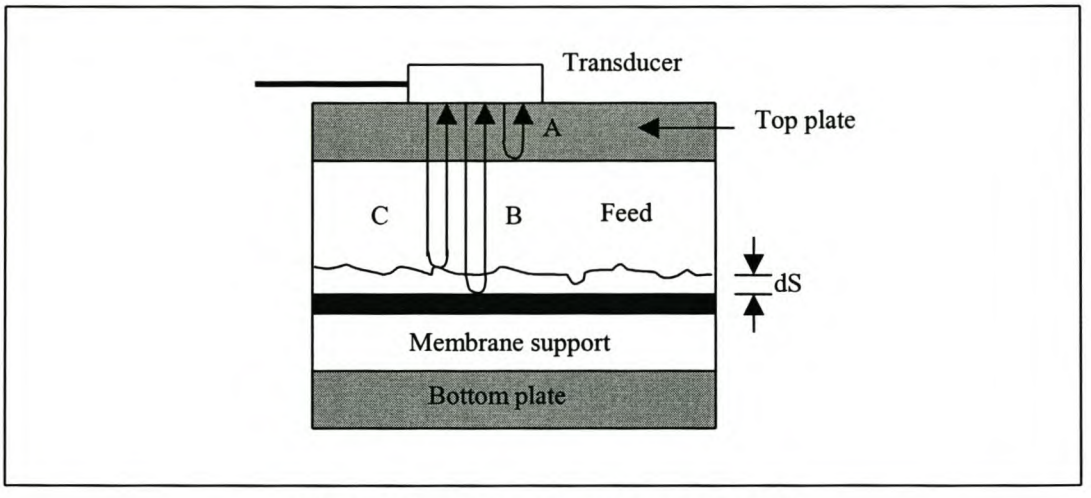

Figure 3-4 – Cross sectional view of RO cell

If the fouling layer is thick enough to be measured by the ultrasonic signal i.e. it falls within the spatial resolution capabilities of the system, a new echo C will be formed as a consequence of the new feed/fouling interface. Further, if the difference in arrival times between echoes B and C, dT, is measured, the thickness of the fouling layer, dS, can be measured with the following equation:

Eq. 20.....dS = 0.5 C dT

where C = velocity of the ultrasonic wave

Thus, the detection of the interface echoes allows fouling to be monitored in real-time.

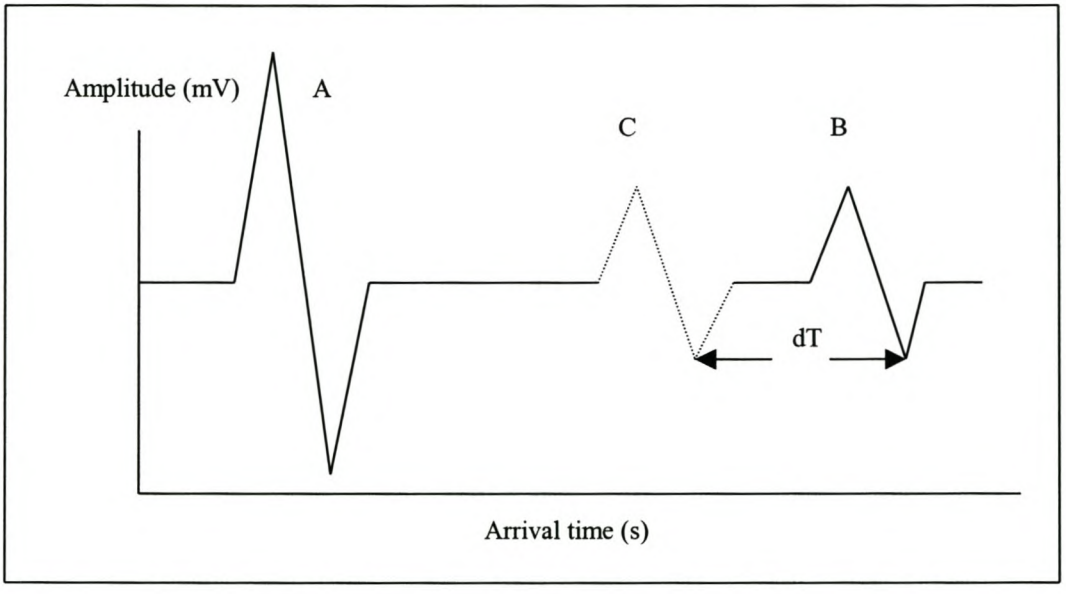

Figure 3-5 – Amplitude vs. time curve for pulse echo operation in flat sheet cell.

As mentioned before (Figure 2-1), Mairal did not experience the formation of a second echo (echo C) that represents fouling. His results showed a decline in the membrane echo amplitude (echo B) as a fouling layer started to form on the membrane. The fact that he used a stainless-steel cell may have had a negative influence on his results, as attenuation in stainless-steel will be much higher than in aluminium. The sensitivity of the UTDR technique was thus reduced by the usage of a stainless-steel flat sheet cell.

3.4 Ultrasonic set-up

The design of the ultrasonic measurement system involves selection of appropriate hardware including ultrasonic transducers, a pulsar/receiver, and an oscilloscope. Suitable software should also be available for generation and processing of the ultrasonic signals. The ultrasonic equipment used during this study consisted of a Panametrics pulsar-receiver (Model 5058PR), a Hewlett Packard oscilloscope (Model 54602B), and Panametrics Videoscan transducers.

3.4.1 Pulsar-Receiver settings

The sensitivity of the UTDR technique was reduced by the 4mm thick aluminium top plate of the cell. The surfaces of the module were polished in order to get a very smooth finish.

Numerous experiments were done in order to find the optimum conditions for the pulsar/receiver and the oscilloscope. The best results were obtained by using almost maximum power, in this case an excitation pulse of 400 V, and the lowest damping for the received signals. The internal trigger was set at 200 Hz repetition. Very stable operating conditions and minimum attenuation made the use of filters for noise unnecessary.

3.4.2 Oscilloscope settings

The oscilloscope was set at a sweep speed of 200 ns/div while 4000 data points (thus 2000 time-amplitude pairs) could be downloaded at any specific time. The data was saved as waveforms in either comma-separated (.CSV) or tab-separated (.PRN) form and could be opened in a spreadsheet program like Excel for further processing.

3.4.3 Transducers

The various frequency transducers that were investigated are the Panametrics V106-RB, 2.25 MHz; V182-RB, 3.5 MHz; V109-RB, 5 MHz; V120-RB, 7.5 MHz and V111-RB, 10 MHz. After numerous experiments it was found that the 7.5 MHz transducer gave the best response for the system under investigation. In all the final experiments that were chosen for data gathering, the V120-RB, 7.5 MHz transducer was thus used.

3.5 Experimental features

3.5.1 Axial position of the transducer

It was not possible to scan the whole membrane area with one transducer, so the axial position of it had to be decided. Studies performed by Mairal (1999) revealed that fouling would most likely initiate at the end of the rectangular cell. He used six transducers at various axial positions in order to get a profile over the membrane. Although he discovered no drastic changes over the length of the cell, it did prove that fouling initiation would start at the end of the vessel where flow is likely to be less. It was thus decided to place the transducer at an axial position close to the end of the cell and to keep it there for all the experiments.

3.5.2 Membranes used

All experiments were carried out using Hydranautics ESPA3 Polyamide membranes. It was cut from manufacturer-supplied long rolls, 1 m wide and several meters long. The membrane specifications is the following:

Maximum applied pressure	4.16 MPa (41 bar)
Maximum Chlorine Concentration	< 0.1 PPM
Maximum operating Temperature	113 °F (45 °C)
Feedwater pH range	3.0 –10.0
Maximum feedwater Turbidity	1.0 NTU
Maximum Feedwater SDI (15 min)	5.0
Maximum feed flow	75 GPM (17.0 m^3/h)
Minimum ratio of Concentrate to Permeate Flow for any element	5:1
Maximum pressure drop	10 psi
Permeate flow	15 000 gpd (56.8 m^3/d)
Membrane area	400 ft^2 (37.3 m^2)

Permeate flux	63.5 L/m^2h

Test conditions:

The stated performance is initial (data taken after 30 min of operation) on the following conditions:

1500 PPM NaCl solution

150 psi (1.05 MPa) Applied Pressure

77 °F (25 °C) Operating temperature

15 % Permeate recovery

6.5 – 7.0 pH range

3.5.3 Operating conditions

All experiments were carried out in the pressure range of 2 - 2.5 MPa (20 - 25 bar) with flowrates varying between 0 - 100 ml/min. Feed concentrations varied between 0.5 – 2 g/l while the temperature was controlled at 25 ± 1 °C.

3.5.4 Preliminary compaction experiments

The UTDR technique measures signal bounce and therefore it is very sensitive to any changes in thickness perpendicular to the signal. In theory, it should thus be sensitive to compaction of the membrane and membrane support at very high pressures. In order to investigate these phenomena, experiments were conducted where the time response (i.e. the membrane reflection) at different operating pressures was collected. These experiments were conducted under both dead-end and cross-flow conditions with clean water at 25 ± 1 °C. The pressures under consideration were varied between 5 and 30 bar. It was found that the membrane echo is indeed a function of the applied pressure inside the cell. The higher the pressure, the more compressed the membrane and support, and thus the distance between the membrane and the top part of the cell increases. This resulted in a shift of the membrane echo in the time domain, (Figure 3-6), as the signal had to travel further in the bulk solution on top of the membrane. Both the dead-end and cross-flow experiments obtained the same results repeatedly. These experiments showed that the UTDR technique was able to measure compaction very accurately, and had to be taken into account before designing the final fouling experiments. For more information on compaction, the interested reader is referred to the thesis of R. Peterson (Peterson, 1996)

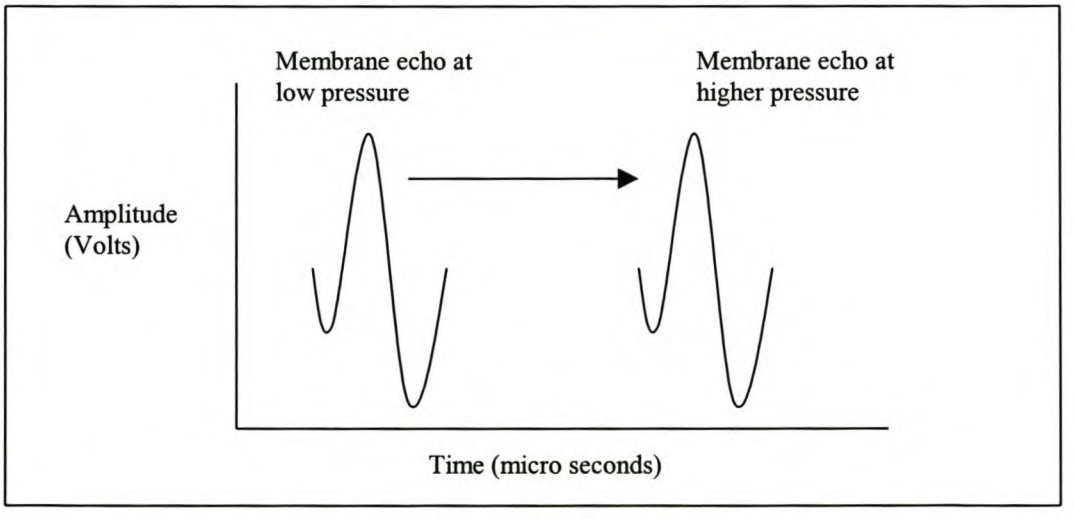

Figure 3-6 - Membrane echo shift at higher pressures

The fact that the membrane as well as the support/spacer combination could be compressed, was useful as it could be used to find the membrane peak on the oscilloscope, i.e. any pressure increase would result in the movement of the membrane echo.

3.5.5 Static membrane experiment

A static experiment was used as a quick test to determine the difference between the results obtained from a clean and a fouled membrane respectively. If the results of the static test (where the UTDR result from a membrane with a known visual fouling layer was compared to that of a clean one) is good, enough credibility would be provided to assume that the UTDR technique can be used for fouling layer monitoring in real time. The chosen membrane, Hydranautics ESPA 3, was operating in an industrial RO water desalination plant at SASOL. It was removed from the plant after compaction was experienced as a result of working at too high pressure for too long. A very low permeate flow was the result. The membrane was in fact damaged and attempts to clean it were unsuccessful. A destructive membrane autopsy was performed with SEM and EDX analysis. It revealed that the membrane was fouled with calcium carbonate, calcium sulphate, silicone, sulphur and a few organic substances.

For the UTDR experiment, a piece of the fouled membrane was prepared by first soaking it for 24 h in clean water. The membrane was then placed inside the rectangular cell and experiments were conducted at the normal operating pressure of the membrane at 20 bar.

3.5.6 Fouling experiments

The final fouling experiments were carried out using 2 different fouling species i.e. calcium sulphate and calcium carbonate. Cross-flow as well as dead-end situations were investigated. All cross-flow experiments were carried out in the laminar area range with axial velocities between 0 - 5 cm/s.

Each experiment consisted of three phases. First, the membrane was soaked in pure water for at least 24 h prior to the start of the experiment. Then the membrane was placed inside the cell and exposed to clean pressurised water at the desired operating conditions of the experiment. Once steady state with respect to the permeate flux and the ultrasonic signal was achieved, the feed was switched to the fouling solution to initiate the third phase in which the changes in the measured variables occurred due to concentration polarisation and fouling. The pure water phase ensured that processes such as membrane compaction and adsorption of trace organic ions on the surface stabilised before initiation of the fouling phase, thereby facilitating an unambiguous interpretation of UTDR and flux behaviour. The experiments were allowed to continue until the ultrasonic response and permeate flux had stabilised. The module was then opened and fouled membrane samples were collected for morphological analyses.

3.5.7 Cleaning experiments

The potential ability of the UTDR technique to detect the presence of a fouling layer may also make it suitable for monitoring the removal of a fouling layer. Cleaning experiments were therefore carried out to demonstrate the potential of the UTDR technique for such an application. The membranes were first fouled to steady-state levels as described in the previous section, after which clean water was introduced to clean the membranes. Experiments were carried out at the same operating pressures as that of the fouling phase. At the end of the cleaning experiments, membrane samples were removed for morphological characterisation.

3.5.8 Morphological characterisation of the fouling layer

The purpose of the morphological study of the fouled membrane samples using scanning electron microscopy (SEM) was deemed necessary in order to establish a correlation between the behaviour of the measured variables and the fouling layer.

Although the SEM analysis resulted in high resolution images which provided important insight into the morphological growth of a fouling layer, it was still limited by the fact that the sampling area was very small relative to the overall size of the membrane as well as the part of membrane that was scanned by the transducer.

To deal with this problem, the samples were prepared in two stages. First, a piece of membrane was removed underneath the area the transducer was scanning. The sample was then analysed under an optical microscope for general features and trends, and a representative area was identified for preparing the SEM sample. By doing so, a representative sample was always taken.

3.6 *Experiments on an industrial spiral wrap RO module*

A number of experiments were done on an industrial spiral-wrap RO module to test the potential application of the ultrasonic A-scan technique on the membrane configuration. The idea was not to undertake a complete study, as the reflections from the various interfaces was too complicated to understand. A thorough study on a spiral wrap module is needed to completely understand the complex signals.

3.6.1 Experimental set-up

An 8-inch diameter spiral wrap RO module was used for the tests. (See Appendix 9 for more detail). Modifications on the module were necessary due to the inability of the ultrasonic signals to penetrate the thick fibreglass casing of the pressure vessel. To deal with this problem, aluminium access ports were built into the pressure vessel wall and the transducer was placed in direct contact with the ports. A set-up of the system is shown in Figure 3-7, with an image of the module in Figure 3-8.

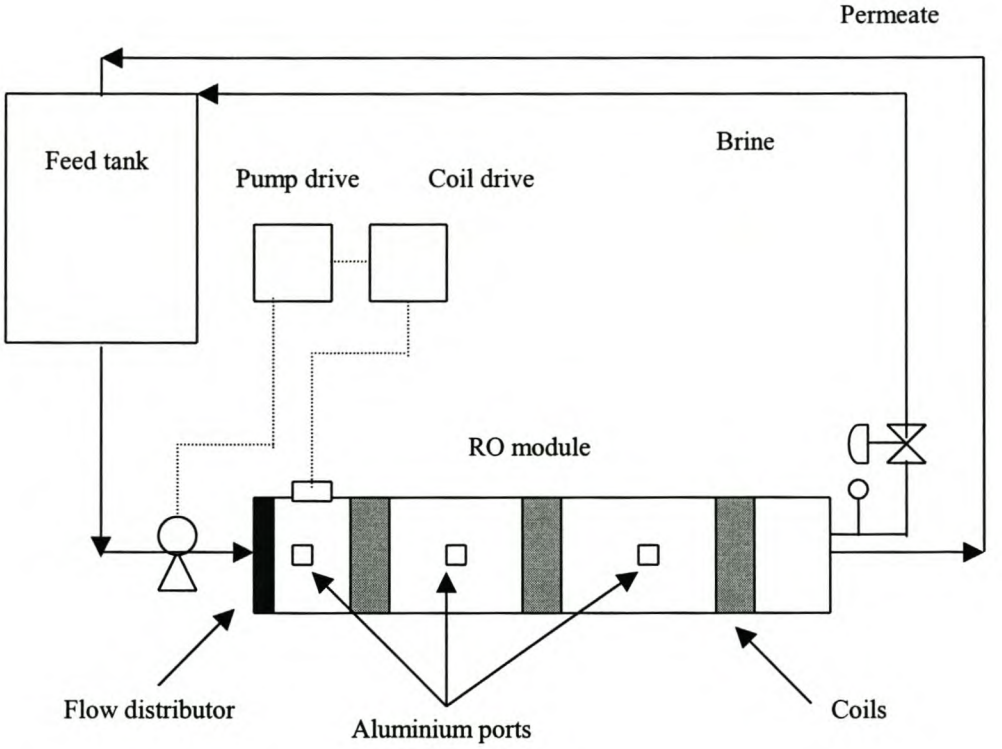

Figure 3-7 – Spiral wrap experimental set-up

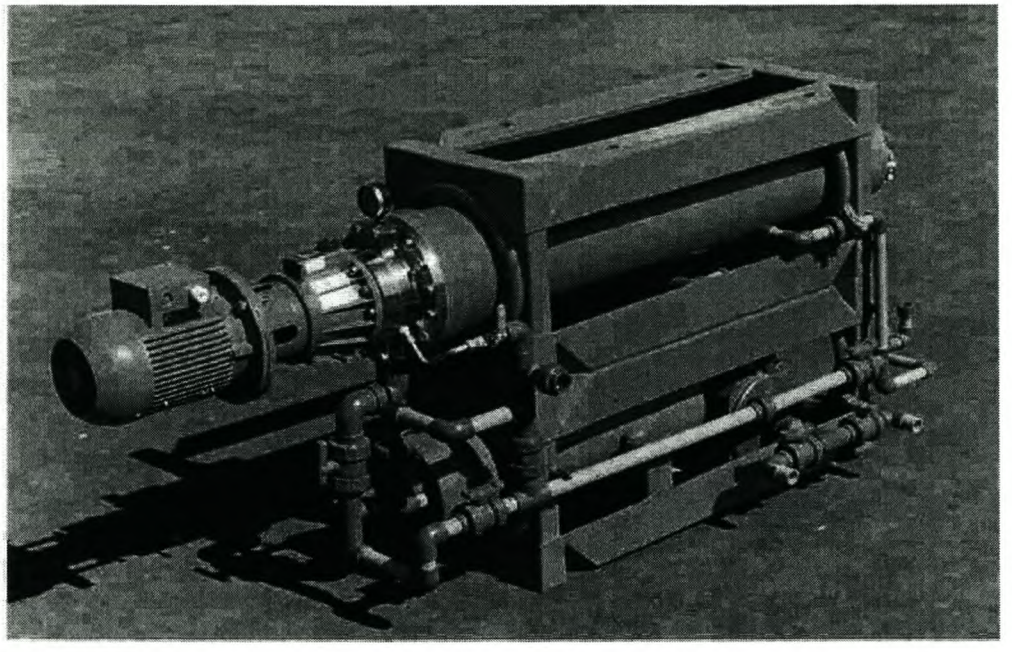

Figure 3-8 - MWD test unit

3.6.2 Experimental characteristics

The influence of the flow distributor as well as the magnetic fields (induced by an electric current in the coils around the module) were investigated. Please refer to Appendix 9 for more detail.

Feed tank:

A 1000-l tank was used. To improve circulation in the tank, a submersible pump was operating continuously inside it.

Coils:

A coil drive made it possible to switch the coils on and off as needed. The module had 3 groups of coils, stretching over the length of it. The access ports were made between the various groups.

RO module:

An eight-inch diameter module was used with the same membranes as during the flat sheet cell tests (Hydranautics ESPA3). Flow rate to the module could be varied by changing the pump workspeed through the pump drive, while the pressure was controlled by the valve on the brine passage. The pressure indicator at the end of the vessel was monitored.

Fouling agent:

Calcium carbonate was used as fouling agent with concentrations just below the maximum soluble value of 2 g/l.

4 Mathematical model

A mathematical model of the reflections inside the flat sheet cell was developed and the results were compared to the actual cell dimensions. The model revealed excellent correlation between the echoes received and the measured cell dimensions. Figure 4-1 is a cross section view of the cell with the received reflections where

T_1 = echo between the honey and the top surface of the cell
T_2 = echo of the cell/water interface, and
T_3 = echo of the membrane.

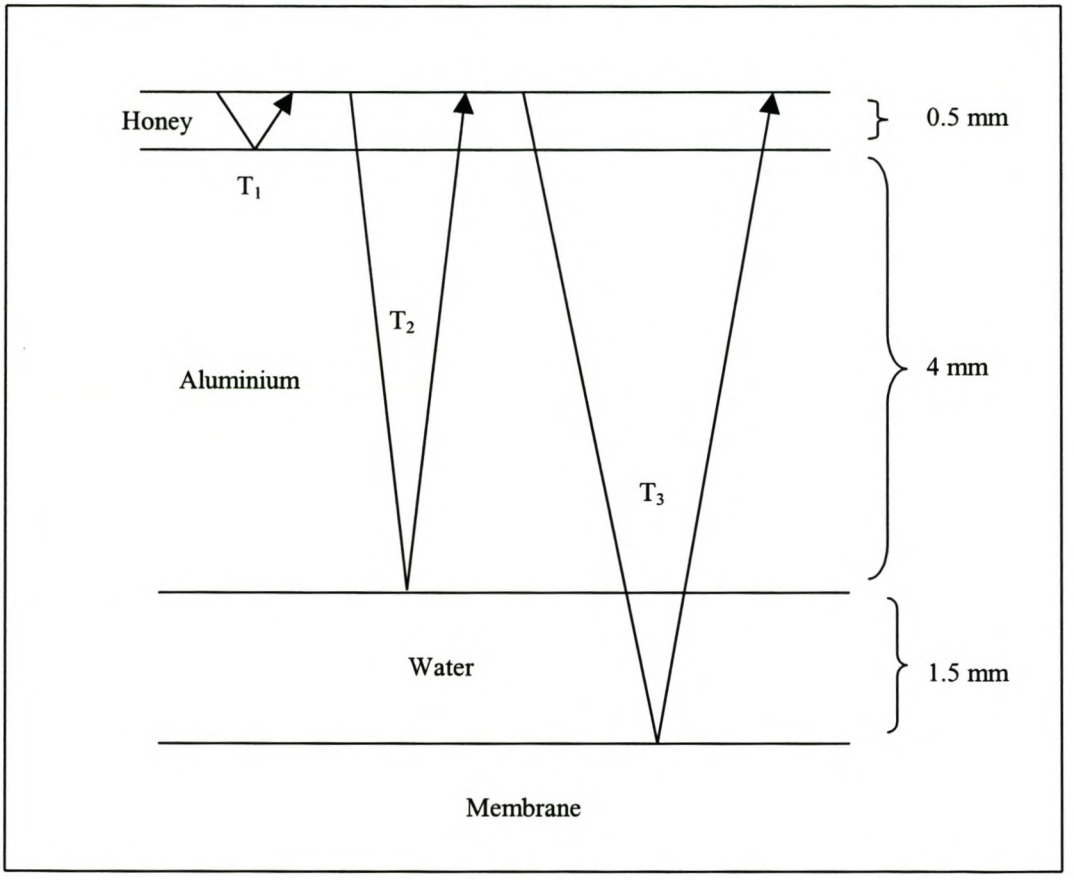

Figure 4-1 – Mathematical model

A typical experiment with a new, clean membrane and working pressure of 20 bar resulted in Figure 4-2, where the different reflections T_1, T_2, and T_3 can be seen. It is not 100 % clear why the first echo is in fact split up into 3-4 parts, but it is believed that 100 % coupling between the transducer and the honey is impossible. This would mean that the reflections can be explained as those coming from an air/honey/air/ aluminium interface.

The time domain reflections of the signals as measured by the oscilloscope was:

$T_1 = 1.62\ \mu s$

$T_2 = 2.84\ \mu s$

$T_3 = 4.94\ \mu s$

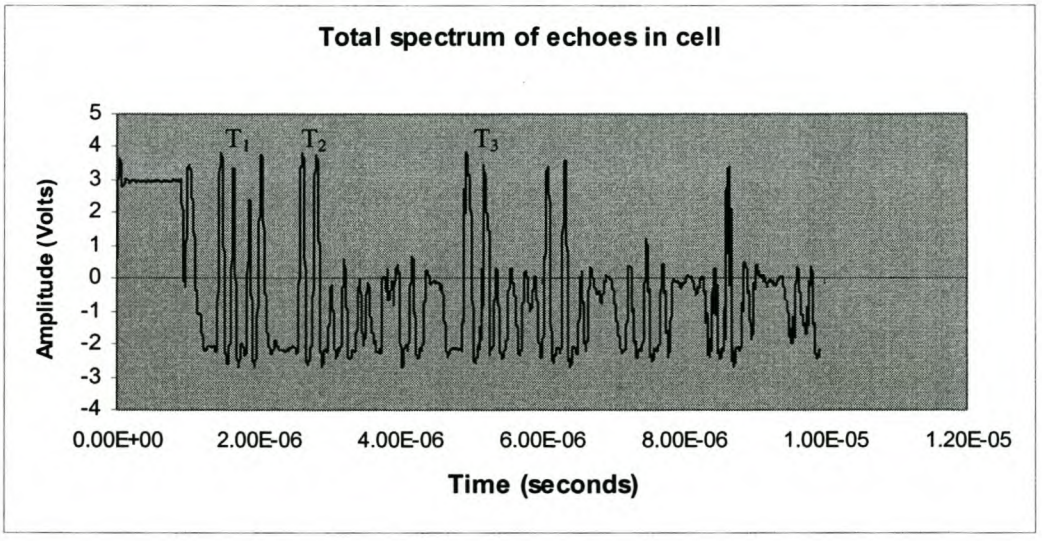

Figure 4-2 - Echo spectrum inside cell

The measured thickness of the aluminium top plate and thus the distance the ultrasonic signal must travel through the aluminium is ± 4 mm. From the preliminary compaction experiments it is also known that the thickness of the water film on top of the membrane is in excess of 1 mm, depending on the pressure.

If the speed of sound in aluminium and water is known, together with the positions of the different interface echoes inside the cell, the thickness of the respective layers can be mathematically correlated by using the received echo time reflection parameters and

Eq. 20……..dS = 0.5 C dT

with

C_{alum} = 6420 m/s

C_{water} = 1430 m/s

$s_{alum} = 0.5 \times C_{alum} \times (T_2 - T_1)$

$= 0.5 \times 6420 \times (2.84 - 1.62)$

$= 3.93E\text{-}3$ m

= 3.93 mm

$s_{water} = 0.5 \times C_{water} \times (T_3 - T_2)$

$= 0.5 \times 1430 \times (4.94E\text{-}6 - 2.84E\text{-}6)$

$= 1.50E\text{-}3$ m

= 1.5 mm

The calculated aluminium thickness of 3.93 mm is very close to the measured value of 4-mm, while the thickness of the water film on top of the membrane at a pressure of 20 bar is 1.5 mm.

5 Results

This chapter presents the results of experiments carried out in the development of UTDR by using the experimental methodology described in the previous chapter. The data generated during real-time measurement of membrane fouling include the permeation rate, system pressure and ultrasonic responses from the membrane surface as digitised waveforms. Each generated ultrasonic data set consists of 4000 data points. This is quite a substantial amount of data that made files very big and frustratingly slow to handle. For the sake of easy handling, only the membrane echo as well as the fouling echo (if present) were thus used in the discussions. The interested reader should refer to Appendix 9-1 for complete characterisation of all the relevant echoes around the membrane.

5.1 Preliminary compaction experiments

The compaction experiments were carried out to investigate the resolution capabilities of the UTDR technique. The membrane echo was captured as a function of the pressure, which varied between 0,5 - 3 MPa (5 – 30 bar). Clean water at 25 ±1 °C was used. Results of a typical experiment is given in Figure 5-1.

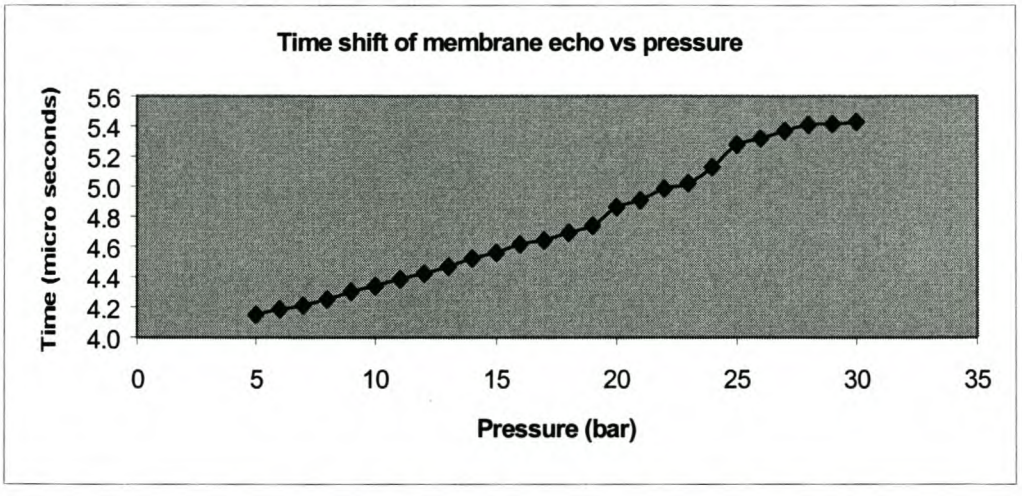

Figure 5-1 - Membrane echo vs pressure

Figure 5-1 illustrates an almost linear relationship exist between the applied pressure and the membrane echo, with asymptotic behaviour at pressures near 30 bar. Maximum compressibility is thus obtained at pressures in excess of 30 bar.

From own experience in working with membranes, fouling layer thickness have been found to vary between 10 – 800 μm (depending on the fouling agent). As membrane movement away from the aluminium top surface of up to 48 μm could be measured, the compaction experiments proved that the resolution of the system was sensitive enough to pick up the presence of a fouling layer.

5.2 *Fouling experiments*

If fouling occurs on the membrane surface, changes in the reflected signal could be expected due to modifications in the morphology of the membrane-solution interface. A new interface signal (Figure 3-5) will be observed in the time-domain if the fouling layer thickness approaches a critical value relative to the resolution of the ultrasonic measurement system.

5.2.1 Static experiment.

A membrane that was fouled as a result of too high-pressure exposure was used for the experiment. The very high-pressure lead to membrane compaction with no cleaning possibilities. Figure 5-2 is the ultrasonic response at 2 MPa (20 bar) pressure and a cross-flow velocity of 50 ± 15 ml/min. The calculated fouling layer thickness according to Eq. 20 and Figure 5-2 is 70 μm.

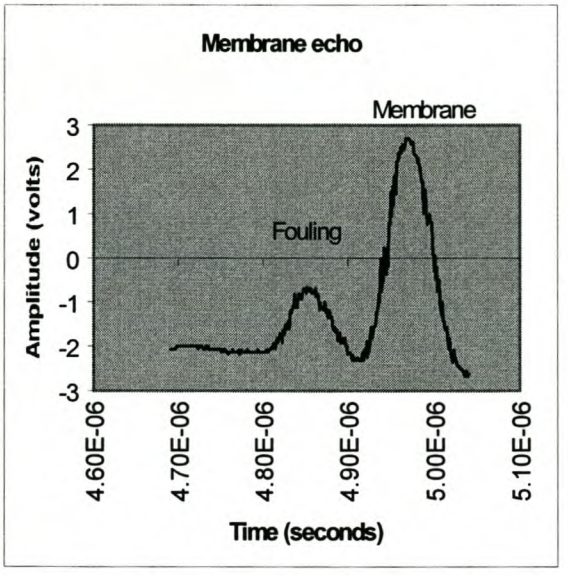

Figure 5-2 - Ultrasonic response of static experiment with compact membrane.

Scanning electron microscope analysis of a membrane sample revealed Figure 5-3.

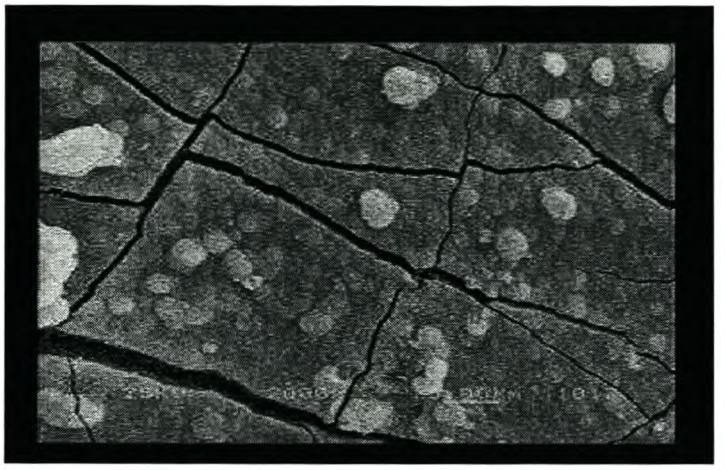

Figure 5-3 - Fouled membrane scanning electro microscope image (photo taken after membrane section was allowed to dry)

The characteristic fouling layer is visible in a comparison between the clean membrane image and the fouled membrane.

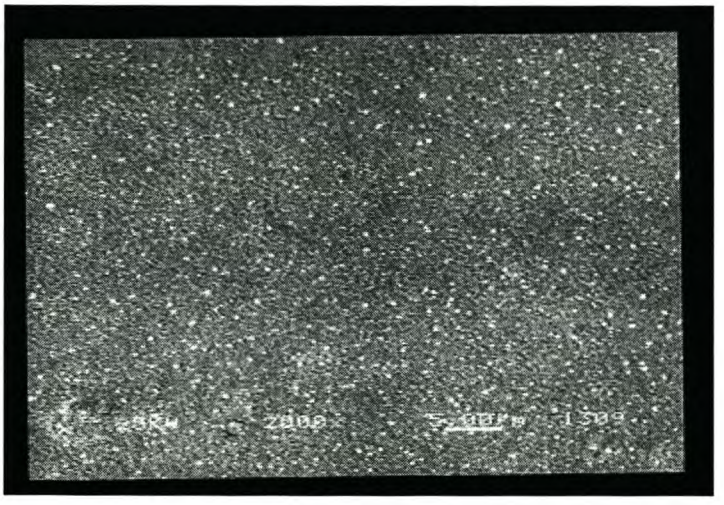

Figure 5-4 - Clean membrane SEM image

The cracks in Figure 5-3 are a result of the membrane that dried out. The fouling layer cracked similar to mud when it dries.

The static test proved that the system was able to distinguish between a fouling layer and the membrane. More fouling test were therefore done in which the fouling agent and system parameters were controlled.

5.2.2 Cross-flow experiments

Experiment with 2 g/l calcium sulphate feed concentration and 50 ml/min cross-flow (1.1 cm/s) velocity.

The pressure was controlled at 21 bar and permeate measurements were taken every 30 min. A graduate decrease in permeate flow was experienced and after 7 hours the experiment was stopped. Ultrasonic echoes were taken every hour. Figure 5-5 is the permeate flow vs. time curve for the experiment.

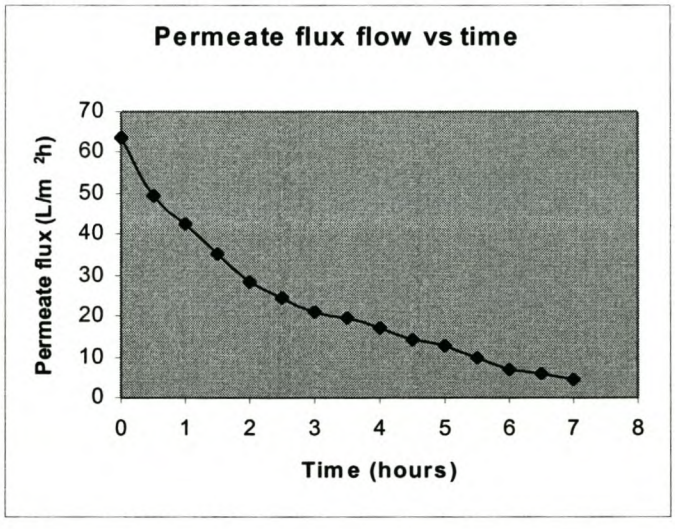

Figure 5-5 - Permeate flow data for calcium sulphate fouling experiment with 1.1 cm/s cross-flow velocity.

Ultrasonic responses:

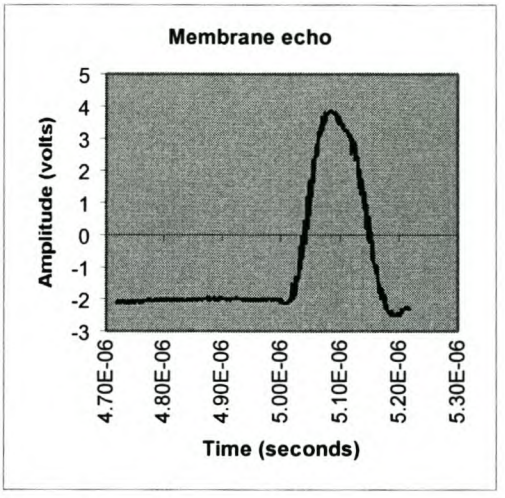

0 hour

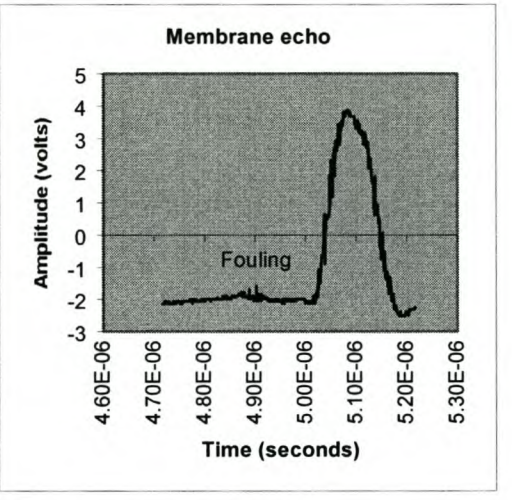

1 hour

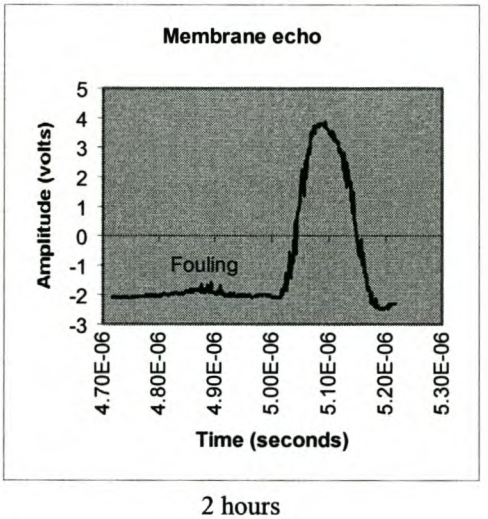

2 hours

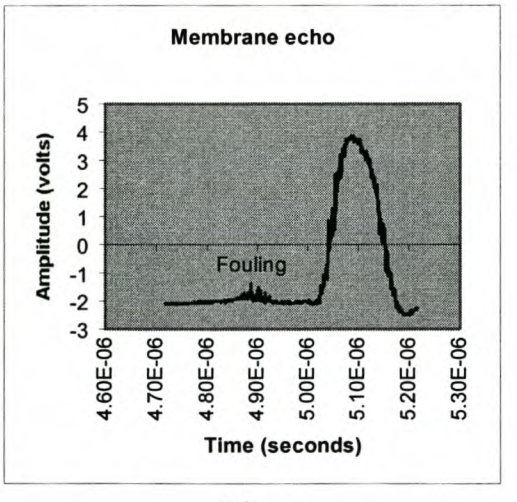

3 hours

Figure 5-6 - Ultrasonic responses at the start and after 1, 2 and 3 hours of operation for the calcium sulphate experiment with 1.1 cm/s cross-flow velocity.

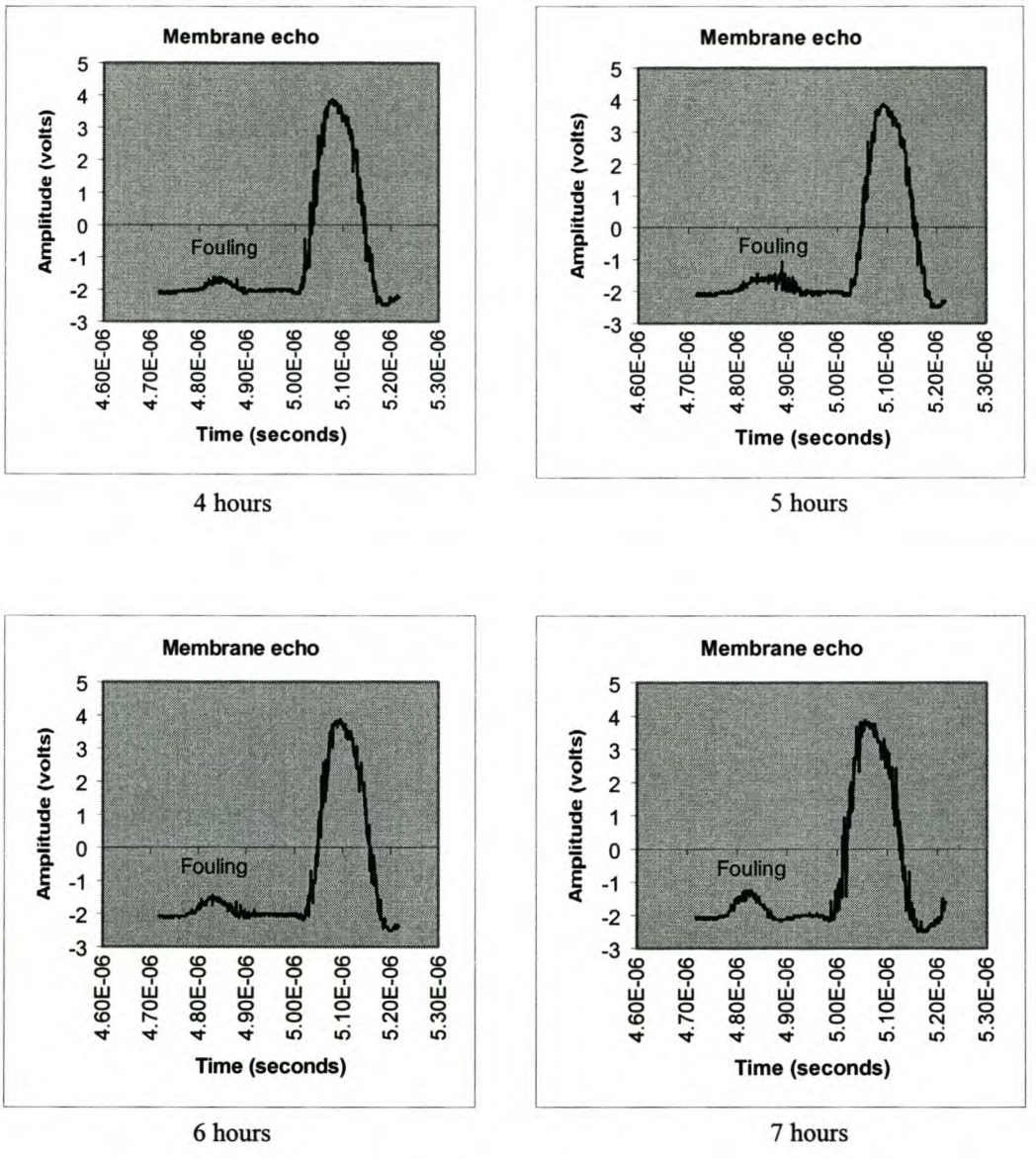

Figure 5-7 - Ultrasonic responses after 4, 5, 6 and 7 hours of operation for the calcium sulphate experiment with 1.1 cm/s cross-flow velocity.

The large peak represents the membrane. This has been confirmed by adding permeate side spacers (see Appendix 9-1). The peak width could be a function of the composite structure of the desalination membrane having a denser face and a more porous and compressible substrate. One can see in some experiments a lower shoulder indicative of this composite membrane geometry (especially evident in Figure 5-32). The formation of the second echo representing concentration polarisation and fouling, was observed within the first hour of operation. This is also

shown by the flux decline behaviour. As fouling layer growth progressed, an increase in echo amplitude (giving a sharper and clearer echo) was observed.

In Figure 5-8 the flux rate is plotted as a function of the fouling layer echo amplitude value (absolute value). The relationship between the decrease in flux rate with an increase in fouling echo amplitude is clear from the figure.

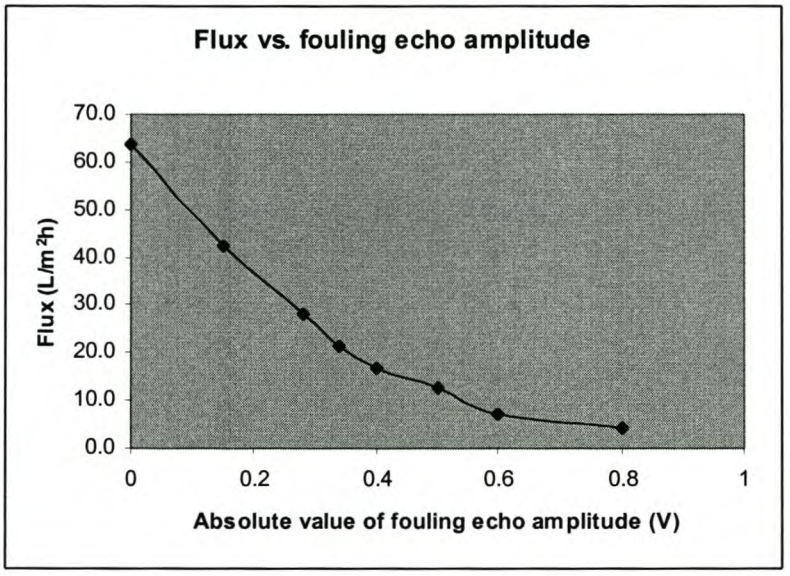

Figure 5-8 - Flux vs. the absolute value of the fouling layer echo for the calcium sulphate experiment with 1.1 cm/s cross flow velocity.

Morphological characterisation of the membrane after 7 hours revealed complete membrane coverage with calcium sulphate crystals. The thickness of the fouling layer as measured by the ultrasonic technique was calculated to be 150 μm.

SEM analysis showed that the fouling layer consisted of needle shaped crystals. A cross-section image confirmed that the thickness of the fouling layer varied between 100-300 μm. (Figure 5-10)

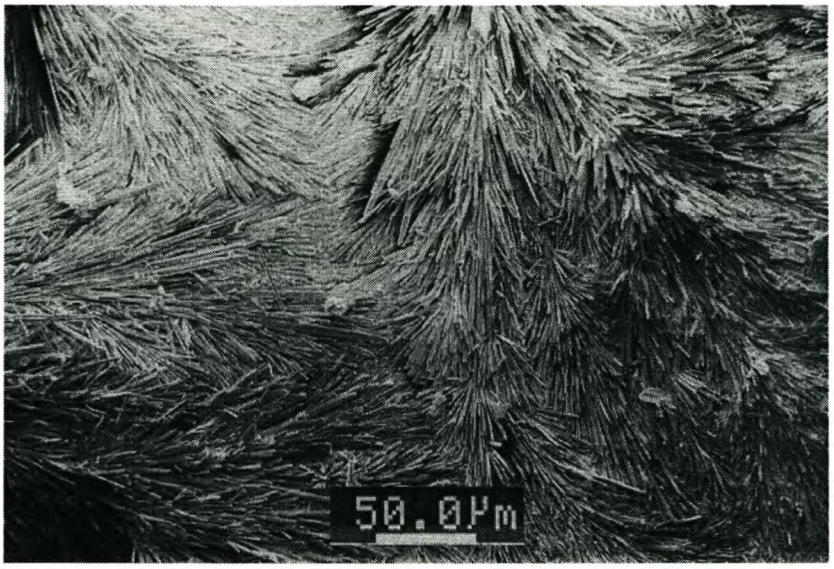

Figure 5-9 – SEM image of fouling layer in calcium sulphate fouling experiment

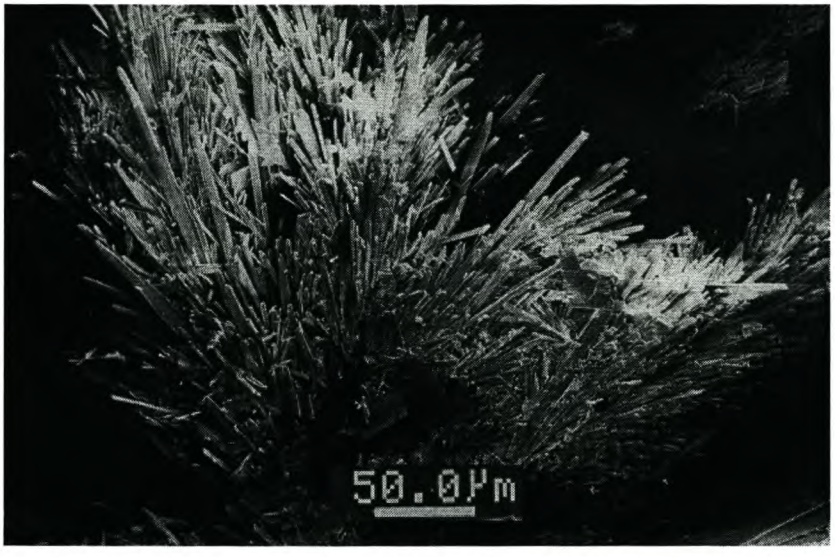

Figure 5-10 – Cross-section image of fouling layer in calcium sulphate fouling experiment

Experiment with 1 g/l calcium sulphate feed concentration and a cross-flow velocity of 100±15 ml/min (2.2 cm/s).

In the next experiment the cross-flow velocity as well as feed concentration were changed. The pressure was controlled at 22 ± 0.5 bar. The higher cross-flow velocity as well as reduced feed concentration resulted in slower fouling and thus longer experimentation time. After 21 hours permeate flow was too low to be measured accurately. Figure 5-11 is the permeate flow vs.time curve.

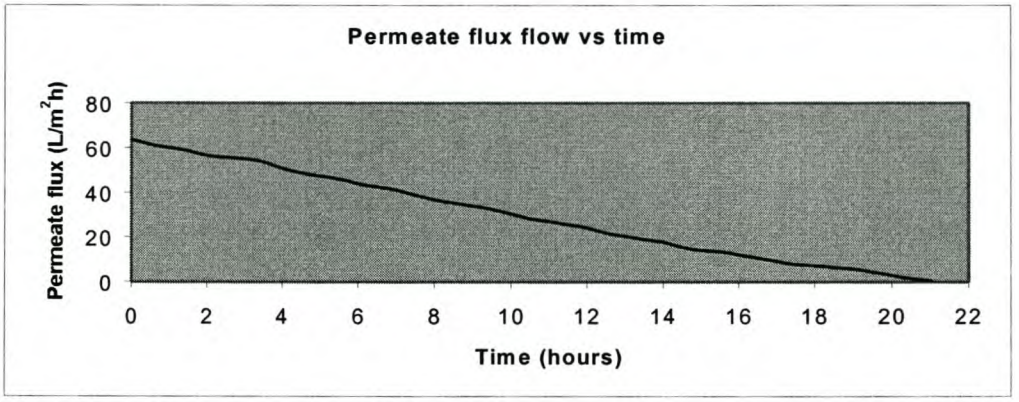

Figure 5-11 - Permeate flow data for calcium sulphate fouling experiment with 100 ml/min cross-flow (2.2 cm/s) and a feed concentration of 1 g/l.

Ultrasonic responses:

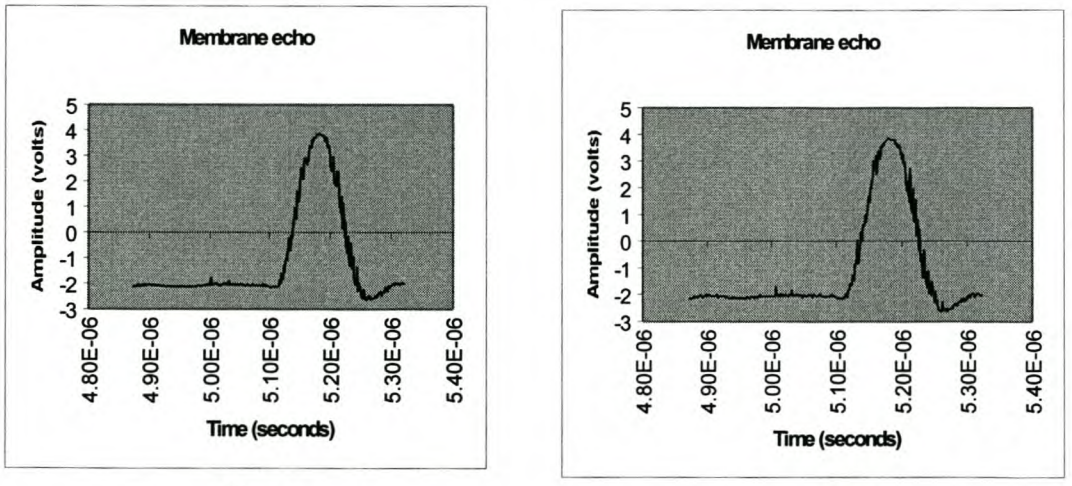

0 hour 1 hour

Figure 5-12 - Ultrasonic responses for calcium sulphate experiment with 2.2 cm/s cross-flow velocity at the start and after 1 hour of operation.

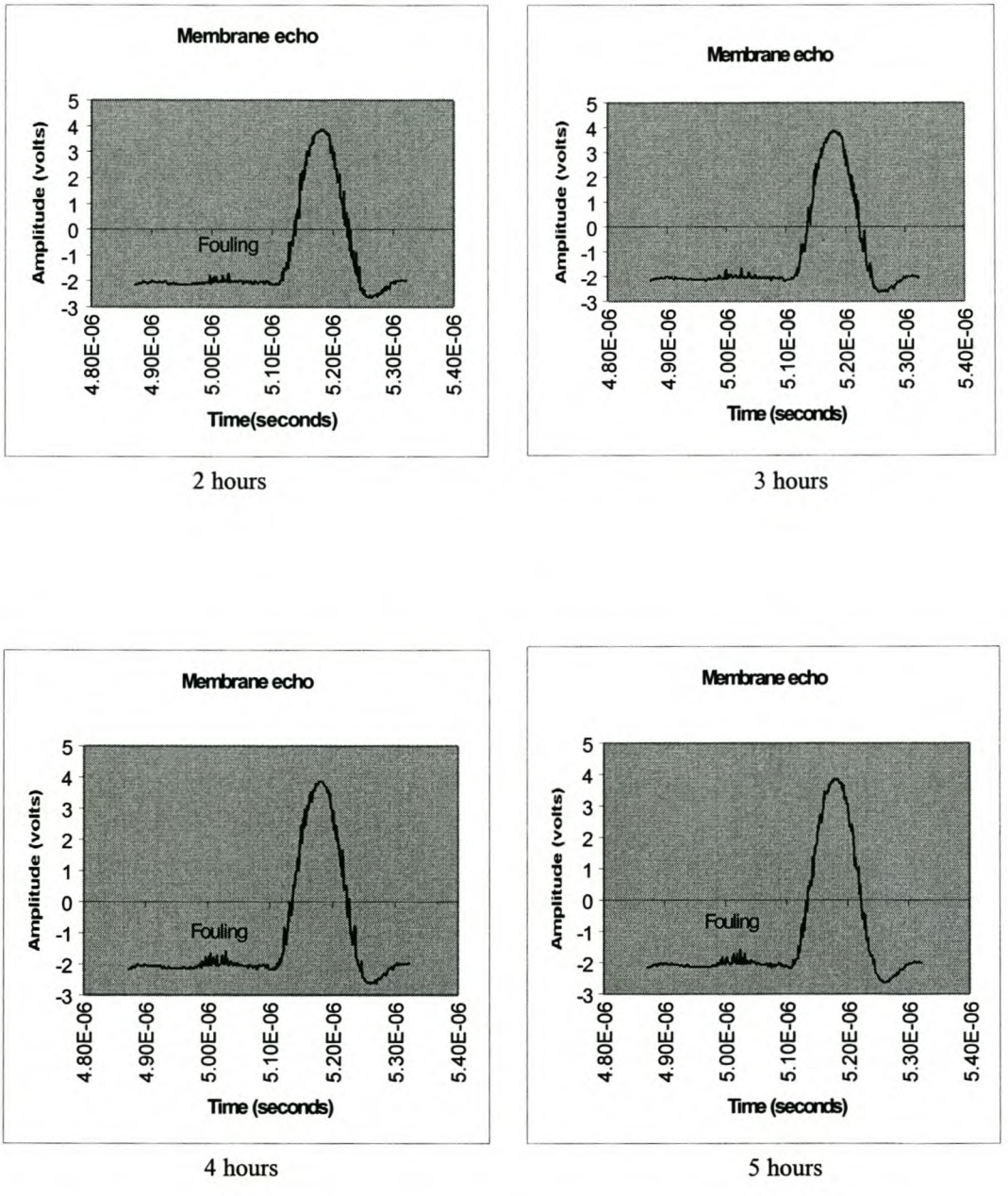

Figure 5-13 - Ultrasonic responses of calcium sulphate experiment with 2.2 cm/s cross-flow velocity after 2, 3, 4 and 5 hours of operation.

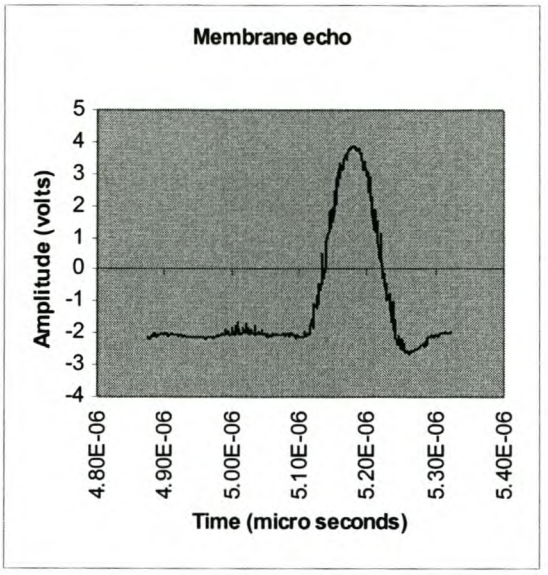

6 hours

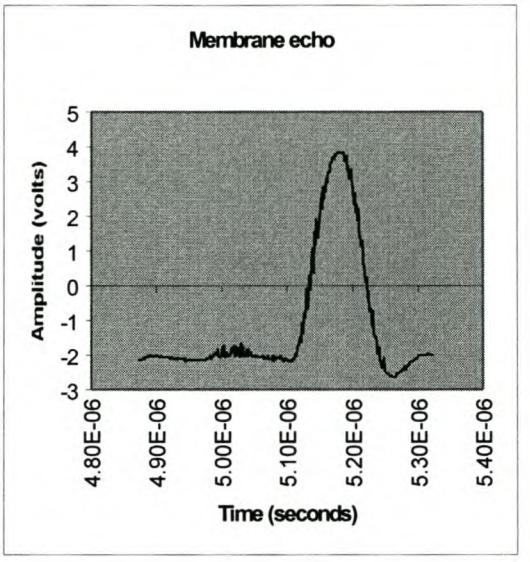

7 hours

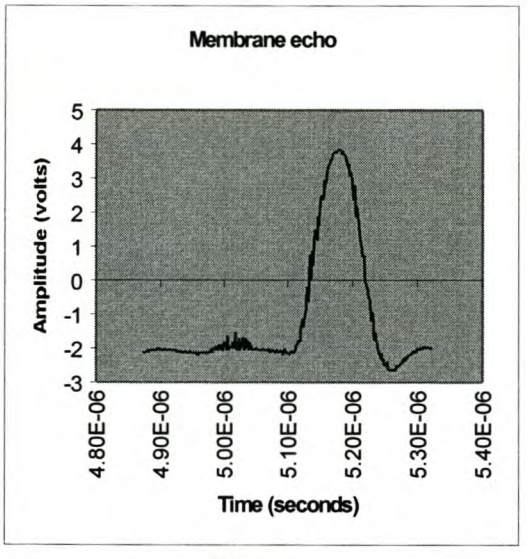

8 hours

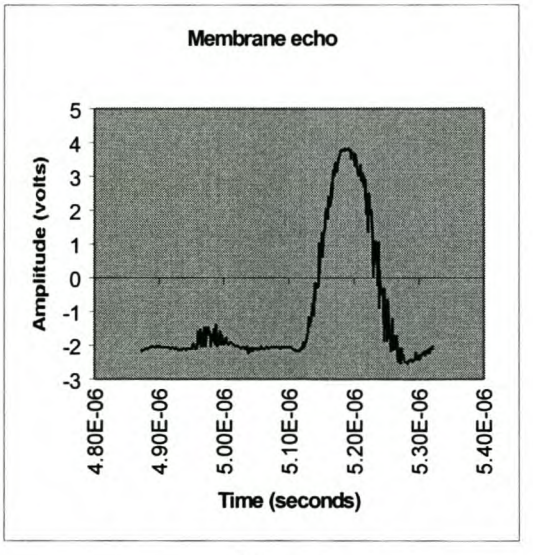

9 hours

Figure 5-14 - Ultrasonic responses for calcium sulphate experiment with 2.2 cm/s cross-flow velocity after 6, 7, 8 and 9 hours of operation.

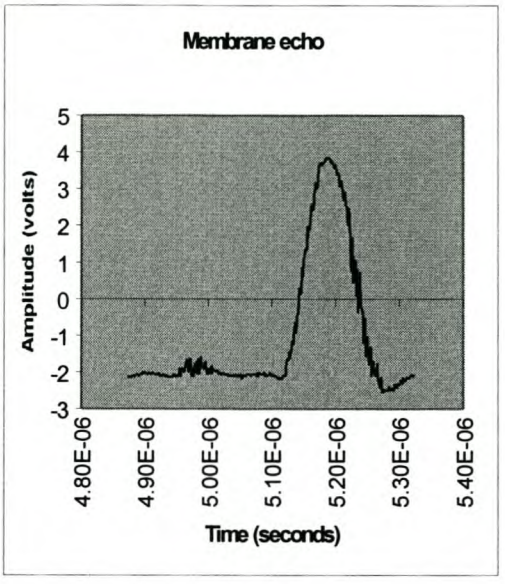

10 hours

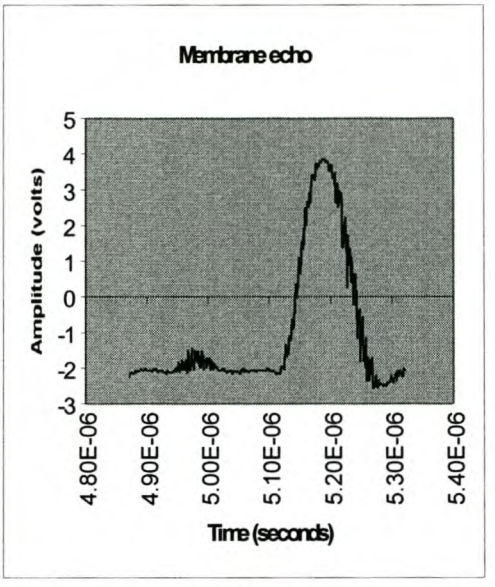

11 hours

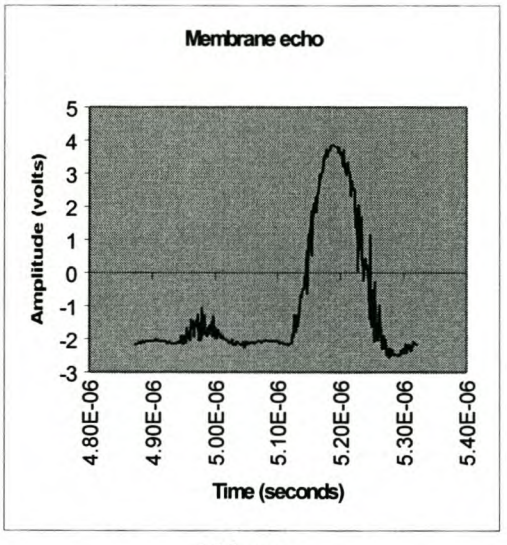

12 hours

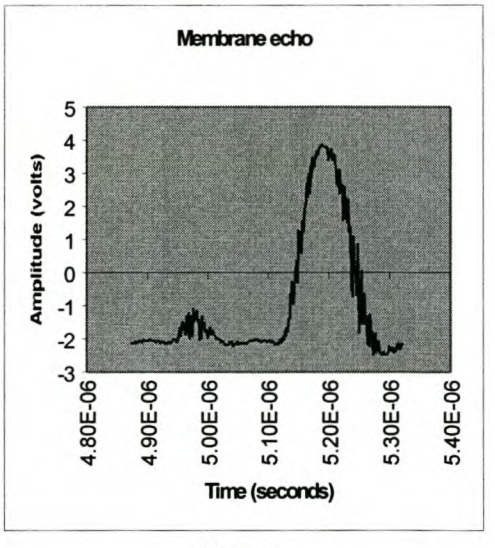

13 hours

Figure 5-15 - Ultrasonic responses of calcium sulphate experiment with 2.2 cm/s cross-flow velocity after 10, 11, 12 and 13 hours of operation.

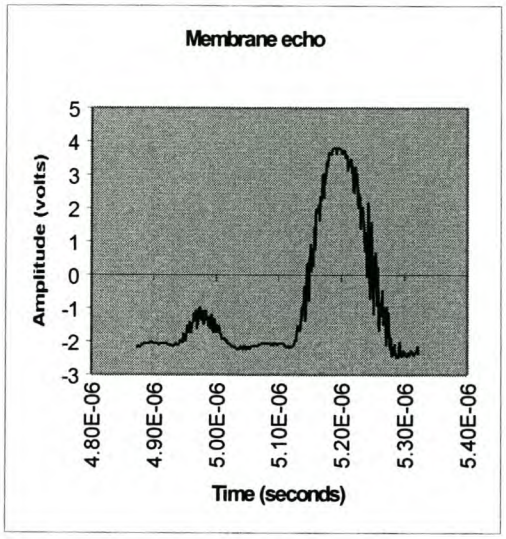

14 hours

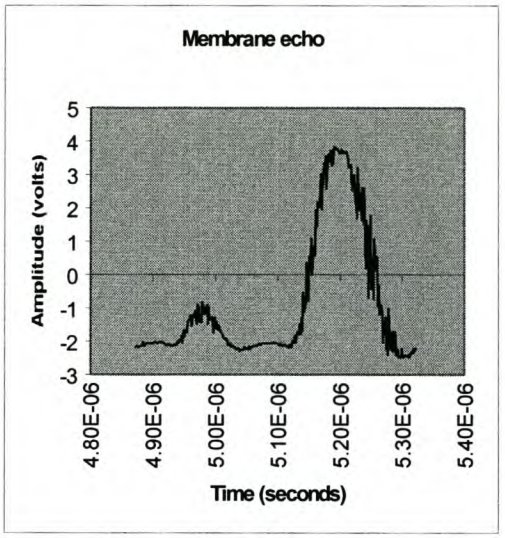

15 hours

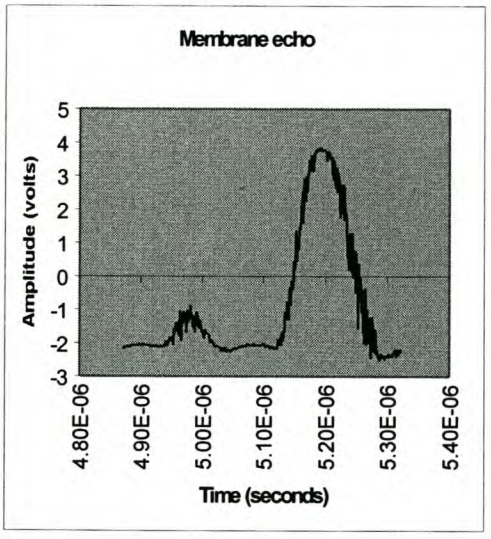

16 hours

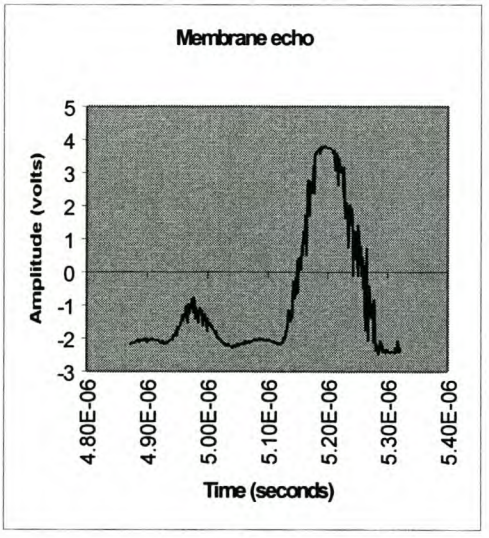

17 hours

Figure 5-16 - Ultrasonic responses for calcium sulphate experiment with 2.2 cm/s cross-flow velocity after 14, 15, 16 and 17 hours of operation.

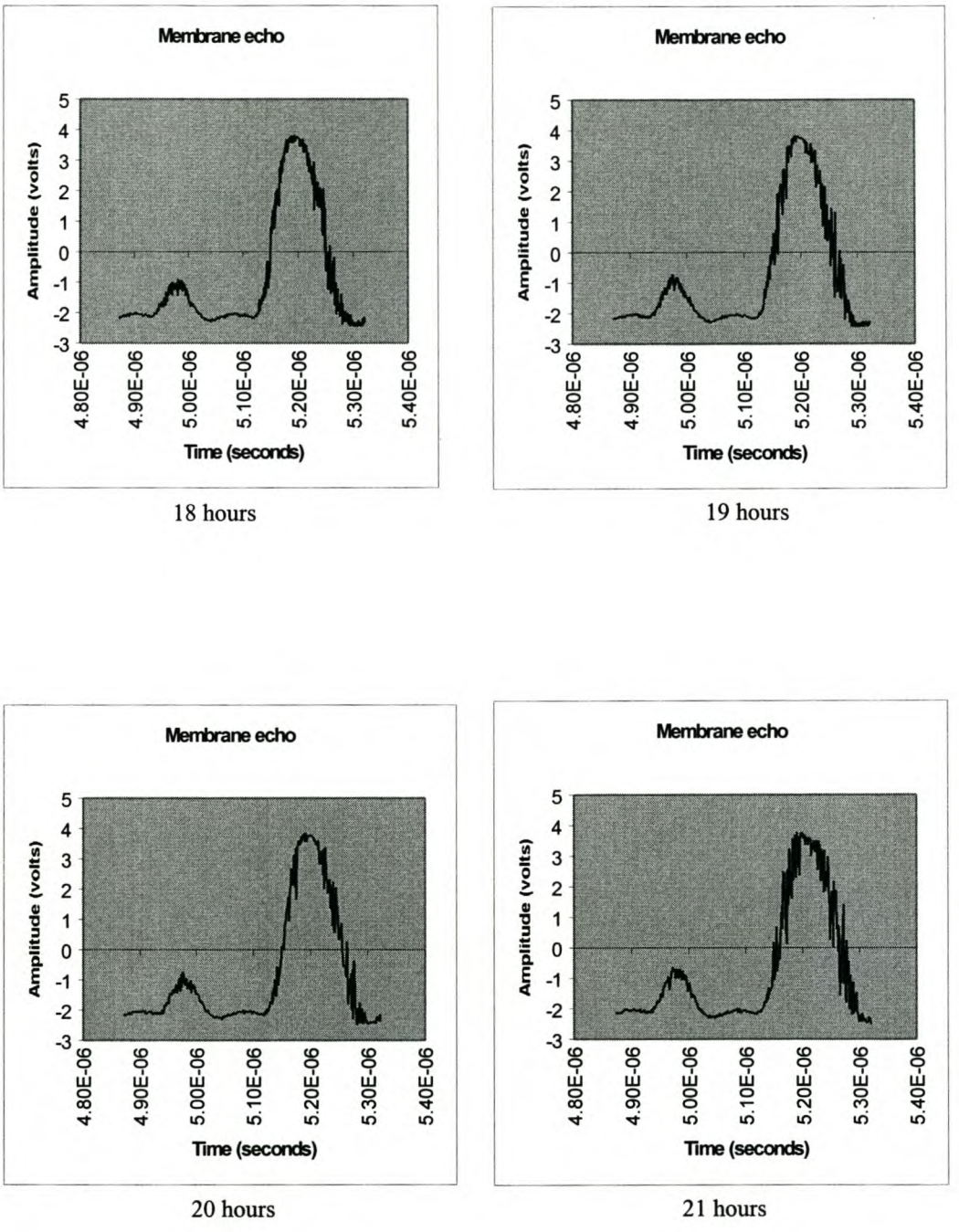

18 hours

19 hours

20 hours

21 hours

Figure 5-17 - Ultrasonic responses for calcium sulphate experiment with 2.2 cm/s cross-flow velocity after 18, 19, 20 and 21 hours of operation.

Morphological analysis again revealed complete membrane coverage. (Figure 5-18)

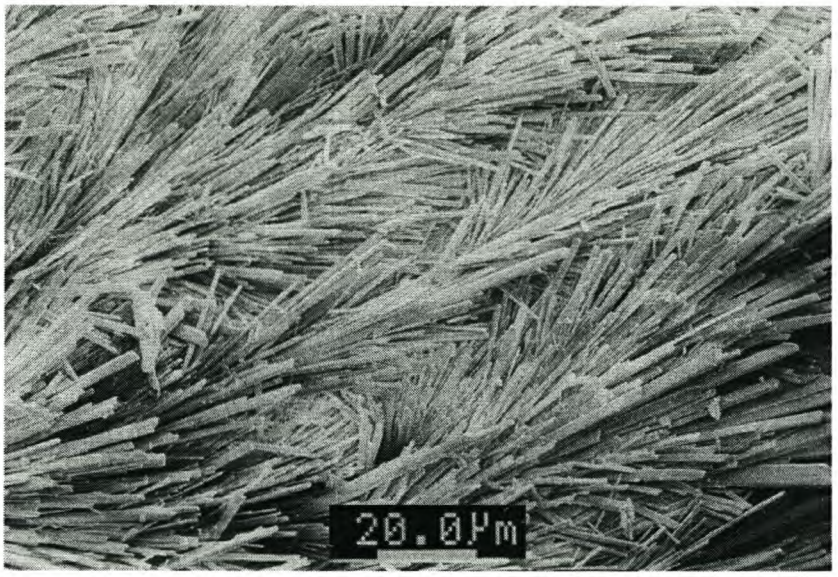

Figure 5-18 - SEM image of fouling layer.

A very noticeable feature from the longer fouling experiments is the unstability of the membrane echo over time. After 9 hours of operation, the echo started to show unstable characteristics with multiple small echoes on the main signal. It is believed that the high pressure on the feed side of the membrane led to the formation of deep stagnant pockets in the areas where the support plate pores are. This phenomenon was seen when the membrane was removed from the cell for morphological characterisation. These pockets could have had an influence on the membrane echo, which resulted in the multiple-echo-behaviour that was found above. The fact that the fouling layer echo remained rather stable is perhaps proof of it. However, more experimentation is needed before making definitive conclusions about any such effect. Another noticeable feature from this experiment was the movement of the fouling layer echo that was seen after 9 hours of operation. It seemed that an increase in fouling layer thickness was responsible for the time-domain movement of the signal. The initial fouling layer thickness was measured as 115 µm, but it changed to160 µm.

Figure 5-19 is the corresponding plot for the fux rate vs. the fouling layer echo amplitude.

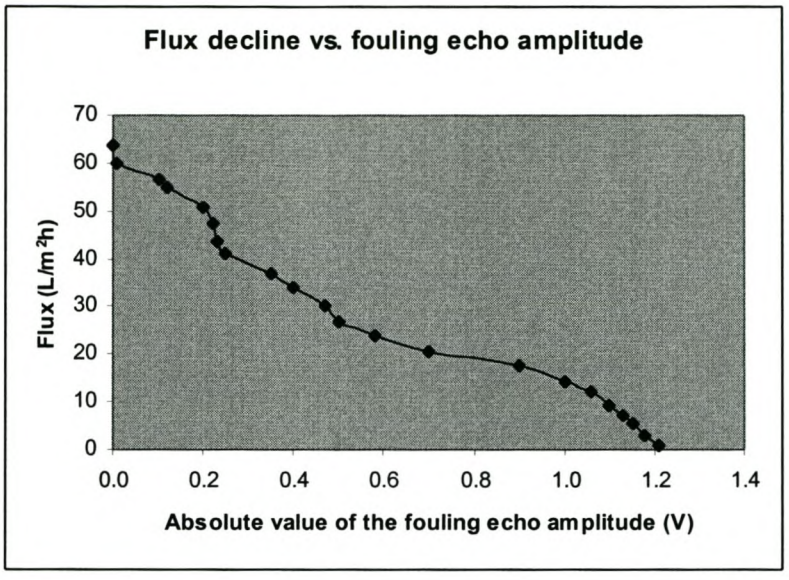

Figure 5-19 - Flux decline behaviour vs. the absolute value of the fouling layer echo amplitude for the calcium sulphate experiment with 2.2 cm/s cross-flow velocity.

Experiment with 2g/l calcium carbonate feed concentration and a cross-flow velocity of 50±15 ml/min (1.1 cm/s).

In the following experiment calcium carbonate fouling was investigated. The pressure was controlled at 22 ± 0.5 bar. Permeate flow behaviour of the 7 hour experiment is summarised in Figure 5-20.

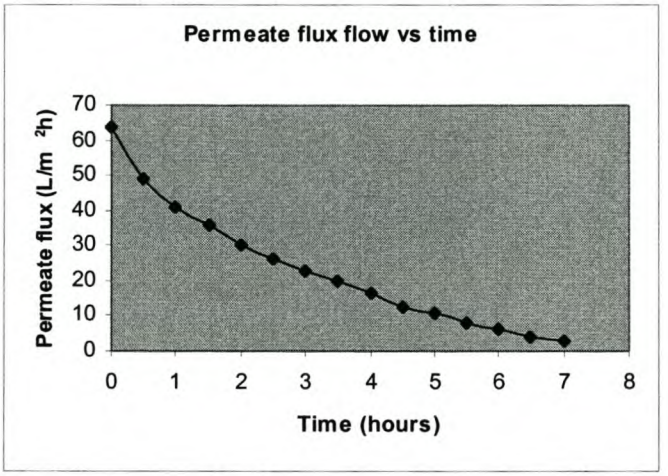

Figure 5-20 - Permeate flow vs. time data for calcium carbonate fouling experiment with 1.1 cm/s cross-flow velocity.

Ultrasonic responses:

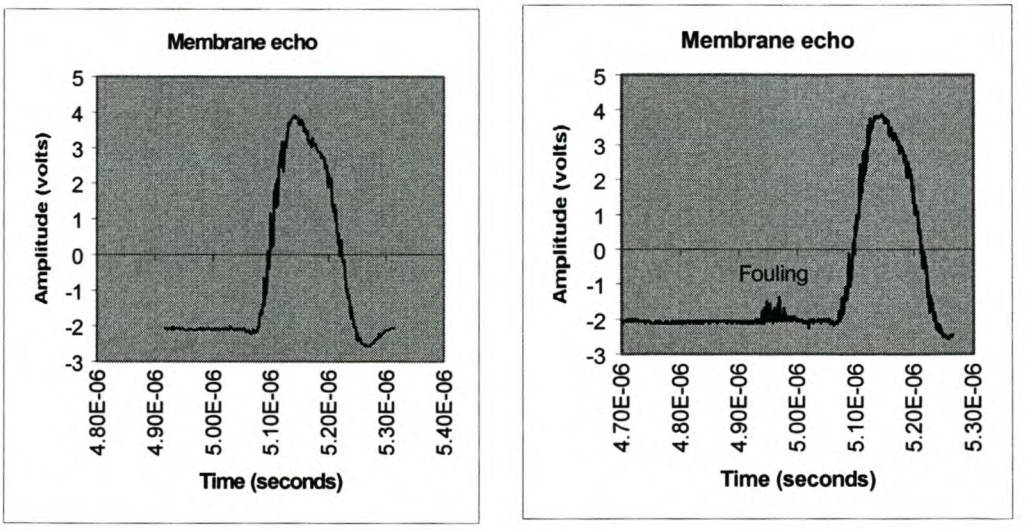

0 hour 1 hour

Figure 5-21 - Ultrasonic responses at the start and after 1 hour of operation for the calcium carbonate fouling experiments with 1.1 cm/s cross-flow velocity.

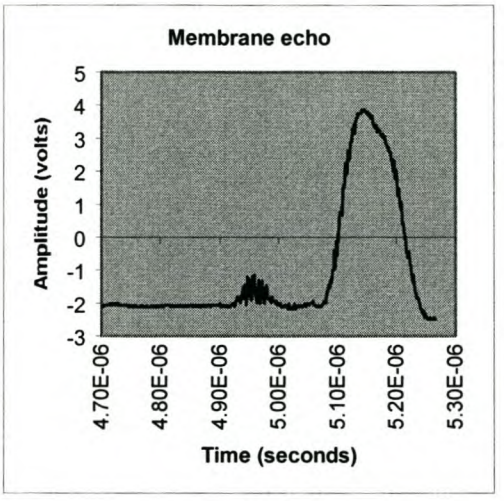

2 hours

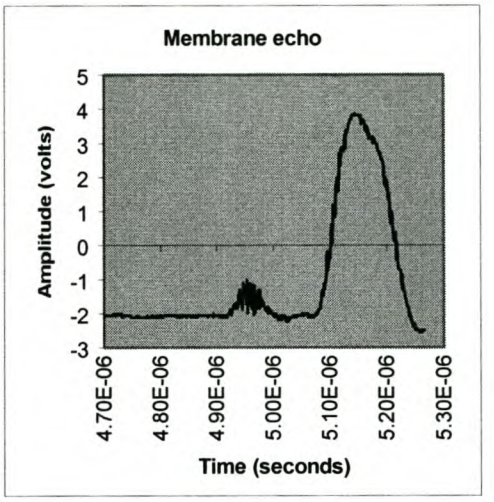

3 hours

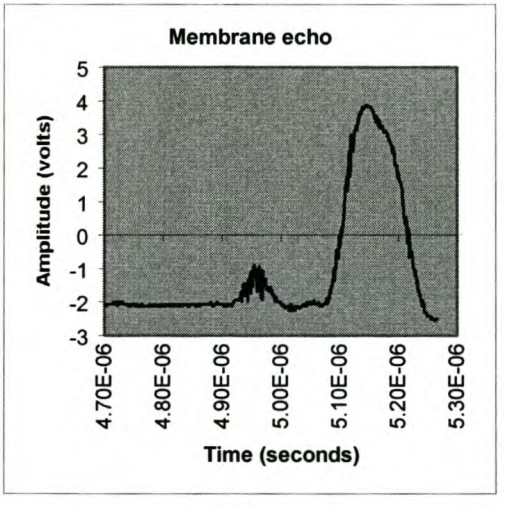

4 hours

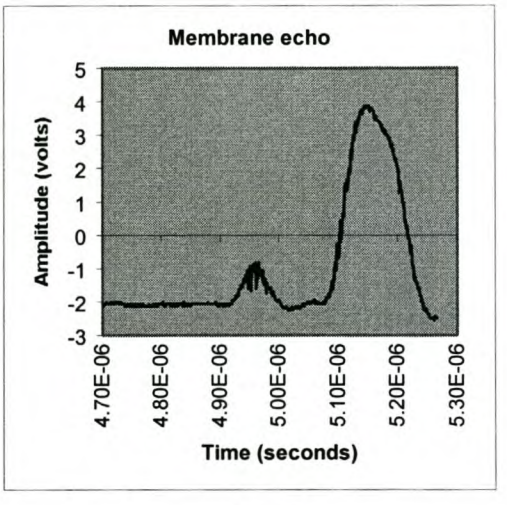

5 hours

Figure 5-22 - Ultrasonic responses for calcium carbonate experiment with 1.1 cm/s cross-flow velocity after 2, 3, 4 and 5 hours of operation.

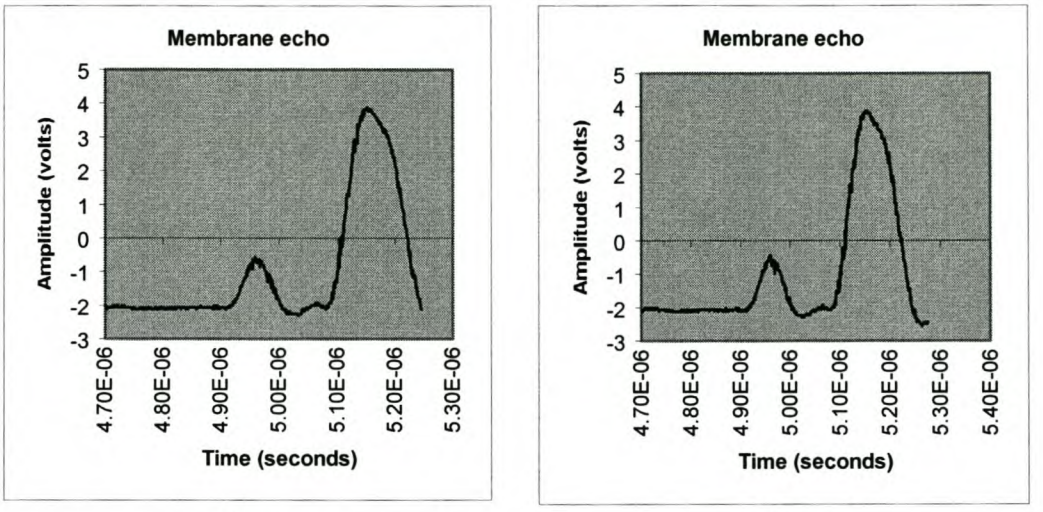

6 hours 7 hours

Figure 5-23 - Ultrasonic responses for calcium carbonate experiment with 1.1 cm/s cross-flow velocity after 6 and 7 hours of operation.

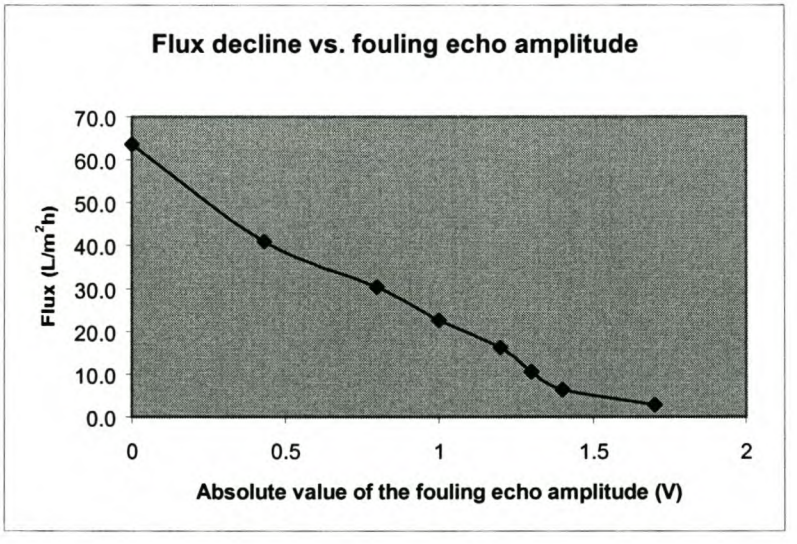

Figure 5-24 - Flux decline vs. the absolute value of the fouling echo amplitude for the calcium carbonate experiment with 1.1 cm/s cross-flow velocity.

The measured fouling layer thickness using UTDR was calculated as 130 μm.

In order to study membrane coverage, 4 experiments were done under exactly the same fouling conditions, with each experiment stopped after a specific time. Membrane samples were taken for SEM analysis after 1 hour, 2 hours, 3 hours and 7 hours of operation.

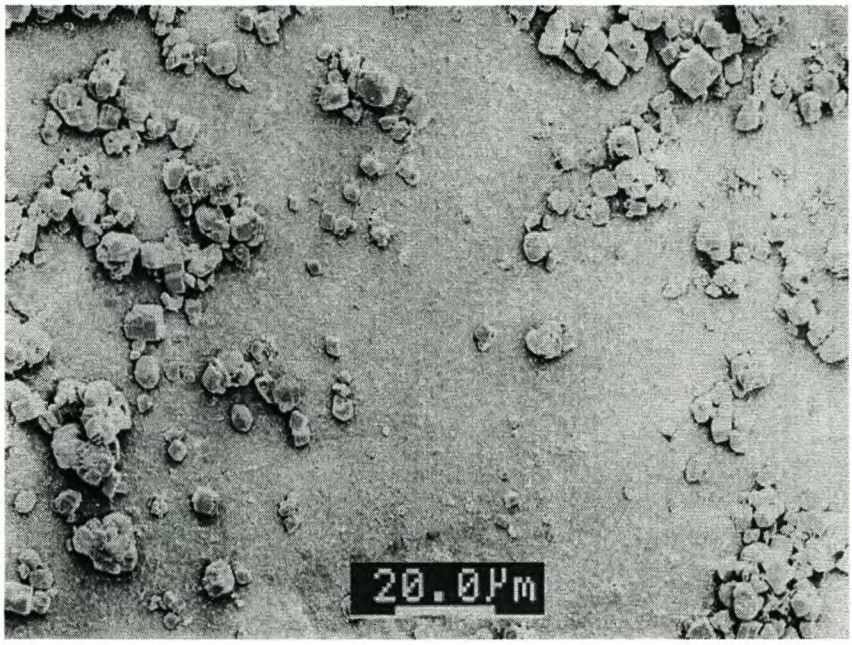

Figure 5-25 – Fouling layer after 1 hour of operation for the calcium carbonate experiment.

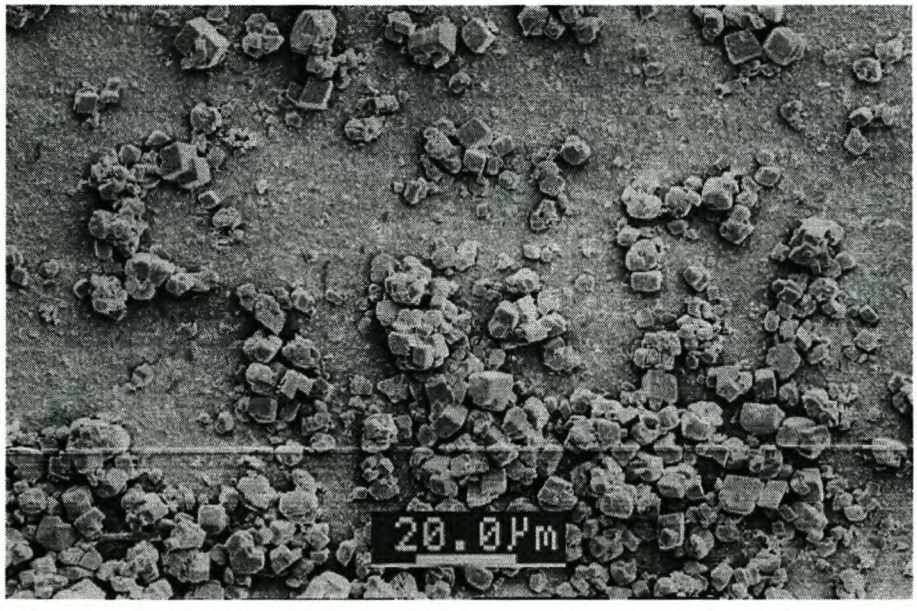

Figure 5-26 - Fouling layer after 2 hours of operation for the calcium carbonate experiment.

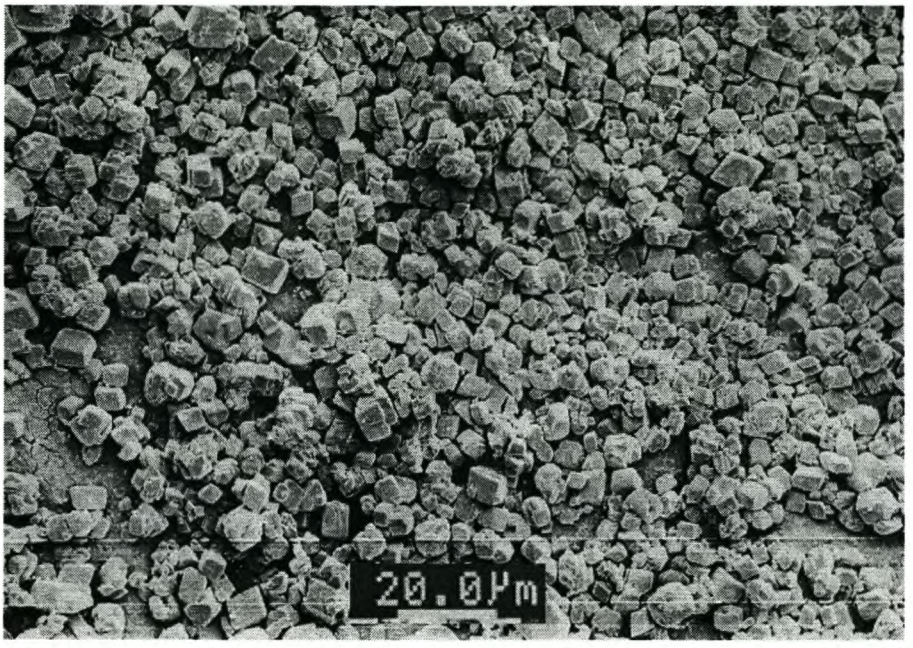

Figure 5-27 - Fouling layer after 3 hours of operation for calcium carbonate experiment.

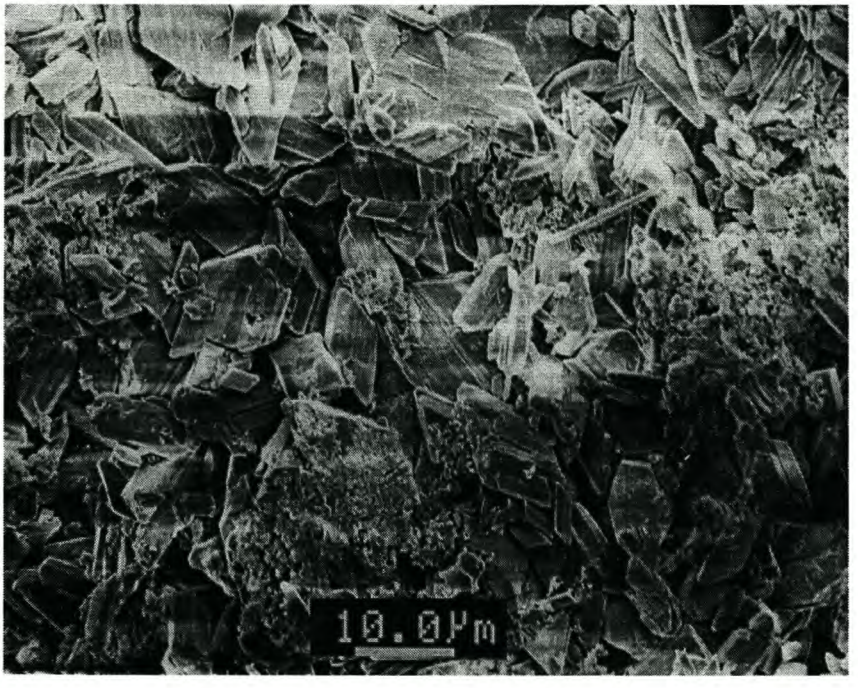

Figure 5-28 - Calcium carbonate fouling layer after 7 hours of fouling.

5.2.3 No cross-flow i.e. dead-end

The dead-end experiments showed the most significant changes in a very short time. Permeation rate values dropped to very low levels within 20 minutes and permeate measurements could not be performed accurately. The formation of a second echo in the time domain was almost immediately noticeable in the ultrasonic response. Morphological analysis of the fouled membranes revealed complete coverage of the surfaces.

Results of two different experiments will be discussed - one with the use of calcium carbonate as fouling agent, and the other with calcium sulphate.

Experiment with 2 g/l calcium carbonate feed concentration at 2.2 MPa (22 bar).

Ultrasonic responses:

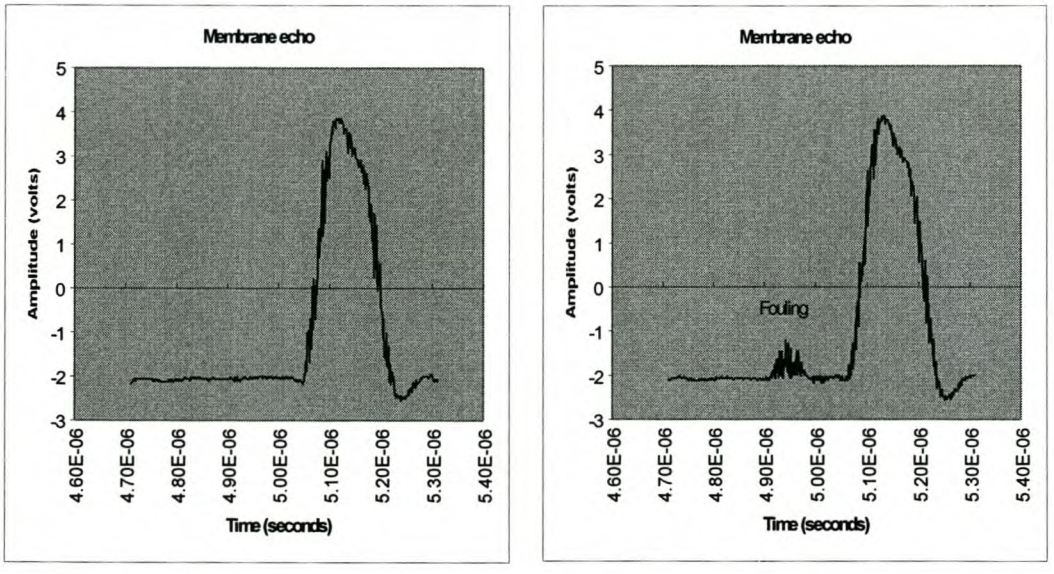

0 min 10 min

Figure 5-29 - Ultrasonic responses for calcium carbonate dead-end experiment at the start and after 10 min of operation.

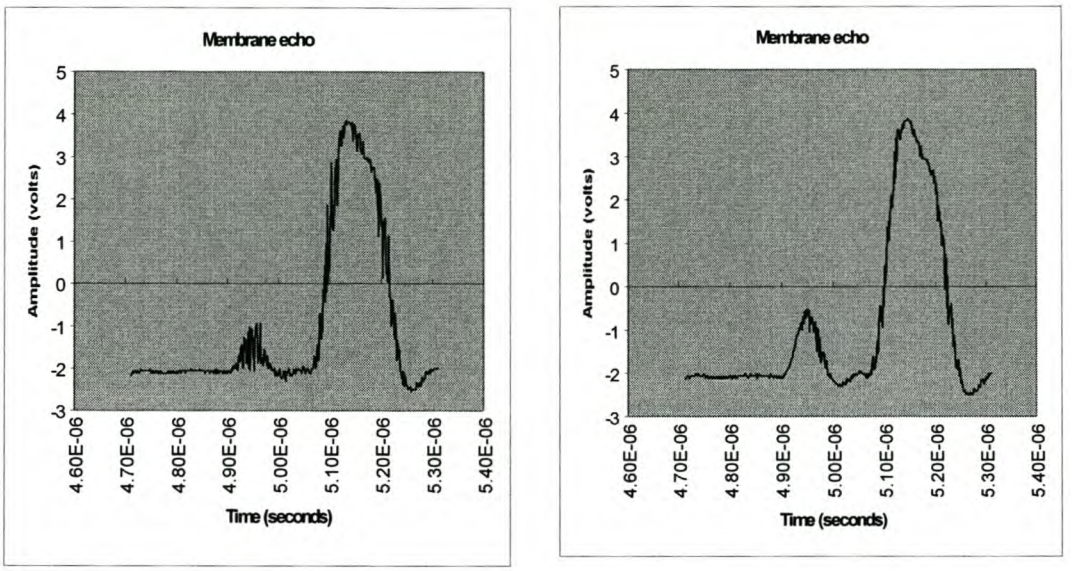

20 min 30 min

Figure 5-30 - Ultrasonic responses for the calcium carbonate dead-end experiment after 20 and 30 min of operation.

The UTDR fouling layer thickness was calculated on 135 μm.

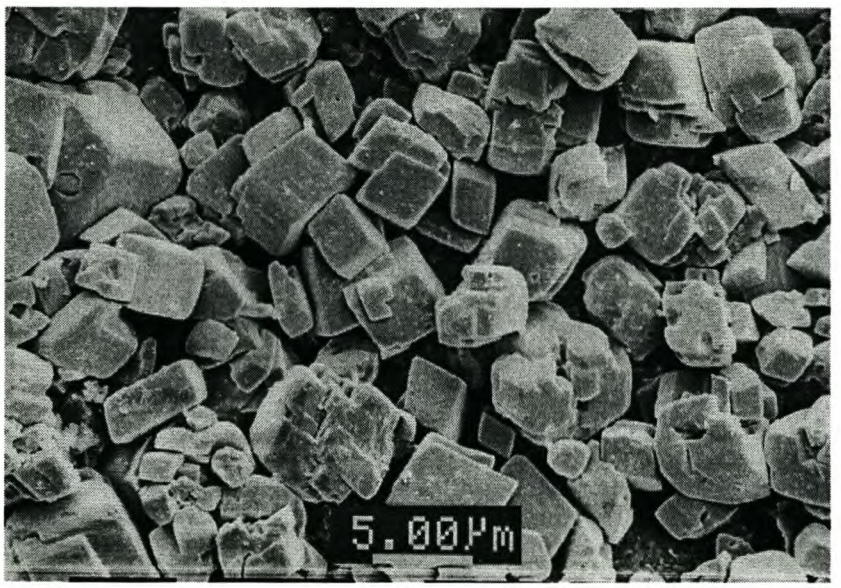

Figure 5-31 - Fouling layer of dead-end calcium carbonate experiment. Complete membrane coverage was observed.

Experiment with 2 g/l calcium sulphate feed concentration at 2.2 MPa (20 bar).

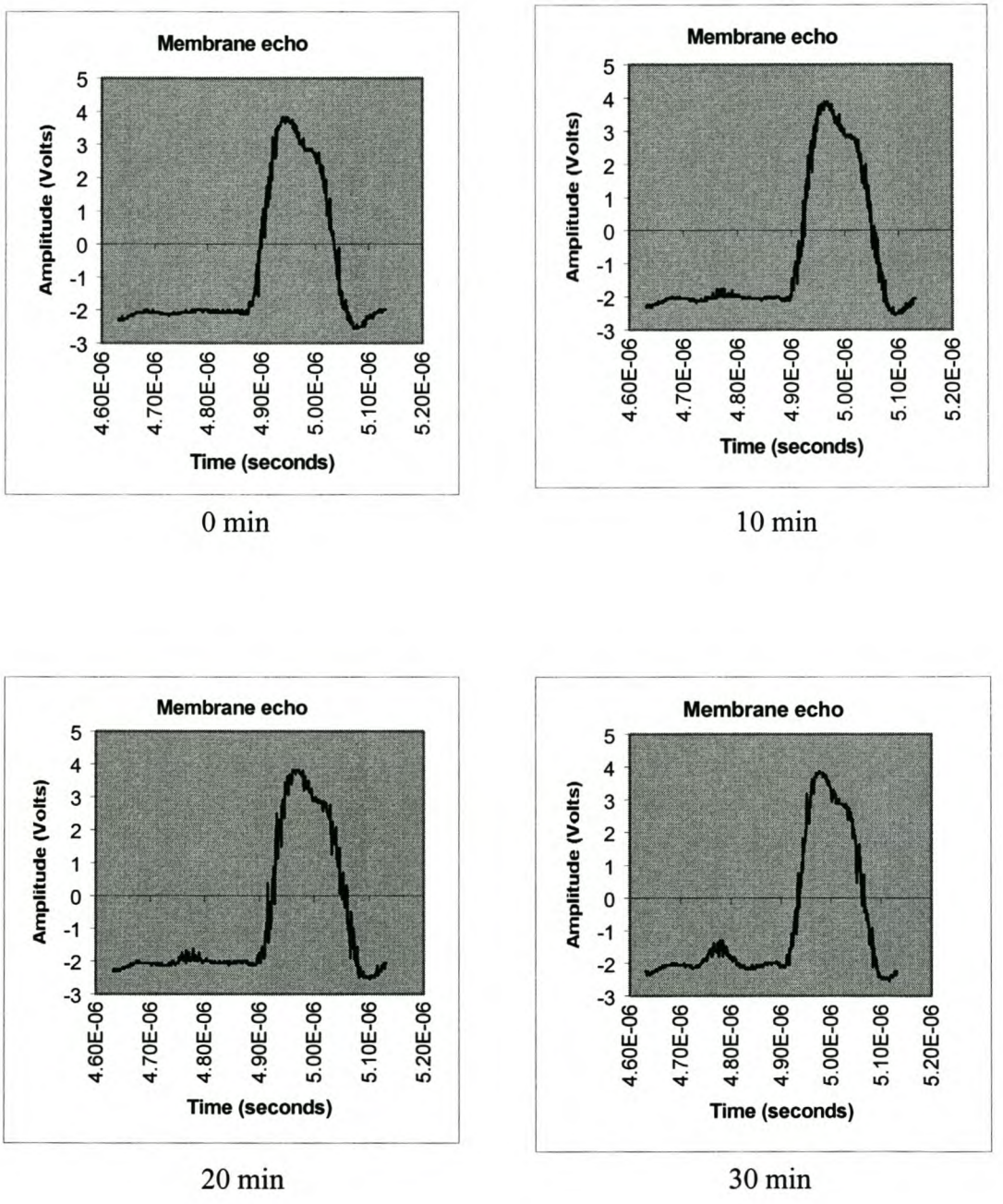

Figure 5-32 - Ultrasonic responses at the start and after 10, 20 and 30 min of operation for the calcium sulphate dead-end experiment.

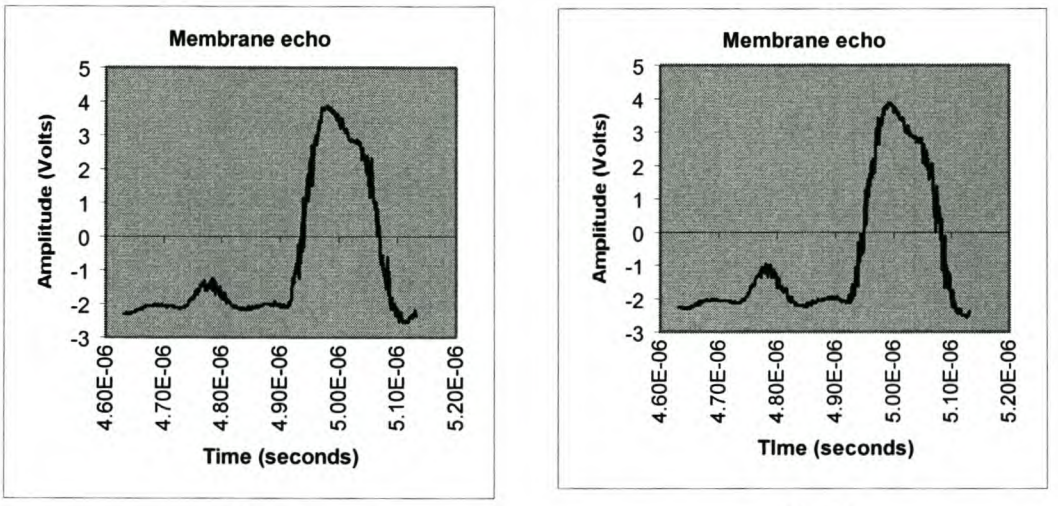

40 min 50 min

Figure 5-33 - Ultrasonic responses after 40 and 50 min of operation for the dead-end calcium sulphate experiment.

Complete membrane coverage was observed with a UTDR measured fouling layer thickness of 150 μm.

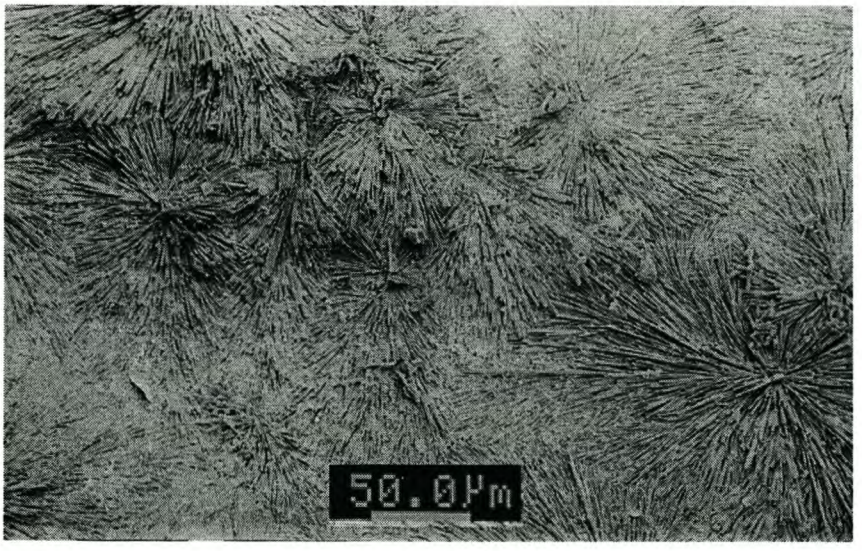

Figure 5-34 - Complete membrane coverage was observed with the SEM analysis.

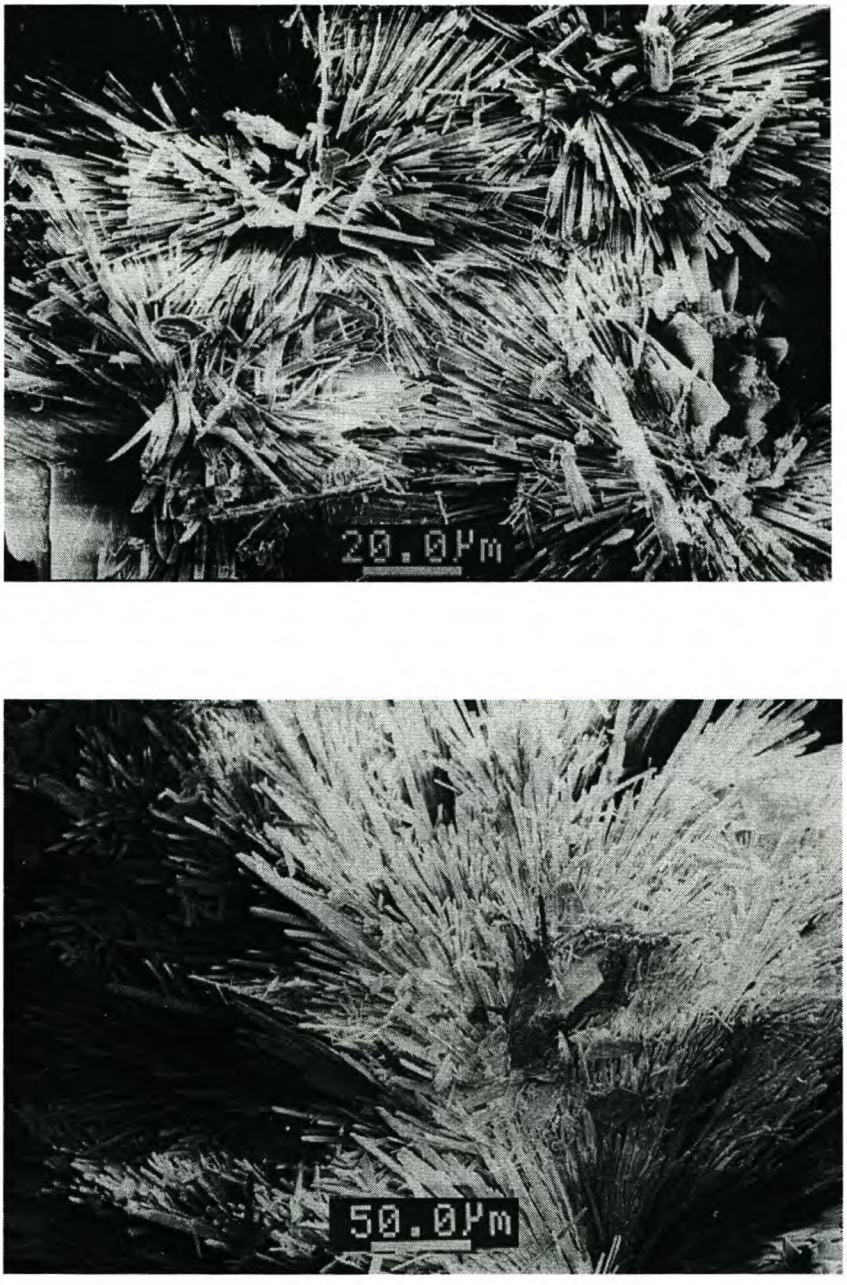

Figure 5-35 – SEM images of the fouling layer formed during the dead-end calcium sulphate experiment.

5.3 *Cleaning experiment*

To investigate the possibility of utilising the UTDR technique for monitoring fouling removal in real time, several experiments were carried out. The experimental procedure was to foul a membrane to steady state levels, after which it was cleaned with deionized water. No backwashing or flow reversal was done during the cleaning phase. The only change being the use of deoinized water. Both the fouling and cleaning phases were carried out at the same pressure and cross-flow velocity. Results of a typical experiment where a membrane was fouled with 2 g/l calcium carbonate and a cross-flow velocity of 50 ± 15 ml/min (1.1 cm/s) will be discussed. The pressure was controlled at 20 ± 0.5 bar.

5.3.1 Fouling phase

The fouling phase of the experiment was stopped after 9 hours of operation when permeate flow was too low to be measured accurately. (less that 0.1 ml/min) Measurements were made every 30 min. Figure 5-36 is a representation of the results.

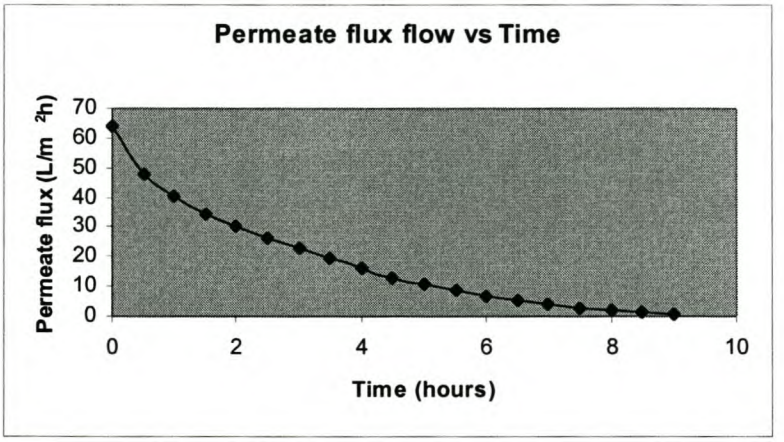

Figure 5-36 - Permeate flow data for the fouling phase of the cleaning experiment.

Ultrasonic responses:

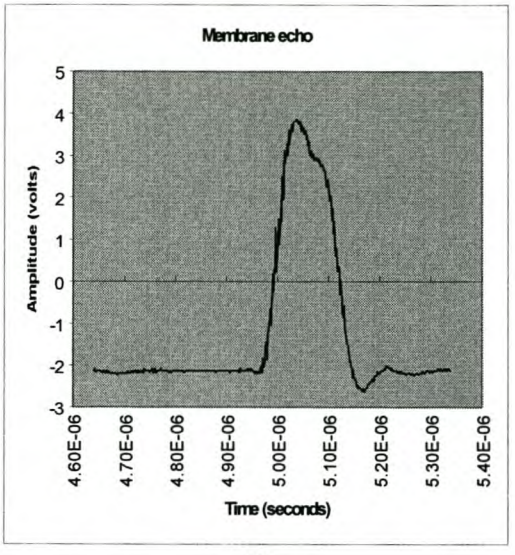

0 hour

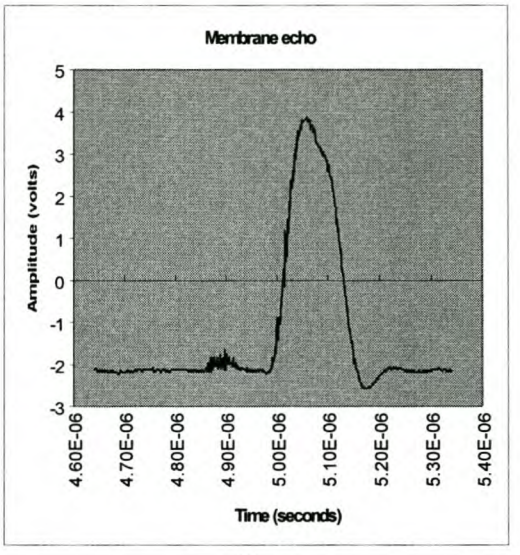

1hour

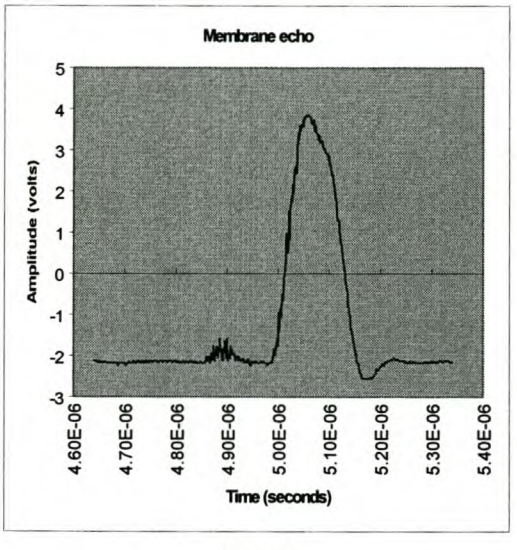

2 hours

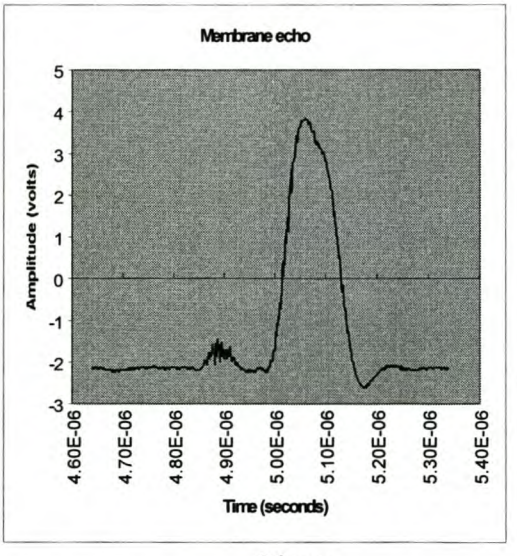

3 hours

Figure 5-37 - Ultrasonic responses at the start and after 1, 2 and 3 hours of operation for the fouling phase of the cleaning experiment.

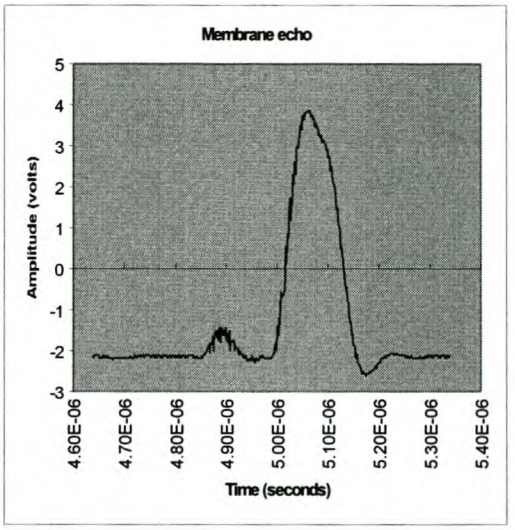

4 hours

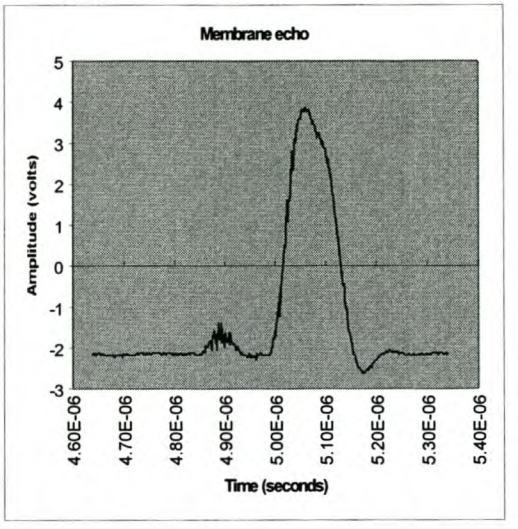

5 hours

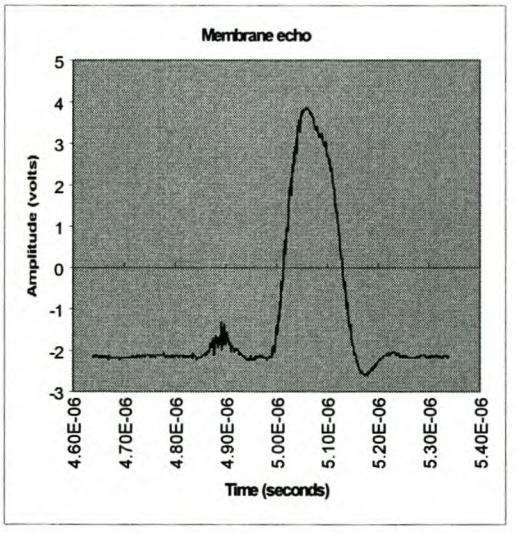

6 hours

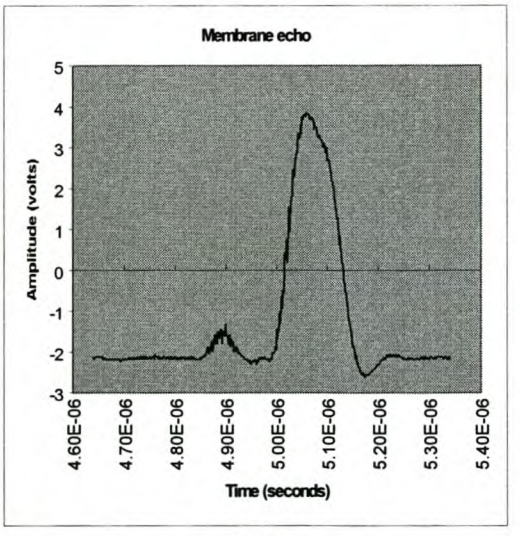

7 hours

Figure 5-38 - Ultrasonic responses after 4, 5, 6 and 7 hours of operation for the fouling phase of the cleaning experiment.

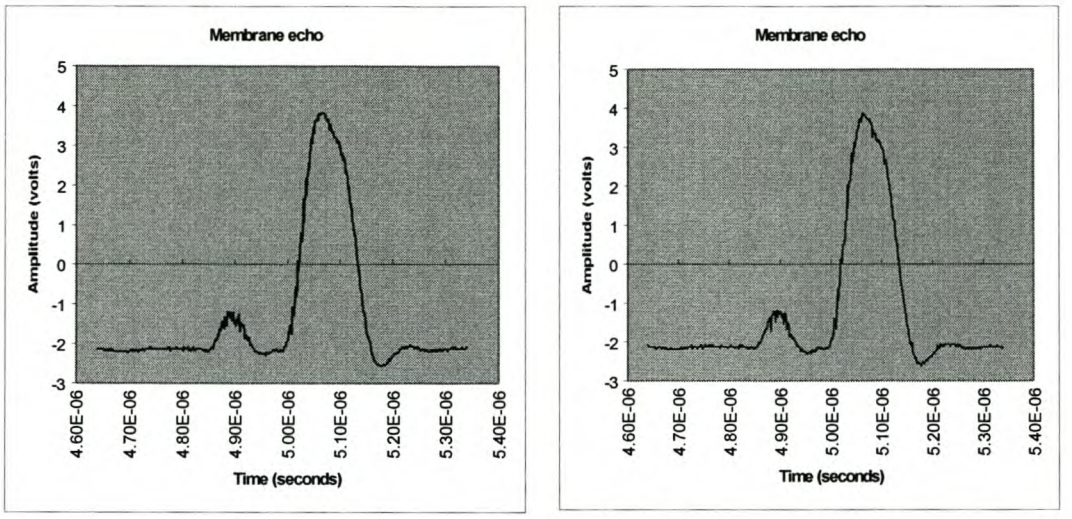

8 hours 9 hours

Figure 5-39 - Ultrasonic responses after 8 and 9 hours of operation for the fouling phase of the cleaning experiment.

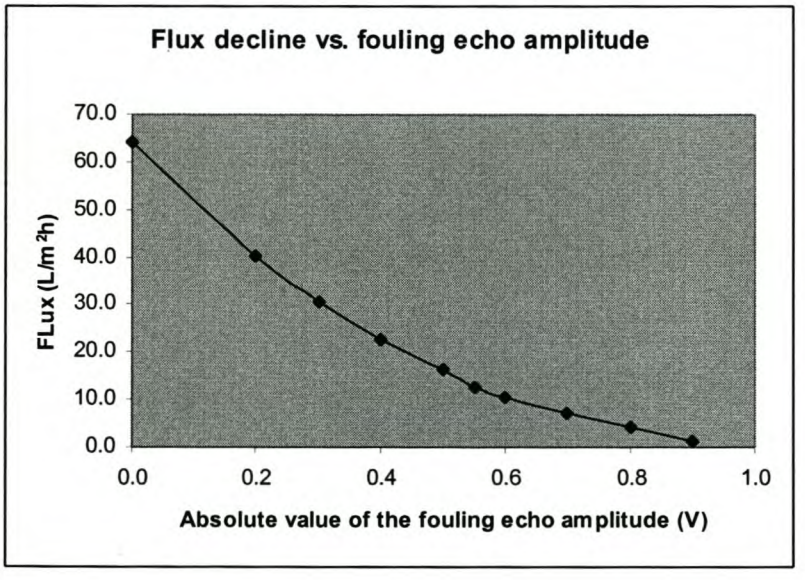

Figure 5-40 - Flux decline vs. relative absolute value of the fouling echo amplitude for the fouling phase of the cleaning experiment.

5.3.2 Cleaning

The cleaning phase was completed after 3 hours when no additional changes in the permeate flow and ultrasonic responses were seen. Although an increase in permeation rate was observed, the flowrate of the clean membrane at the start of the experiment was not obtained, even after 30 min of HCl treatment.

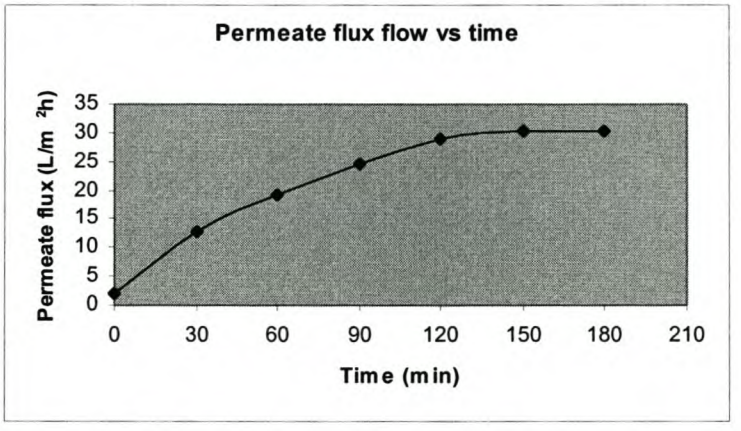

Figure 5-41 - Permeate flow vs. time curve for the water cleaning phase of the cleaning experiment.

Ultrasonic responses for the cleaning phase:

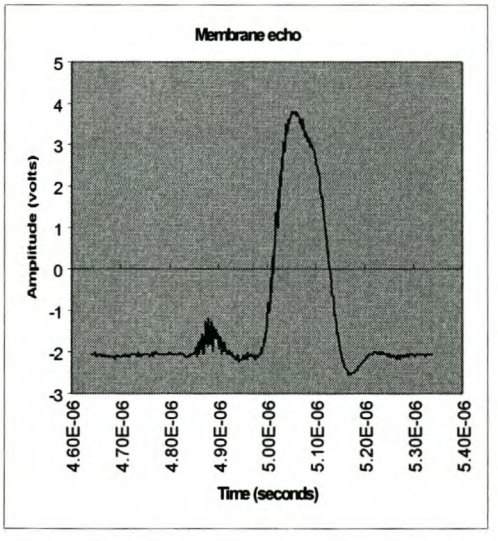

Start (0 hour)

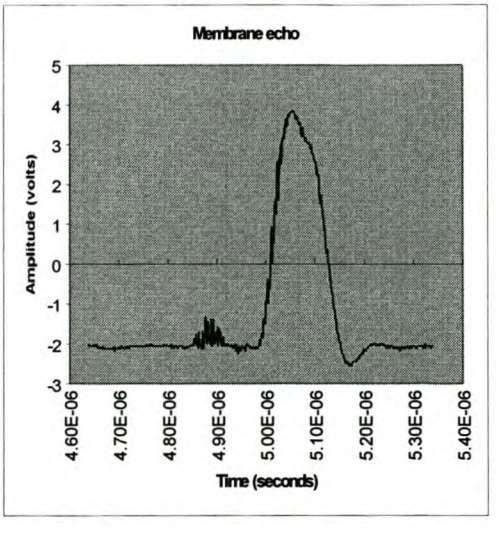

30 min

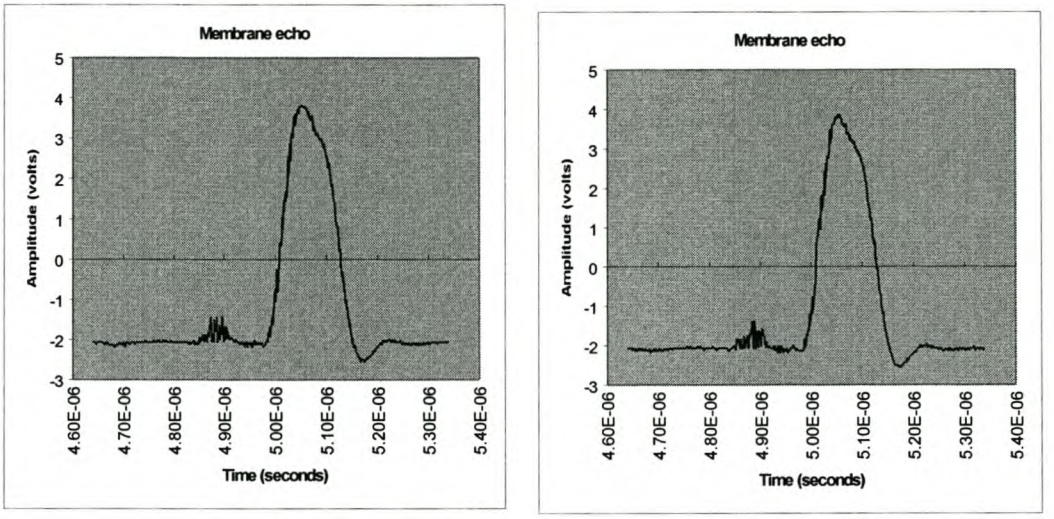

60 min

90 min

Figure 5-42 - Ultrasonic responses at the start and after 30, 60 and 90 min of operation for the cleaning phase of the cleaning experiment.

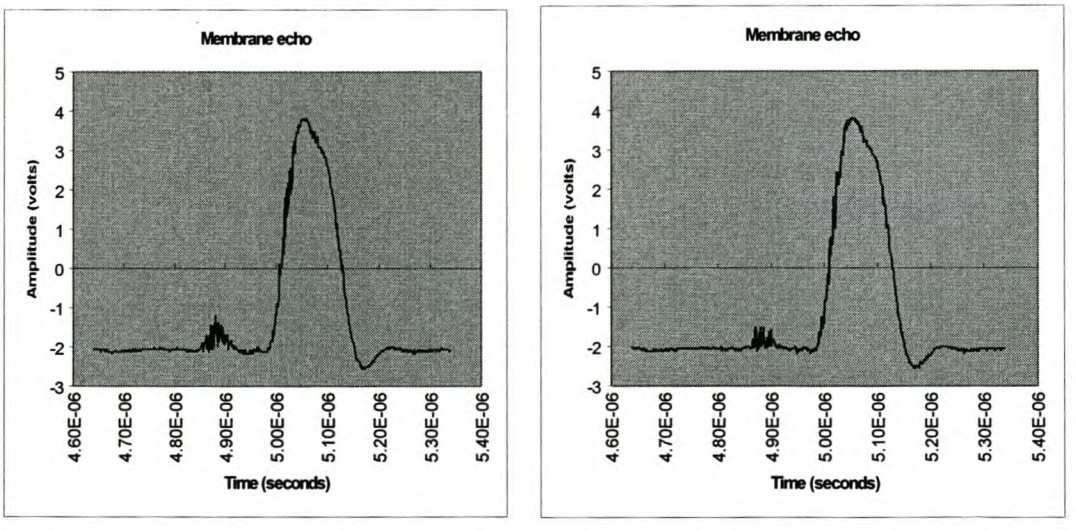

120 min

150 min

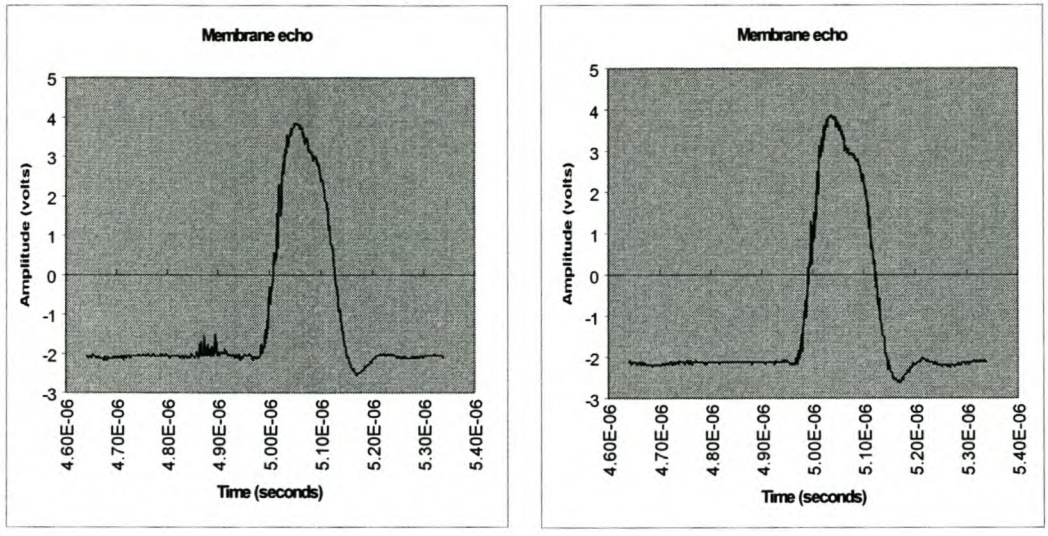

180 min

After 30 min treatment with diluted HCl

Figure 5-43 - Ultrasonic responses after 120, 150 and 180 min of operation, as well as the response after treatment with hydrochloric acid, for the cleaning phase of the cleaning experiment.

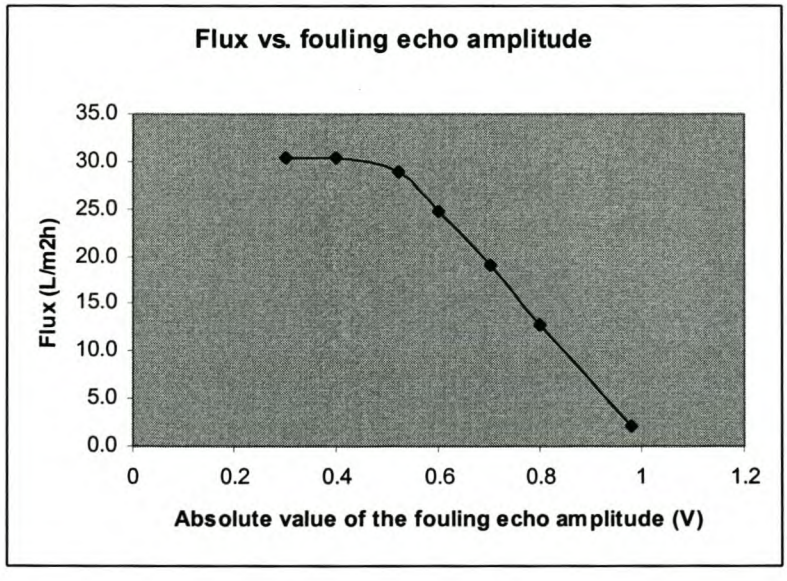

Figure 5-44 - Flux rate vs. the absolute value of the fouling echo for the cleaning phase of the cleaning experiment.

Morphological analysis of the membrane after the cleaning phase with pure water revealed that a fouling layer was in fact still visible on the membrane. After treatment with diluted HCl, the membrane was almost 100% clean. (Figure 5-46)

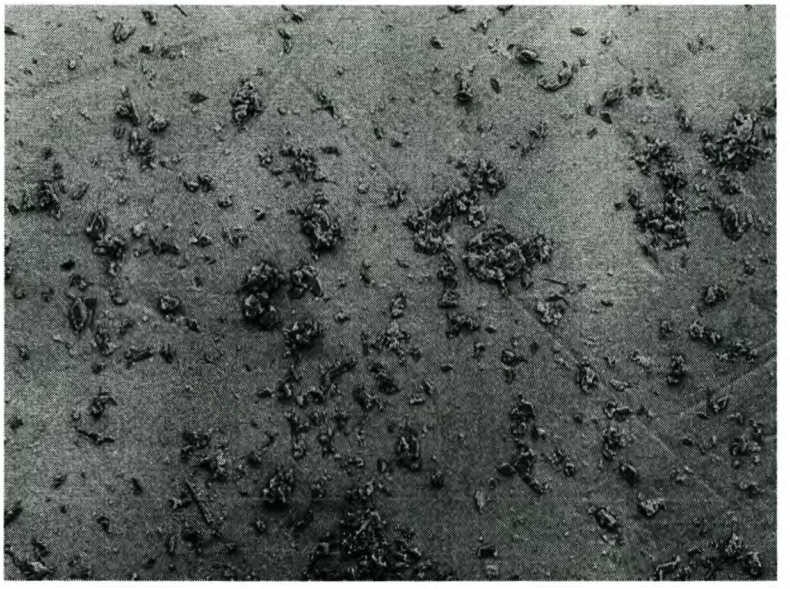

Figure 5-45 - Fouling layer after 180 minutes of cleaning with water

Figure 5-46 - Membrane after 30 min treatment with diluted HCl

5.4 Interpretation of results

During fouling conditions, rejected particles will deposit on top of the membrane and form a cake layer, which is the starting point for fouling. The particle layer on top of the membrane has a different acoustic impedance than the bulk solution, and thus the UTDR technique is able to observe its presence. The formation of the second echo before the main membrane echo, is a result of the acoustic impedance change between the bulk solution and the particles in the fouling layer.

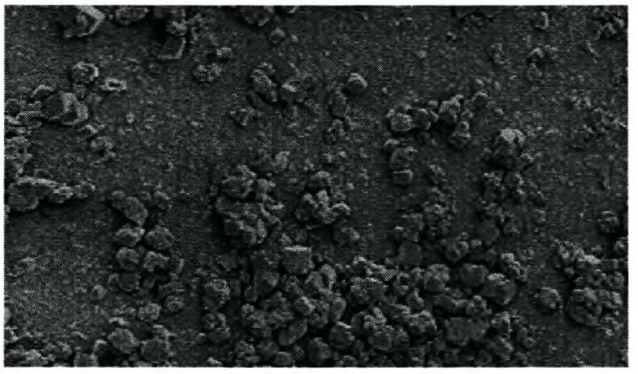

Figure 5-47 – Cluster growth fouling on the membrane

As fouling growth proceeds, time-domain movement of the fouling echo was expected as a result of an increase in the fouling layer thickness. Although experienced during one of the experiments, it was not a general trend. At fouling initiation, the UTDR technique measured the same spread of layer thickness as when the membrane was completely fouled; the only difference had been in the fouling echo's amplitude. This behaviour is difficult to explain, but it is believed that the ultrasonic signal measures the layer thickness caused by concentration polarisation at the salt activation point, but this is not necessarily an indication of the fouling layer cake thickness at early times. The smaller echo is a result of the fact that the acoustic impedance change between the bulk solution and this layer is very small and a sharp, clear echo is not obtained. However, an increase in fouling and formation of the cake layer as seen in the SEM images, is responsible for a sharper and clearer fouling layer echo.

SEM analysis showed that fouling initiation and growth starts in the form of clusters that grow on the membrane. The longer the fouling experiment, the more clusters formed until the whole membrane was covered with a uniform fouling layer. If more clusters are covering the membrane, a denser fouling layer is formed, and a bigger acoustic impedance change between the membrane and the layer is expected. This would mean a sharper reflection, and thus an echo with bigger amplitude is seen on the oscilloscope. Figure 5-48 and Figure 5-49 illustrates this theory.

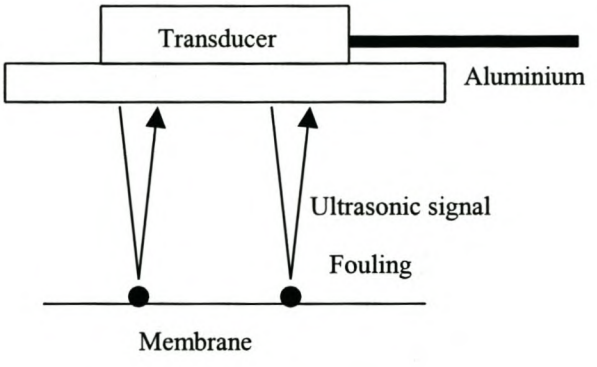

Figure 5-48 - Fouling initiation

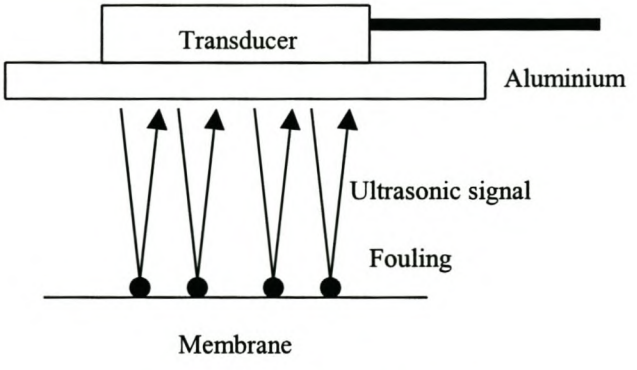

Figure 5-49 - Fouling layer growth

The phenomena that the ultrasonic technique is in fact measuring fouling layer thickness, is proved by the static experiment (Figure 5-2) as well as the cleaning experiments. During the static experiment, clean water was flowing over the membrane during cross-flow conditions, so no cake layer could have been formed as a result of a seeded feed. The only layer on top of the membrane was the compact fouling layer, which was measured to be 70 μm.

This hypothesis was also proved during the cleaning experiment when pure water was flowing over the membrane. During cleaning, the technique measures only the fouling layer, as no cake layer can form on top of the membrane as a result of a fouling agent in the water. Still, no movement of the echo was seen, with the only change being the fouling echo amplitude that vanished over time. Of course one can argue that the cleaning phase is responsible for fouling layer dissolution, and a decrease in particle concentration is experienced on top of the membrane. This might not mean all particles decrease equally in size, so that part of the barrier is actually as thick as the original fouling layer. This situation would give a signal similar to the cake layer, but with a reduced amplitude, and could continue until the fouling layer is completely dissolved. The time-domain measurement could thus not always be an accurate indication of fouling layer thickness. However, the important factor to realise is the disappearance of the second echo, which is a clear indication of fouling layer removal.

Results from the dead-end experiments indicate that the ultrasonic technique is able to monitor rapid fouling layer growth very effectively. The unstable fouling layer echo that formed during these experiments is typical of rapid particle movement and clogging on top of the membrane. In fact, fouling layer growth during dead-end conditions is very exciting, as it was so rapid that the naked eye could see changes in the fouling layer echo within seconds. This makes it very useful to study cleaning techniques.

These results show that UTDR is an effective way to monitor concentration polarisation and fouling on membranes.

5.4.1 Differences in calcium carbonate and calcium sulphate fouling

A membrane fouled with calcium carbonate seems to give a sharper, clearer echo than with calcium sulphate. Both dead-end and cross-flow conditions gave the same results. The fouling layer of calcium sulphate consists of needle shaped crystals or rosettes, stretching randomly over the membrane, while calcium carbonate appear to have more consistency in forming a uniform fouling layer.

The sharper echo is a result of the more uniform fouling layer that has higher density. Due to the higher density, the acoustic impedance change between the membrane and the fouling layer is bigger and a better reflection is seen. This phenomenon is seen in the clear, sharp reflection from the compact membrane fouling layer that is very dense and uniform. (Figure 5-2)

Under the same fouling conditions (cross-flow velocity and concentration of fouling agent), the rate of clogging between calcium carbonate and calcium sulphate seem to be more or less the same, although calcium carbonate gives a better, sharper reflection. The URDR technique was unable to indicate any significant difference in fouling layer thickness between calcium carbonate and calcium sulphate fouling respectively.

5.5 *Results of tests performed on the spiral-wound module*

5.5.1 Experiment with the flow distributor used

Figure 5-50 – Ultrasonic reflections at the 1st port with the flow distributor used

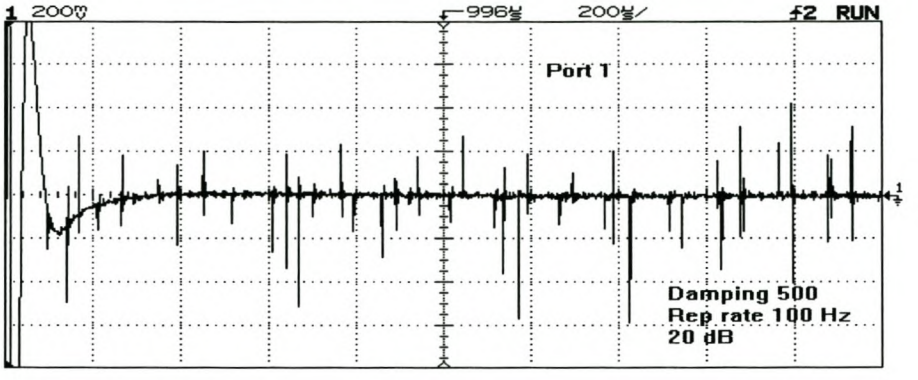

Figure 5-51 – Ultrasonic reflections at the 2nd port with the flow distributor used

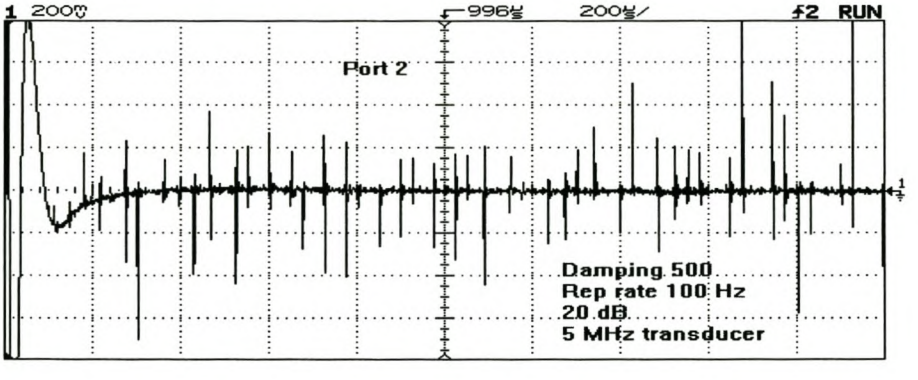

Figure 5-52 – Ultrasonic responses at the 3rd port with the flow distributor used

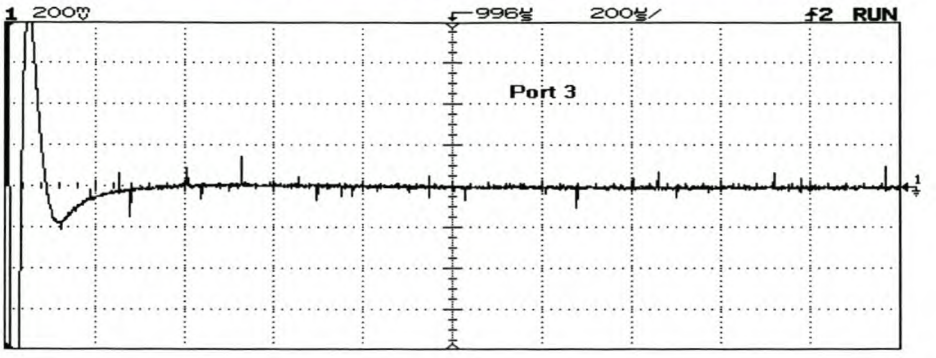

Figure 5-50, Figure 5-51 and Figure 5-52 are reflections that were taken from the various ports after an hour of operation at 2g/l calcium carbonate concentration, 20 bar operating pressure and 15 % permeate recovery. At port 3, (Figure 5-52) which is at the end of the module, no echo was found. This behaviour can be explained as the existence of an air barrier in one of the membrane outerlayers. It is very significant, as it indicated a stagnant zone in the membrane; i.e. the whole membrane was not wetted and thus used. However, it should be mentioned that the membrane that was used was brand new and the running time was perhaps not long enough to completely wet the membrane, especially because it was at the end of the module where flow is likely to be less.

A definite difference in the number of reflections between the first- and second port images are clear from a comparison between Figure 5-50 and Figure 5-51. At the first port (Figure 5-50), less reflections is seen. This is most probably the influence of the flow distributor. Due to very high turbulence at the beginning of the module, it is possible that some of the signals "get lost" in air bubbles. It is believed that carbon dioxide is formed while the fluid is forced through the flow distributor, as analysis of the permeate and brine passages showed traces of it. The mechanism is believed to be similar to cavitation. Cavitation can be accompanied by release of heat as the microspheres collapse. An increase in water temperature is most likely the result of this behaviour. The carbon dioxide is probably formed according to the following reaction (Furukawa, 1999):

$$H^+ + HCO_{3-} = H_2CO_3$$

$$H_2CO_3 = H_2O + CO_2$$

Two-phased flow could therefore be created while the fluid is passing through the flow distributor. If this were indeed the case, concentration polarisation would also be affected in the sense that ions are carried away from the membrane surface more rapidly. The result is lower osmotic pressure at the membrane surface, leading to greater net driving force:

Equation 21.....$J = kA(dP - dp)$ where

J = product flow

k = membrane constant

A = membrane surface area

dP = net driving pressure (applied pressure – product pressure)

dp = net osmotic pressure ($p_{membrane} - p_{product}$) and the osmotic pressure is dependent on concentration

Another effect is that the salt rejection also improves, since the salt passage through the membrane is concentration related.

Equation 22.....$J_i = k_i(C_w - C_p)$ where

J = solute (salt) flux

k_i = membrane permeability coefficient

ß = concentration polarisation coefficient

C_b = concentration in bulk stream

C_p = concentration in product

$C_w = ßC_b$ = concentration at membrane

If the concentration at the membrane surface is less, ($ßC_b - C_p$) is reduced, and less ion transport will be observed, resulting in improved water quality.

To test the hypothesis, the flow distributor was removed and the following images were taken under the same conditions as the previous experiment:

5.5.2 Tests without the flow distributor

Figure 5-53 – Ultrasonic reflections at the 1st port without the use of the flow distributor

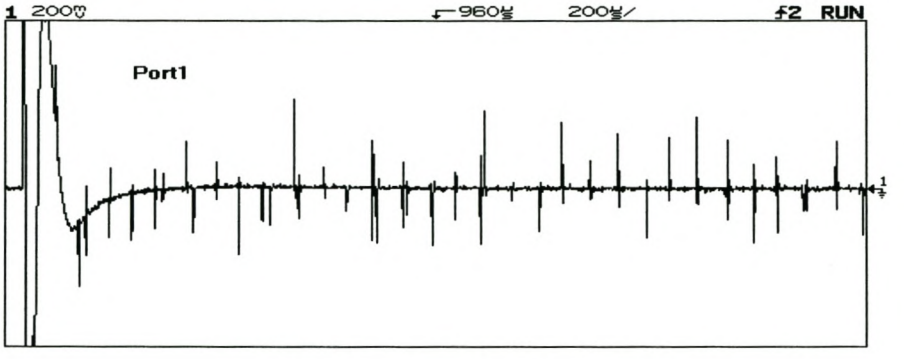

Figure 5-54 – Ultrasonic reflections at the 2nd port without the use of the flow distributor

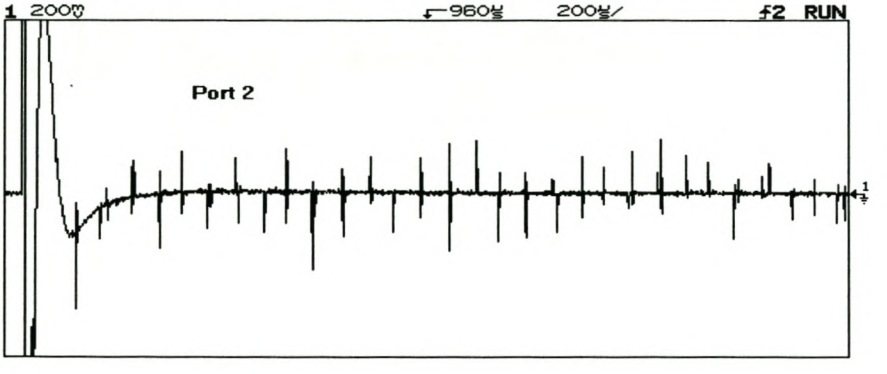

Figure 5-55 – Ultrasonic reflections at the 3rd port without the use of the flow distributor

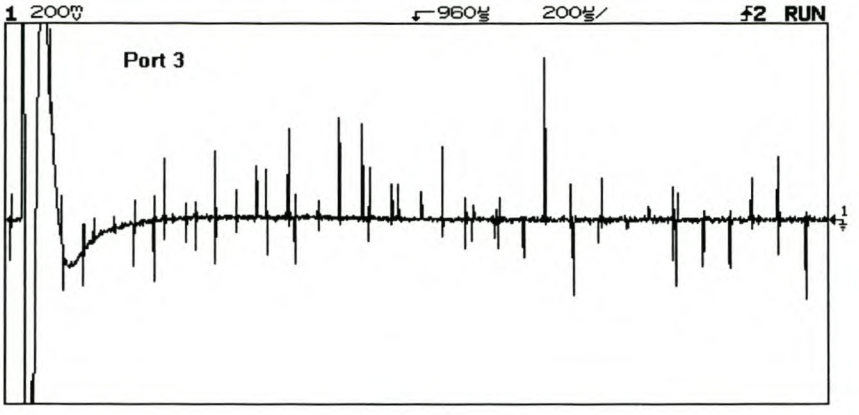

From these images, the phenomenon that was found when the flow distributor was used is not visible. More evenly spaced time-amplitude reflections are seen for the various ports. It is therefore possible to make the assumption that the flow distributor is indeed responsible for gas formation.

The echoes from the third port (Figure 5-55) indicated that an air barrier was in fact responsible for the previous result when no echo was found. The membrane was completely wetted after longer running time was allowed.

5.5.3 Magnetic field effect

Dramatic changes are seen when the electric field is switched on (Figure 5-57). However, some doubt exists in whether these changes are made by changes within the module itself, or whether the electro-magnetic field is influencing the signal in another way. The magnetic fields are responsible for some harmonic effects, but not in a wide frequency band as that which was found in Figure 5-57. The disturbance from the magnetic field comes from noise that is picked up through the transducer cable. This was found by holding the transducer next to the coils when the module was not running. The cable should therefore be coated with a material to weaken this effect.

Figure 5-56 – Ultrasonic reflections at port 2 with the coils switched off

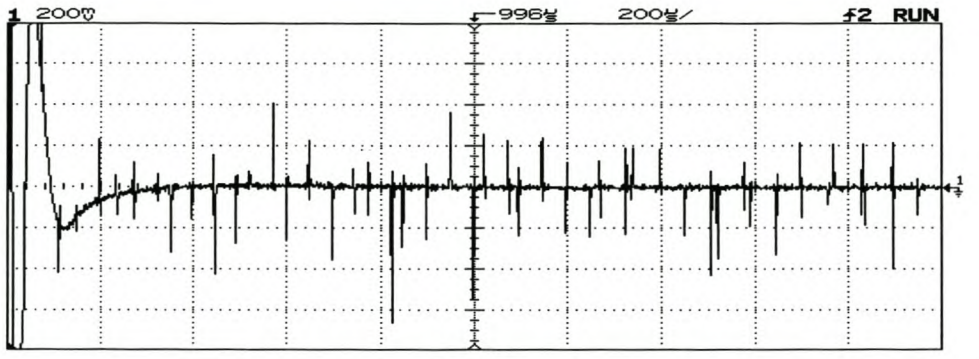

Figure 5-57 – Ultrasonic reflections at port 2 with the coils on.

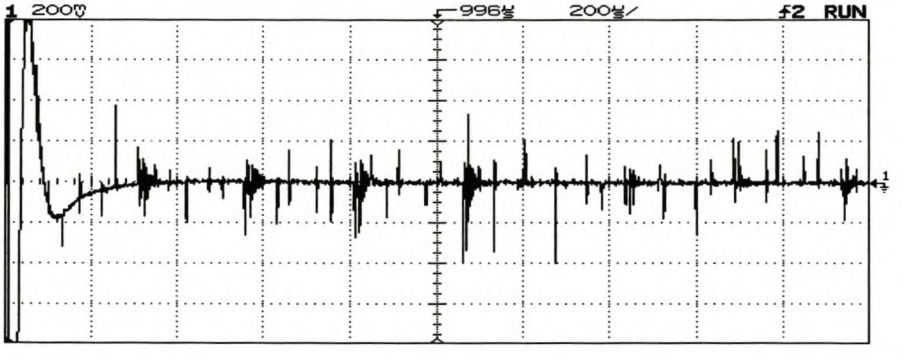

An increase in the bulk solution's density, typical of rapid particle movement away from the membrane can lead to the results that were found above, but it can also be harmonics from the coil drive that is influencing the signal. If the last case was responsible for the phenomena, it is difficult to explain why the echo has such a wide bandwidth, as this was not the case when only the disturbing influences of the magnetic field was investigated.

The membrane was not fouled due to problems with precipitation in the feed tank. After an hour of operation the temperature of the water had increased to 30 deg celcius which resulted in precipitation of the added fouling agent, calcium carbonate, in the.feed tank. A heat exchanger or small cooling tower was needed to keep the temperature down, but were not available. The influence of fouling was thus not investigated. More experiments are needed.

6 Conclusions

The main conclusions of this research can be summarised as follows:

- Ultrasonic-time-domain-reflectometry is capable of visualising membrane compaction and fouling noninvasively in real time.

- The technique's ability to detect changes in the fouling layer will clearly assist in understanding the mechanisms of fouling better.

- The fact that the ultrasonic technique monitors changes on the membrane surface makes it very suitable to study membrane cleaning. The power of the technique lies in its capability to detect changes in fouling layer morphology in real time. The response is much quicker than permeate measurements, which makes it very suitable to study cleaning techniques. The effectivity of various cleaning techniques can be studied with UTDR.

- Fouling layer thickness measurements with **Eq. 20.....dS = 0.5 C dT** are not necessarily an accurate indication of the fouling layer thickness. The second echo's amplitude (fouling layer echo) should more be seen as an indication of the state of the fouling layer. The denser the fouling layer, the better the reflection and thus a bigger amplitude is seen.

- The cell design as used is still far from simulating even a single sheet in a spiral wrap membrane module. It will have to be adapted to bring it a bit closer to the real world in order to really be of assistance. However, even the cell used will already be a great step forward. After some modifications to improve plant simulation, it could be fitted or retrofitted to any industrial desalination or ultrafiltration plant and UTDR monitoring could be combined with other monitoring protocols.

- Tremendous possibilities exist for the application of UTDR direct to other configurations of commercial importance like spiral-wound, hollow-fibre and tubular modules, but more research is necessary to investigate the usage of UTDR in these areas.

- The UTDR technique has significant potential for use in module design. In particular, the technique can provide information regarding stagnation zones within the module. This capability was highlighted in a test that showed no flux-flow in the spiral-wound module.

- The technique can monitor changes through a thick-walled module. Its non-destructive capabilities make it extremely valuable for usage in the membrane industry.

- UTDR is quite sensitive to changes inside the module, which made it possible to study the influence of MWD's flow distributor. The formation of air bubbles, created as the fluid passes through the orifices of the flow distributor, has been noticed.

Overall, UTDR seems very promising, as it is the only non-destructive-real-time testing technique available to study changes inside modules.

7 Future research required

UTDR has tremendous possibilities for usage in the membrane field. Further work is vital to investigate the possible application on other membrane configurations. More work is needed in the following areas:

- Spiral wrap modules.

The complex nature of multiple echoes will make interpretation of the results very difficult. The best way to start further experimentation is by means of a flat sheet cell with multiple membranes inside the cell. The number of membranes can gradually be increased until it is typical of a spiral wrap module.

- Tubular modules

Will be easy to investigate if a curved transducer is used. The curved area has to fit very tight to the outer surface of the tubular wall.

- Capillary or hollow fibre modules

Again the complex nature of multiple echoes will make experimentation difficult but one can start with a few capillary fibres and gradually increase them.

8 References

Altmann, Justus & J. Ripperger. 1997. Particle deposition and layer formation at the crossflow microfiltration. *Journal of Membrane Science* 124: 119 - 128

Baker, John S. & S.J. Judd. 1996. Magnetic Amelioration of Scale Formation. *Water Research* 30 (2): 247 - 260

Baker, John S., S.J. Judd & S.A. Parsons. 1997. Antiscale magnetic pretreatment of reverse osmosis feedwater. *Desalination* 110: 151 – 166

Benson, Robert F., R.K. Carpenter, B.B. Martin & D.F. Martin. 1997. Using magnetic fields to prevent scale. *Chemtech.* [ISSN 0009-2703] 27 (4): 35-37

Belfort, Georges & B. Marx. 1979. Artificial Particulate fouling of hyperfiltration membranes – II Analysis and Protection from fouling. *Desalination* 28: 13 – 30

Blokhra, R.L. & J Joshi. 1994. Effect of magnetic field on membrane transport. *Industrial Journal of Chemistry* 33A: 758 - 759

Brunelle, Michael T. 1980. Colloidal fouling of reverse osmosis membranes. *Desalination* 32: 127 - 135

Carter, J. W. & G. Hoyland. 1976. *5th International Symposium on Fresh Water from the sea* 4: 21

Chai, Xijun, T. Kobayashi & N. Fujii. 1999. Ultrasound-associated cleaning of polymeric membranes for water treatment. *Separation and Purification Technology* 15: 139 - 146

Cooray, G. 1998. *Mineral Water Development*, Stellenbosch, South Africa, 7600 (Personal communication)

DuPont de Nemours, E. I. & Co., Permasep Engineering Manual (1982)

Faller, Kathleen, A (ed). 1999. Manual of Water Supply Practices: *Reverse Osmosis and Nanofiltration*. United States of America: American Water Works Association

Fane, A. G. UNESCO *Centre for Membrane Science and Technology*, The University of New South Wales, Sydney, NSW 2052, Australia. (Personal communications with Mr Fane)

Ford, R. D. 1970. *Introduction to Acoustics*. Amsterdam: Elsevier

France, A. B. & Cabell, S. G. 1890. *U. S. Patent* 438 579

Furukawa, David, H. 1999. *A new approach for mitigating membrane fouling*, Paper presented at: Fouling mitigation in membrane processes workshop, Technicon-Israel Institute of Technology, Haifa, Israel

Grimes, S. M., Tube International, March (1988) 111-118

Grodzinsky, S., Weiss, A., Separation and Purification Methods 14 (1985) 1-40

Gutman, R. G., The Chem Eng., July (1977) 510-513, 521-523

Hiddink, J., De Boer, R., Nooy, P. F. C., J. Dairy Sci. 63 (1980) 204

Higashitani, Ko, A. Kage, S. Katamura, K. Imai & S. Hatade. 1993. Effects of a Magnetic field on the Formation of $CaCO_3$ Particles. *Journal of Colloid and Interface Science* 156: 90-95

Harvey, R. 1965. *US Patent* 3206397

Jagannadh, S. Nadh & H.S. Muralidhara. 1996. Electrokinetics Methods to Control Membrane Fouling. *Industrial and Engineering Chemistry Research* 35: 1133 - 1140

Kremen, Seymour S. 1979. Means by which reverse osmosis desalting costs can be substantially reduced well before 2000. *Desalination* 30: 59 - 68

Kools, W, F, C, S. Konagurthu, A. R. Greenberg, L. J. Bond, W. B. Krantz, T. H. van den Boomgaard, H. Strathmann. 1998. Use of ultrasonic time-domain-reflectometry for real-time measurement of thickness changes during evaporative casting of polymeric films. *Journal of Applied Polymer Science 69*:2013 - 2019

Kronenberg, K. J. 1998. *Magnetic water treatment de-mystified.* http:/www.gcea.com/treatment

Li, H., E. Ohdaria, M.Ide. 1995. *Japanese Journal of Applied Physics 35*(5B)

Li, H., A.G. Fane, H.G.L. Coster, S.J. Vigneswaran. 1998. Direct observation of particle deposition on the membrane surface during crossflow micro-filtration. *Journal of Membrane Science* 149: 83 - 97

Lin, I. J. & S. Nadiv. 1988. Membrane performance under the influence of Magnetic pretreatment. *Magnetic Separation News* 2: 137-143

Lonsdale, H. K. 1982. The growth of membrane technology. *Journal of Membrane Science* 10: 81 - 181

Mackley, M.R. & N.E Sherman. 1992. Cross-flow cake filtration mechanisms and kinetics. *Chemical Engineering Science* 47: 3067 - 3084

Mairal, Anurag P., A.R. Greenberg, W.B. Krantz & L.J. Bond. 1999. Real-time measurement of inorganic fouling of RO desalination membranes using ultrasonic time-domain reflectometry. *Journal of Membrane Science* 159: 185 - 196

Mallevialle, J., P.E. Odendaal & M.R. Wiesner. 1996. *Water Treatment Membrane Processes*. New York: McGraw-Hill

McDonogh, R. M., H. Bauser, H. Stroh & H.Chmiel. 1990. Concentration polarisation and adsorption effects in cross-flow ultra filtration of proteins. *Desalination* 79: 217 - 231

McDonogh, R. M., H. Bauser, H. Stroh, H. Chmiel. 1995. Experimental in situ measurement of concentration polarisation during ultra- and microfiltration of bovine serum albumin and Dextran Blue Solutions. *Journal of Membrane Science* 104: 51 - 63

Ozeki, Sumio, C. Wakai & S. Ono. 1991. Is a Magnetic Effect on Water Adsorption Possible? *Journal of Physical Chemistry* 95 (26): 10557 - 10559

Parsons, Simon A., B.A. Wang, S.J. Judd & T. Stephenson. 1997. Magnetic treatment of calcium carbonate scale-effect on pH control. *Water Research* 31 (2): 339 - 342

Parvatiyar, Madan G. 1996. Interaction of dispersed phase with concentration polarisation. *Journal of Membrane Science* 115: 121-127

Peterson, R. A. 1996. *Use of Acoustic TDR to Assess the effect of crosslinking on membrane compaction.* M.S. Thesis. Boulder: University of Colorado

Peterson, R. A. 1998. Use of ultrasonic time-domain reflectometry for real-time measurement of compressive strain during membrane compaction. *Desalination* 116: 115 - 122

Potts, D. E., R.C. Ahlert & S.S. Wang. 1981. A critical review on fouling of reverse osmosis membranes. *Desalination* 36: 235 - 264

School of Water Sciences. 1996. *Proceedings of the Second International Meeting on Antiscale Magnetic Treatment.* United Kingdom, Cranfield Beds: Cranfield University

Reimers, R. S., Anderson, A. C., White, L.E., Applied Fields (1997)

Sakiadis, B. C. in Perry, R.H., D.W. Green & J.O. Maloney. 1984. *Perry's Chemical Engineer's Handbook.* New York: McGraw-Hill

Shercliff, J. A. 1965. *A textbook of magnetohydrodynamics*. New York: Pergamon Press

Shimichi, W. 1995. *Japan Patent* 0731974

Vermeiren, T. I. S. 1953. *U. S. Patent* 2652925

Wakeman, R. J. 1994. Visualisation of cake formation in crossflow microfiltration. *Trans. IchemE* Part A 72: 530 - 540

9 Appendix

The changes in echo responses from the membrane were investigated by placing a permeate side spacer from a spiral-wound membrane configuration under the membrane. With the addition of the permeate spacer, another echo was seen.

No permeate spacer used:

Figure 9-1 is the response for a clean membrane on top of the porous support, while Figure 9-2 represents the same conditions but with the presence of a fouling layer. In both experiments the pressure was controlled at 2 MPa (20 bar).

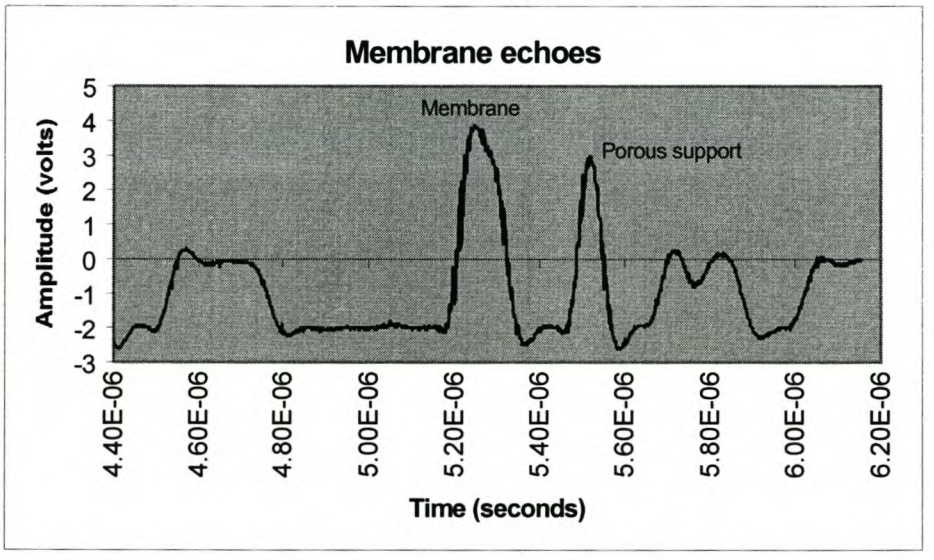

Figure 9-1 - Ultrasonic response of clean membrane and the porous support at 20 bar (no permeate spacer used.)

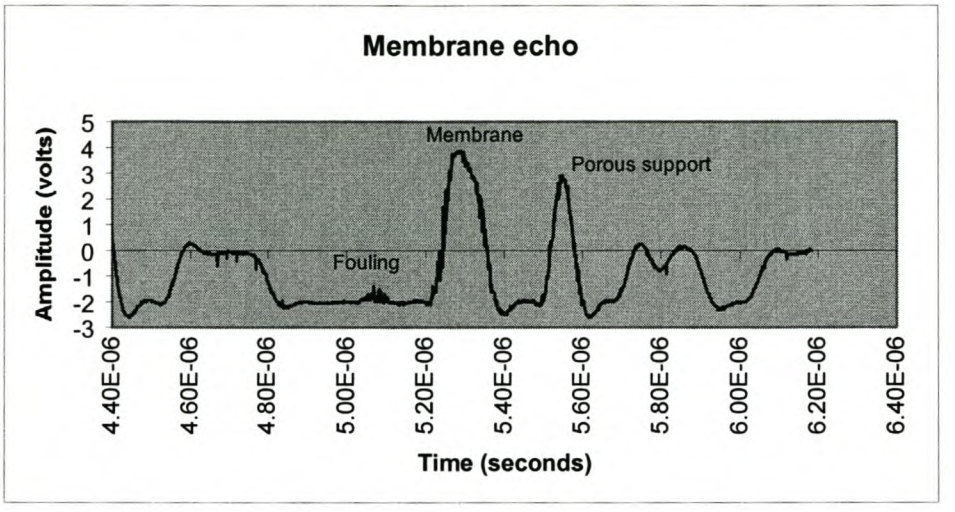

Figure 9-2 - Ultrasonic response of fouled membrane and porous support at 20 bar. (no permeate spacer)

With the permeate side spacer:

By placing the permeate spacer under the membrane, the formation of another echo was seen. This behaviour confirmed that the first echo was in fact the membrane echo.

The influence of pressure on the membrane echo is also clear from the following two images. In Figure 9-3, the membrane echo is in the area of 5.0 μs, (at a pressure of 2 MPa), while it has moved to 5.1 μs in Figure 9-4, as a result of the higher pressure (2.1 MPa).

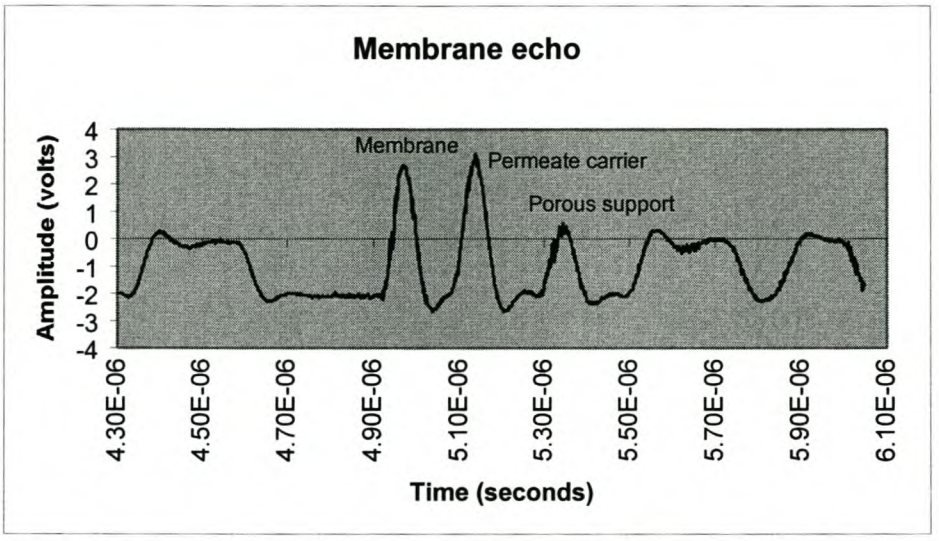

Figure 9-3- Clean membrane ultrasonic response with permeate water spacer support under membrane at 20 bar pressure.

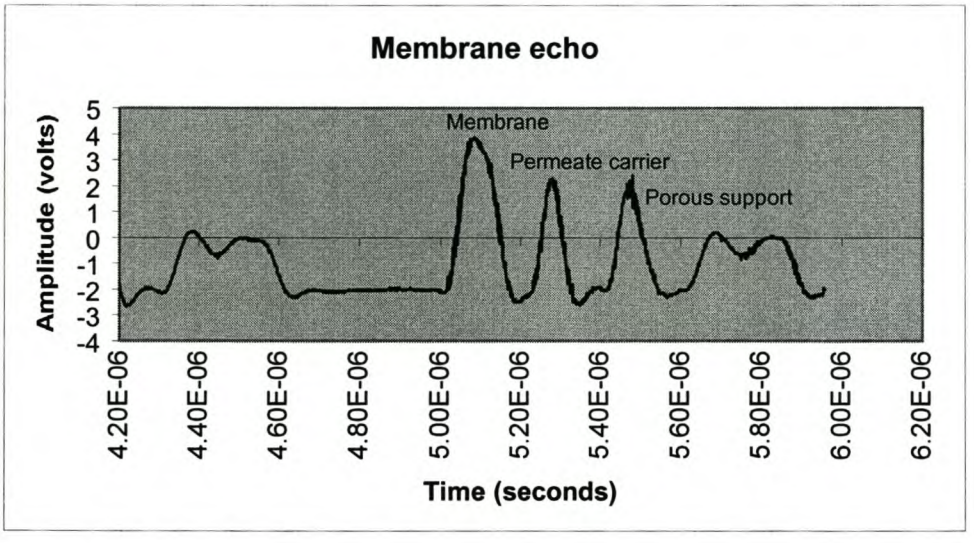

Figure 9-4 - Clean membrane ultrasonic response with permeate spacer support under membrane at 21 bar pressure.

Figure 9-5 is the response for the same membrane and operating conditions as in Figure 9-4, but with the presence of a fouling layer.

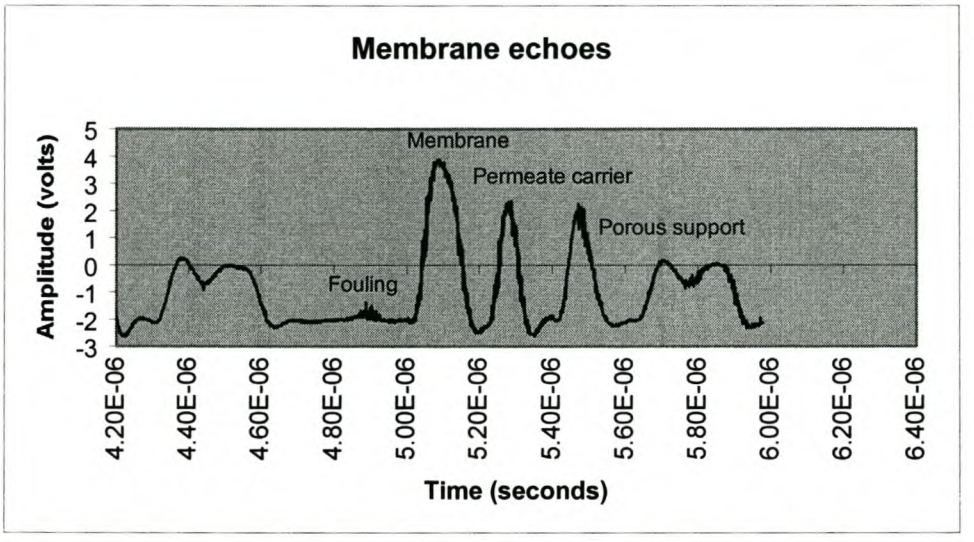

Figure 9-5 - Ultrasonic response with permeate carrier support under membrane at 21 bar pressure and fouling present.

The difference between the fouling layer echo that is captured during real-time fouling conditions, and the echo that is seen from the static experiment with the compact scale membrane (Figure 5-2), is clear from a comparison between Figure 9-5 and Figure 9-6. Figure 9-6 is in fact only an expansion of Figure 5-2, to include all the relevant echoes. From these images it can be seen that the compact fouling layer gives a better reflection. The reason for this behaviour can be explained by the fact that the fouling layer of the compact membrane has a higher density. The membrane pores were completely plugged and a solid, uniform fouling layer was present. (Figure 5-3)

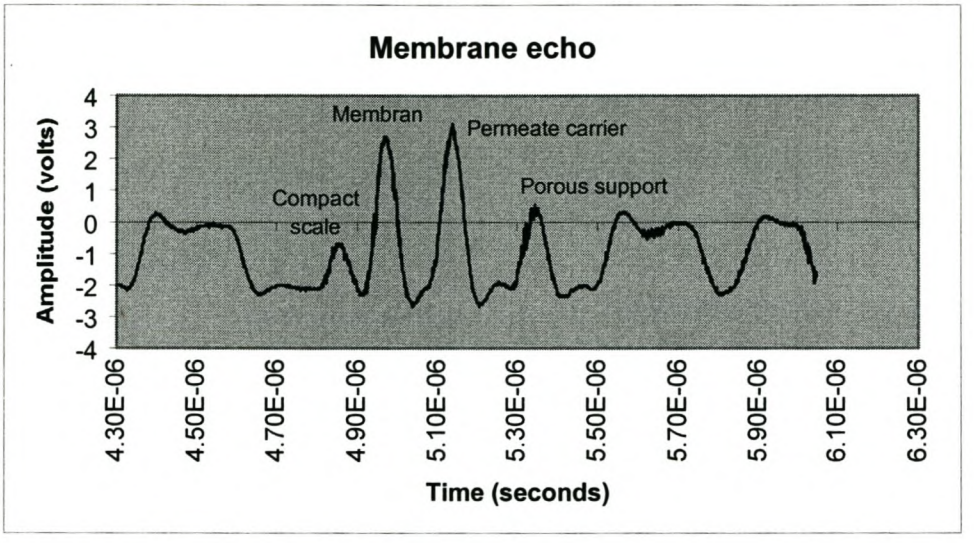

Figure 9-6 - Ultrasonic response of compact membrane with permeate spacer under membrane at 20 bar.

9.1 Background on the spiral wrap RO module used in the study

Mineral Water Development (MWD), a company at Stellenbosch, supplied the spiral wrap module equipment. They are leading suppliers of membrane equipment for the desalination industry.

MWD have successfully designed and patented a technique that inhibits and reduces membranes from fouling. This new design makes use of a flow distributor, as well as coils and electric currents around the membrane. The flow distributor has the ability to focus feed flow more evenly over the membrane area, while the magnetic fields (which form due to the induction effect) are responsible for the 'Self-Cleaning' of the membranes. The fact that the membranes are not fouling as fast as in other reverse osmosis processes and that no chemicals are used results in lower maintenance requirements and in the prolonged life of the unit.

Despite the remarkable results they obtain with their technique, they have no clear explanation for it. Thus they don't know whether they have obtained optimum working conditions and if the technique can be upgraded. Better methods for the control, monitoring and understanding of this process are necessary in order to make full use of its capabilities. This would be the ideal situation for the UTDR technique.

9.2 Spiral-wound membrane configuration

Unlike the flat sheet cell, this design makes use of the spiral-wound membrane configuration. The interpretation of the ultrasonic signals is much more complex in this design, as there are more reflections than in the flat sheet cell.

In this design, (Figure 9-7) two flat sheets of membrane are glued together back-to-back to form an envelope. Inside the envelope is a porous sheet of material called a water carrier. The envelope is glued together on three sides. The forth side is attached to a perforated permeate tube. The only way water (permeate) can exit the envelope is through this tube.

During operation, feed (under pressure) flows across the membrane surface on both sides of the envelope. Water, which permeates through the membrane, flows along the water carrier towards the open end of the envelope and exits through the permeate tube. In large industrial systems several envelopes are attached to the perforated permeate tube in such a way that permeate exiting the envelopes has to enter the same permeate tube. The envelopes are then wrapped or wound around the permeate tube to form a cylindrical membrane element. Before the envelopes are wrapped, a mesh feed spacer is placed between the envelopes. The feed spacer is necessary to provide spaces between membrane envelopes after the envelopes are wrapped into the spiral wound configuration. This space, called the feed channel, allows the feed to flow evenly through the element from one end to the other.

Elements are placed end-to-end in a cylindrical pressure vessel (PV). This casing (PV) is usually made of fibreglass. Permeate tubes of each element are connected to form a permeate channel and allow permeate from the collective elements to exit one end of the PV. Feed enters thus one end of the PV, and concentrate and permeate exits the other.

Figure 9-7 - RO spiral wound membrane configuration

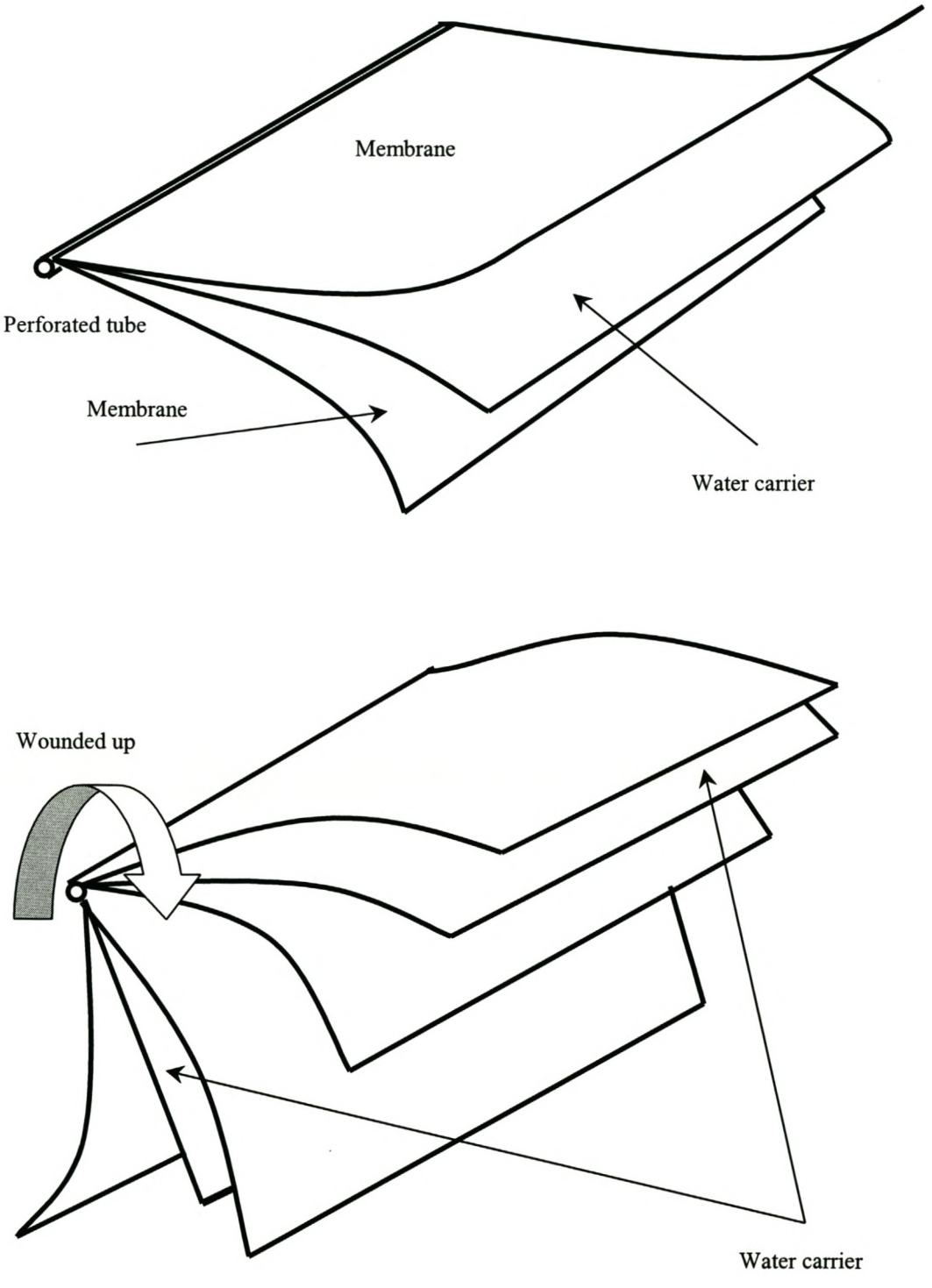

9.3 Problems with System design

The feed spacer inside the element causes problems. It limits the velocity of flux flowing through the element and limits the cleaning ability of the cross flow. The spacer also provides spaces where colloidal particles can be retained and bacteria can grow, increasing the fouling tendency of a spiral-wound element.

As the feed channels in an element become fouled, the flux through the element becomes uneven. The water seeks the path of least resistance resulting in lower cross-flow velocities as the water progresses further along the membrane leaf. This could produce even more fouling, especially if microbiological growth is present. At some point the system must then be shut down and cleaned.

Cleaning the spiral-wound element presents a problem for two reasons. First the flow path used by the cleaning solution is the same one used by the feed. If fouling has distorted the distribution of the feed flow, it also distorts the distribution of the cleaning solution flow. The fouled areas of element are the last to receive the cleaning solution but the most difficult to clean.

The second problem involves the membrane element configuration inside the PV. Elements are rarely removed for cleaning because of the time and labour involved, especially in large systems. This means that elements are usually cleaned while they are in the PV. This is done by connecting hoses or other feed lines to the PV and pumping cleaning solution through the PV. Because the elements are cleaned while mounted in series in the PV, any foulants removed from the first element must pass through the remaining elements before it exits the PV. Each following element does the same, with the exception of the last element in the series.

All of these factors can result in an extensive amount of time required for cleaning. Because the system is not in normal production during cleaning and since labour and cleaning chemicals are expensive, membrane cleaning is not popular. Any way to speed up the cleaning process or increase the time between cleanings is welcomed.

9.4 Magnetism in water treatment

The subject of the magnetic treatment of water to prevent scale is controversial, but the following phenomena have been found after magnetic fields was used to treat some processes:

- reduced formation of hard lime scale in boilers and pipe systems
- elimination of old lime scale deposits
- accelerated plant growth
- desalination of soils
- improvement of concrete
- better cleaning, faster drying
- better taste and smell of drinking water
- changes of freezing modes
- beneficial effect on patients with kidney stones and
- minute changes in some physical constants of water, such as viscosity, IR absorption and surface tension to mention just a few.

The answer to the main question " why does a magnetic field affect the properties of water systems?" has not yet been found, and thus the problem of magnetic treatment of water is discussed more on the engineering, empirical, and technological level, rather than on a purely scientific basis. In practice, however, no one argues whether magnetic treatment is effective or not, the only argument is on how to explain the observed phenomena correctly: by the changes that take place within the water itself, or solely by the influence of the impurities present in the water.

9.4.1 Characteristics of magnetic treatment

In general, there are two features characteristic of magnetic treatment: the poor reproducibility of experimental results (especially under laboratory conditions), and the "memory" of its magnetisation which water seems to show, i.e., the persistence of the magnetisation effects for several hours or even days, if the temperature of the water systems is sufficiently low.

According to some reports the water retains its capability of reducing scale for up to 2 days. Actually, the treated water has its specific scale reducing capability as long as its calcium carbonate is in the solid form of the inert micro crystals. Dr. Kronenberg (1997) and his team from the University of Cottingen, Germany, had done the following studies:

They placed drops of water on glass slides and permitted the water to evaporate under observation with magnifications from 50 to 400 times. The microscope was equipped with polariser and analyser in order to improve the contrast for the optically active $CaCO_3$ crystals. They compared drops of ordinary water as it came from the tap with drops of the same water after it had passed through magnetic fields. The drops were evaporating side by side on the same glass slide under identical conditions.

They found that the area formerly covered with the water was now covered with a lattice of thin dentric crystals and that the rim of the drop was studded with a number of thick, strongly light-polarising dentric crystals which had grown from one point at the glass on the periphery of the drop. The crystals were firmly attached to the glass of the slide and fractured if one attempted to dislocate them with a microscopic needle. By counting the crystals, they found that the number of crystals which had grown on the glass after the water was magnetically treated, was reduced by about two thirds. The effectivity of the treatment with respect to reduction of such glass-attached crystals was therefore 67%.

This simple method of comparing the microscopic crystal count with and without magnetic treatment permits within hours a quantitative estimate of the effectivity of the treatment with regard to scale reduction.

By investigating the inert micro crystals under high magnification for many different waters and varied treatments, some astonishing results were found. By using the interference colours of the polarised light, the thickness of the disk-shaped crystals can be estimated to be from $0.1_{p.}$ to $2.4_{p.}$ (about 4 times the wavelength of red light). Most astonishing was the findings that these crystals keep changing their mode. After about 20 hours they develop holes in their centres and some of their matter turns into thin needles bundled up at the location of the disk. The disk-shape is a meta-stable crystal form of calcium carbonate that transforms into the more stable form of acicular crystals within days. These needle-shaped crystals then dissolve also, most of them last only 2 or 3 days. That is the reason for the fact that the scale-reducing properties of the treated water last for 2 days only.

9.4.2 Influences of magnetic treatment on water

The following phenomena were found after magnetic fields were used to treat water:

1. A reduction in pH (Parsons et al., 1997)
2. Reduction in conductivity (Baker and Judd, 1996)
3. A change in the light absorbency or transmission
4. Reduction in viscosity and surface tension
5. Water absorption change (Ozeki et al., 1991)
6. Influence on IR absorbency
7. Reduction of zeta potential
8. The coagulation rate of colloidal particles in electrolyte solutions is suppressed (Higashitani et al., 1993)
9. A change in particle size and crystallinity type (Grimes, 1988)
10. The degree of the magnetic effect increases with decreasing particle size.
11. A reduction in oxygen saturation levels in water which correspondingly reduces corrosion (Reimers, 1997)

9.4.3 Magnetic behaviour

A material's magnetic behaviour falls in one of four categories:

- ferromagnetism
- ferrimagnetism
- paramagnetism or
- diamagnetism

Paramagnetism, in which the nonzero spin or orbital momentum of the electron in a substance causes the molecule to line up with the applied magnetic field, and diamagnetism, where a magnetic moment is induced in a substance by the application of an external magnetic field, are the two common groups for our purposes.

Russian papers note that in order to be effective, the water to be treated has to move across magnetic fields not stronger than 1000 to 2000 Oersted. It also usually works better for water at a lower temperature, and for a certain flow-velocity the effect is a maximum.

9.4.4 Magnetism and quantum numbers

How does a magnetic field work in order to minimise scale formation? The explanation is given in terms of the change of spin-orbital system entropy arising from the orientation of the atom magnetic moment within an applied magnetic field. The relationship of the entropy to the available spin states is given by the Boltzmann definition of entropy, (Benson et al., 1997)

Eq. 23..... $S_b = k_b.\ln w$

where k_b is the Boltzmann constant and W is the number of permutations based on the spin-orbit coupling and the orbital angular momentum.

In the absence of a magnetic field, the ground-state spin level would be degenerate. However, in the presence of a magnetic field of magnitude B, the energy level splits, and for S = ½, two terms result from m = + ½ and m = -½ (m is the magnetic spin quantum number).

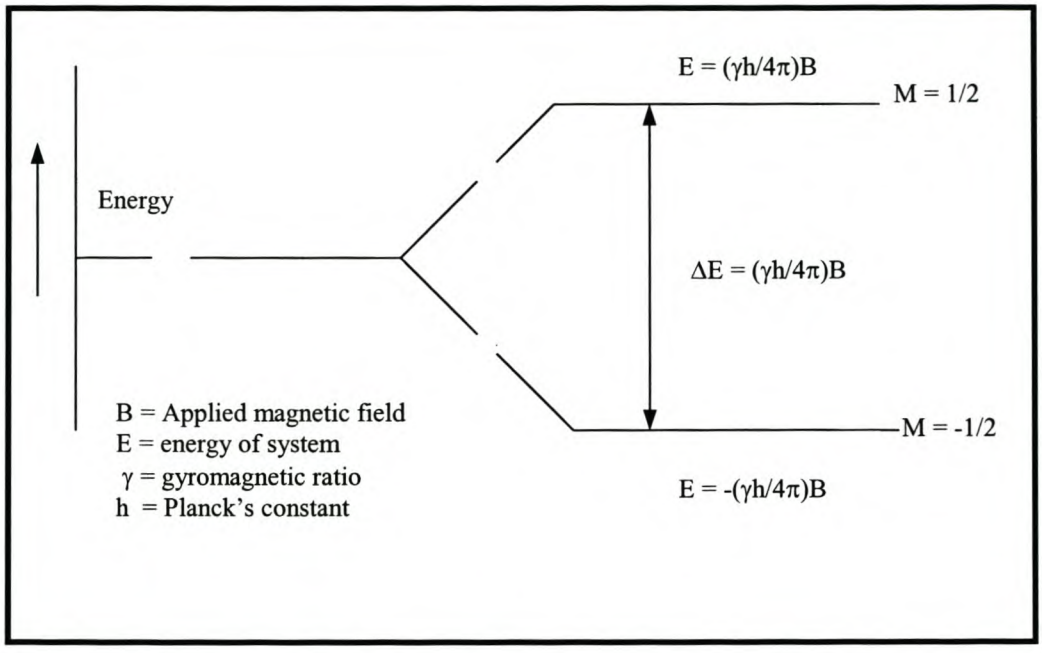

Figure 9-8 – Energy variation of a diamagnetic substance in the presence of a magnetic field

The two energy levels are ± (γh/2π)B and the difference in energy between the two energy levels is a function of the applied field: E = ± (γh/2π)B.

Thus, in the presence of a magnetic field, permutations increase, and two energy levels result for each one that existed before. Consequently, there is a change in entropy between the spin system and the lattice surrounding it as the spins are distributed within the new levels. For paramagnetic substances at low temperatures, the presence of a magnetic field would simply result in the alignment within the magnetic field and lead to reduce entropy. Diamagnetic substances do not align, because the opposing electron spins cancel each other, however, the effect on the lattice remains the same.

An increase in entropy is therefore reflected in an increase in the solubility for aqueous saturated fluids. The effective splitting of the magnetic spin-state degeneracy in the presence of a magnetic field appears to be cancelled when spins are paired. The resultant magnetic moment is shielded from the applied magnetic field. However, a molecule in a solid lattice has many magnetic moment contributions that do not completely shield the resultant magnetic moment. As a result, the number of available permutations of the resultant magnetic moment increases in response to the applied magnetic field.

In terms of the solubility product equilibrium involved in scale formation, the shift in equilibrium can be interpreted in terms of a magnetic perturbation of the system.

Eq. 24.....$\Delta G = -RT\ln K = \Delta H_{soln} - T\Delta S_{soln}$

As is seen from this Gibb's equation, which describes the free energy change of the solubility equilibrium (ΔG), the response seen would arise from changes in the entropy term.

9.4.5 Composition dependence of water

The successful application of magnetism to prevent scaling depends on the water composition (Benson et al., 1997). Calcium carbonate with a magnetic susceptibility of -0.381 cgsu can be controlled, and deposits removed, as can deposits of calcium sulphate (-36.4 cgsu) or sodium fluorosilicate. However, paramagnetic species such as the hydrous oxides of iron and manganese are troublesome due to their greater magnetic susceptibility and may need to be removed. Roughly, a maximum of 1ppm of iron and/or manganese can be tolerated for each 200 ppm of total dissolved solids.

9.4.6 Forces on a particle

Solid or fluid material moving in a magnetic field experiences an e.m.f. If the material is electrically conducting and a current path is available, electric currents

ensue. Alternatively, currents may be induced by change of magnetic field with time. There are two consequences:

- An induced magnetic field associated with these currents appears, perturbing the original magnetic field.
- An electromagnetic force due to the interaction of currents and field appears, perturbing the original motion.

These are the two basic effects of magnetohydrodynamics (MHD), the science of the motion of electrically conducting fluids under magnetic fields. The situation is essentially one of mutual interaction between the fluid velocity field and the electromagnetic field; the motion affects the magnetic field and the magnetic field affects the motion.

These forces act on the current carrying entity, the ion. Positively charged particles will move in a direction in accord with the Right-hand Rule, where the electric and magnetic fields are represented by the fingers and the force by the thumb. Negatively charged particles will move in the opposite direction. This force is in addition to any mixing in the fluid due to turbulence. The result of these forces on the ions is that, in general, positively charged ions (calcium and magnesium, primarily) and negatively charged ions (carbonate and sulphate, primarily) are directed toward each other with increased velocity. The increased velocity should result in an increase in the number of collisions between the particles, with the result being formation of insoluble particulate matter. Once a precipitate is formed, it serves as a foundation for further growth of the scale crystal. The treatment efficiency increases with increasing hardness since more ions are present in solution; thus each ion will need to travel a shorter distance before encountering an ion of opposite charge.

An important feature of MHD is the ability of the electromagnetic force to be sometimes pseudo-viscous and dissipative and sometimes pseudo-elastic and conservative in a way that must depend on some dimensionless expression of the degree of conductivity.

Electrical properties of fluid

MHD differs from ordinary hydrodynamics in that the fluid is electrically conducting. It is not magnetic; it affects a magnetic field not by its mere presence but only by virtue of electric currents flowing in it. The fluid conducts because it contains free charges that can move indefinitely, but it may also be a dielectric and contain bound charges that can only move a limited extent under electric fields. This migration of bound charges is described in terms of the usual polarisation vector **P** (coulomb/m^2).

Electric and magnetic fields

A charged particle such as an electron suffers forces of three kinds.

1. It is repelled or attracted by other charged particles and the total force on the particle per unit of its charge due to all the other charges is the *electrostatic field* **E** (volt/m). From Coulombs law it follows that **E** is irrotational (**curl E = 0**), where **E** can also be represented as the negative gradient of an electrostatic potential V, where **E = -grad V**. It also follows that **E** is solenoidal in regions devoid of charge.
2. A charged particle moving with velocity **v** m/s relative to a certain frame of reference experiences a magnetic force **v** × **B** (Newton's) per unit of its charge, with **B** the *magnetic field*.
3. If the magnetic field **B** is changing with time relative to a certain frame of reference, then per unit of its charge a particle will suffer a further force **E**, the *induced electric field*, defined by **div E = 0** and Faraday's law **curl E** = $-\partial\mathbf{B}/\partial t$. Since div **curl** vanishes, $(\partial/\partial t)$ div **B** = 0, and therefore div **B** = 0.

The total force on a particle per unit of its charge is called the *Lorentz force* (Shercliff, 1965) and is defined by

Eq. 25……..……..E + v × B.

9.4.7 Starting from Faraday's law

Presume a uniform magnetic field has been established perpendicular to the fluid flow in a pipe. Next, presume that two conductors, one on each side of the pipe, are placed on the walls of the pipe and connected by a galvanometer. Further presume that the fluid is an ionic medium. The fluid is a moving conductor through the magnetic field, and the flux linkages created by this conductor change (due to its movement) are generating an electromotive force. This force can be calculated from Farady's law (Benson et al, 1997):

Eq.26.....$E = -Nd\Phi/dt$,

Where **E** is the electromotive force of mutual induction, **N** is the number of ampere turns per meter, and $\mathbf{d\Phi/dt}$ is the rate of change of magnetic flux with time. When the current produced by the induced electromagnetic field (EMF) reaches its Ohm's law value, the flux ceases to change and the induced EMF becomes zero.

The EMF induced in a circuit caused by a change in magnetic flux will be in the direction current could flow to oppose this change in flux (Lenz's law). Because the conductor (moving fluid) is passing through a magnetic field, the EMF generated is called "motional" or "generated" EMF. If dt is substituted by the distance, ds, divided by the velocity v,(m/s) one obtains Faraday's law as modified for motional electromotive force and in the form applicable to conducting fluid treatment:

Eq. 27.....$E = -Nd\Phi/dt = BL(ds)/(ds)/v = BLV$

where **B** is the magnetic flux density perpendicular to the fluid flow and **L** is the diameter of the pipe containing the fluid.

9.5 Areas where MTW is successfully applied:

Based on analyses of existing technical literature on the magnetic treatment of water and its ability to alter water properties, there are many basic areas where the utilisation of this method has great practical merit, such as elimination of scales due to high temperature, control of incrustations on equipment, reduction of salt deposits in piping systems, intensification of bactericidal function of disinfectants, acceleration of reagent diffusion, increasing the efficiency of ion exchange resin (ionits), removal of fine particles in the purification of recycling of waste water, extraction of valuable metals from ores by flotation concentrate, acceleration of the solidification of certain cements and increasing the density and strength of casting moulds.

10 Glossary

PRF rate	Repetition rate - stepwise selection of crystal-controlled frequencies: 20, 50, 100, 200, 500, 1k, 2kHz
High pass filter	A filter that selectively passes high-frequency inputs to the output while blocking low-frequency inputs from reaching the output.
Low pass filter:	A filter that selectively passes low-frequency inputs to the output while blocking high-frequency inputs from reaching the output.
Gain	Toggle switch selects 40 dB (x100) or 60 dB (x100) maximum system gain, excluding the auxiliary amplifier.
Main bang	The action of the transducer when it is triggered by a voltage signal to deliver a high frequency ultrasonic signal.
Interface ringdown	Typical of an undamped transducer. The transducer takes a while to recover after the main bang and is still "buzzing" Under these circumstances it will be unable to resolve closely positioned reflections. A high-dampened transducer should always be used where good resolution is of primary importance.
Auxilary amplifier	An interior chassis-mounted preamplifier of the Pulsar receiver Model 5058 PR.